

**THEORETICAL AND EXPERIMENTAL STUDY OF
ERBIUM-DOPED FIBER LASER CHAOTIC CONDITIONS IN
RESPONSE TO ACOUSTIC VIBRATIONS FOR PIPE
LEAKAGE MONITORING**

By

ONUBOGU NNEKA OBIANUJU

A thesis submitted to the Department of Electrical and Electronics
Engineering, Lee Kong Chian Faculty of Engineering and Science,
University Tunku Abdul Rahman,
in partial fulfillment of the requirements for the degree of
Doctor of Philosophy (Engineering)

June 2023

ABSTRACT

THEORETICAL AND EXPERIMENTAL STUDY OF ERBIUM-DOPED FIBER LASER CHAOTIC CONDITIONS IN RESPONSE TO ACOUSTIC VIBRATIONS FOR PIPE LEAKAGE MONITORING

Onubogu Nneka Obianuju

Pipelines undergo deformation leading to leakage several times throughout their service life. Hence, there is a need for Structural Health Monitoring (SHM) to ensure the safety of pipelines. Various conventional SHM and fiber optics technology methods for pipeline leakage detection have been explored in the past, most of which are expensive; have slow response time; limited coverage, and limited sensitivity. This thesis presents a cost-effective and highly sensitive Erbium-doped fiber laser (EDFL) sensor that was designed and tested for its effectiveness in pipeline leakage and location detection. Results obtained showed an overall sensor accuracy of 90 % for leak location detection. However, during the tests, some instabilities were observed in the sensor. This led to the experimental and theoretical study of the behavior (including chaotic conditions) of the modulated EDFL to understand the cause of the instabilities. Two EDFL configurations (linear cavity – EDFLL and ring cavity – EDFRL) both under pump and external cavity-loss modulations were analyzed experimentally and theoretically. The bifurcation diagrams obtained showed resonance peaks, regions of chaos, and optical bi-stability confirming that the existence of bifurcation is the root cause of the EDFL's unstable

behavior. For the theoretical analysis, a modified model built from two rate equations of a class B laser was presented. The model generates all spectral characteristics obtained during experimental pump and external cavity-loss modulations of the two EDFL configurations and can therefore be used to quickly predict the results of the EDFL sensor for further improvement in the future.

It has been proven that the dynamic response of the pump-modulated EDFLL and EDFRL can be theoretically predicted with total average accuracies of: 91.09 % (EDFLL) and 86.60 % (EDFRL) in terms of the “resonance peaks”; and 91.58 % (EDFLL) and 90.79 % (EDFRL) in terms of the “frequency after which saturation occurred”. Similarly, it has been proven that the dynamic response of the cavity-loss modulated EDFLL and EDFRL can be theoretically predicted with total average accuracies of: 91.04 % (EDFLL) and 91.07 % (EDFRL) in terms of the “resonance peaks”; and 91.70 % (EDFLL) and 95.96 % (EDFRL) in terms of the “frequency after which saturation” occurred. The EDFLL and the EDFRL are highly sensitive to external perturbations such as acoustic waves even at low frequencies ranging from 100 Hz to 100 kHz and can be used for pipeline monitoring.

ACKNOWLEDGEMENT

This project execution would have been impossible without the help of God Almighty. To Him be all the glory.

I would like to express my deepest gratitude to my main supervisor Assoc. Prof. Dr. Pua Chang Hong for all his guidance throughout the research work. I also thank him for his advice, support, and motivation toward making me an advanced and independent researcher. Special thanks to my co-supervisor Prof. Ts. Dr. Faidz Abd Rahman who guided me at the beginning of the project and helped me figure out my mistakes. He also shared his ideas with me on the project to help me understand the project better.

Special thanks to UTAR for providing the lab facilities and all the equipment used in carrying out the experiments and numerical simulations throughout the research. Greatest thanks to TRGS, the Ministry of Education Malaysia, and UTARRF, UTAR for their financial support for the first two years of the project.

Also, I would like to acknowledge my colleagues in the Photonics group whom I worked with at the beginning of the project: Law Zi Jian, Sin Ling Woon, and Wen Hao. They all helped me understand the research area as they were all already in the research group before I joined the project. Special thanks to Law Zi Jian for always helping me move my heavy equipment to the lab when I needed to do experiments and for his special guidance on how to

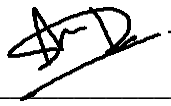
use some of the instruments for the experiments and also the software. More so, I will forever be grateful to my research partner Prof. William Rose from the University of Delaware who is the backbone of the simulation code used in this project. He guided me thoroughly on various methods to solve the rate equations theoretically using MATLAB and took his time to direct me on how to re-modify the code over and over again until it became perfect. Great thanks go to Prof. Rider Jaimes Reategui from the University of Guadalajara, Mexico, for sharing his codes and thesis with me which aided me a lot in formulating my codes used for the theoretical analysis.

Lastly, I must acknowledge my direct family (my very supportive husband and two daughters) who understood when and why I did not have much time for them and still showered me with love, and encouragement and gave me emotional and financial support during the research project. My parents, siblings, relatives, and friends kept encouraging me no matter how difficult it got, most especially my father (Engr. Godwin Onubogu) who contributed a lot emotionally, financially, and also by sharing his great ideas with me towards the project. I specially thank my mum for all her numerous prayers for me and for even flying all the way to Malaysia twice during the project duration to assist me with my kids while I carry out my research. I thank you all for your continuous encouragement and unfailing support throughout the research period.

APPROVAL SHEET

The thesis entitled "**THEORETICAL AND EXPERIMENTAL STUDY OF ERBIUM-DOPED FIBER LASER CHAOTIC CONDITIONS IN RESPONSE TO ACOUSTIC VIBRATIONS FOR PIPE LEAKAGE MONITORING**" was prepared by ONUBOGU NNEKA OBIANUJU and submitted as partial fulfillment of the requirements for the degree of Doctor of Philosophy (Engineering) at Universiti Tunku Abdul Rahman.

Approved by:



(Assoc. Prof. Dr. PUA CHANG HONG)

Date: 12/6/23.....

Main Supervisor

Department of Electrical and Electronic Engineering

Faculty of Engineering and Science

Universiti Tunku Abdul Rahman



(Prof. Ts. Dr. FAIDZ ABD-RAHMAN)

Date: 13/6/2023.....

Co-supervisor

Department of Electrical and Electronic Engineering

Faculty of Engineering and Science

Universiti Tunku Abdul Rahman

FACULTY OF ENGINEERING AND SCIENCE

UNIVERSITI TUNKU ABDUL RAHMAN

Date: 12/06/2023

SUBMISSION OF THESIS

It is hereby certified that **Onubogu Nneka Obianuju** (ID No: **18UEM04510**) has completed this thesis entitled “THEORETICAL AND EXPERIMENTAL STUDY OF ERBIUM-DOPED FIBER LASER CHAOTIC CONDITIONS IN RESPONSE TO ACOUSTIC VIBRATIONS FOR PIPE LEAKAGE MONITORING” under the supervision of Assoc. Prof. Dr. Pua Chang Hong (Supervisor) from the Department of Electrical and Electronics Engineering, Faculty of Engineering and Science, and Prof. Ts. Dr. Faidz Abd Rahman (Co-Supervisor) from the Department of Electrical and Electronics Engineering, Faculty of Engineering and Science.

I understand that the University will upload a softcopy of my thesis in pdf format into UTAR Institutional Repository, which may be made accessible to UTAR community and the public.

Yours truly,



(*ONUBOGU NNEKA OBIANUJU*)

DECLARATION

I, ONUBOGU NNEKA OBIANUJU hereby declare that this thesis is based on my original work except for quotations and citations which have been duly acknowledged. I also declare that it has not been previously or concurrently submitted for any other degree at UTAR or other institutions.



(ONUBOGU NNEKA OBIANUJU)

Date 12/06/2023

TABLE OF CONTENTS

	Page
ABSTRACT	ii
ACKNOWLEDGEMENT	iv
APPROVAL SHEET	vi
SUBMISSION OF THESIS	vii
DECLARATION	viii
TABLE OF CONTENTS	ix
LIST OF TABLES	xii
LIST OF FIGURES	xv
LIST OF ABBREVIATIONS	xxi
LIST OF PUBLICATIONS	xxii
CHAPTER	
1. INTRODUCTION	1
1.1 Research Background	1
1.1.1 Conventional methods of SHM	1
1.1.2 Fiber Optics Technologies for SHM	2
1.2 Problem Statement	8
1.3 Research Questions	9
1.4 Research Objectives	10
1.5 Thesis Outline	10
2. LITERATURE REVIEW	13
2.1 Introduction	13
2.1 Erbium-Doped Fiber Laser (EDFL) and its Working Principle	13
2.1 Erbium-Doped Fiber Laser Dynamic Behaviour for Sensing	18
2.2 Laser Dynamics of the Erbium-doped Fiber Laser Triggered by Pump Modulation	27
2.3 Laser Dynamics of Erbium-doped Fiber Laser Triggered by Loss Modulation	43
2.4 Summary	50
3. METHODOLOGY	52
3.1 Introduction	52

3.1	Design of the EDFL Sensor for Test on a Water Pipeline	55
3.2	Testing of the EDFL Sensor on a Real Water Pipeline to Detect the Presence of Leakage and the Location of the Leakage.	57
3.3	Experimental Analysis to Understand the Cause of the Instability in the EDFL Sensor	64
3.3.1	Experimental Configuration of the EDFLL	64
3.3.2	Experimental Configuration of the EDFRL	66
3.3.3	Experimental Pump Modulation of the EDFLL	67
3.3.4	Experimental Pump Modulation of the EDFRL	70
3.3.5	EDFLL subjected to experimental external loss modulation	75
3.3.6	EDFRL Subjected to Experimental External Loss Modulation	76
3.4	Amplitude modulation of the EDFRL	77
3.5	Theoretical Analysis of the EDFL under Pump Modulation to Predict the Experimental Results	78
3.6	Summary	89
4. PUMP MODULATION OF THE EDFLL AND EDFRL		91
4.1	Pump modulation of the EDFLL	92
4.1.1	Experimental and Theoretical Results of the Pump-modulated EDFLL1	95
4.1.2	Experimental and Theoretical Results of the Pump-modulated EDFLL2	100
4.1.3	Experimental and Theoretical Results of the Pump-modulated EDFLL3	103
4.1.4	Experimental and Theoretical Results of the Pump-modulated EDFLL4	106
4.2	Pump Modulation of the EDFRL	113
4.2.1	Experimental and Theoretical Results of the Pump-modulated EDFRL1	116
4.2.2	Experimental and Theoretical Results of the Pump-modulated EDFRL2	123
4.2.3	Experimental and Theoretical Results of the Pump-modulated EDFRL3	126
4.2.4	Experimental and Theoretical Results of the Pump-modulated EDFRL4	128
4.2.5	Experimental and Theoretical Results of the Pump-modulated EDFRL5	131

4.2.6	Experimental and Theoretical Results of the Pump-modulated EDFRL6	135
4.3	Pump Modulation of the EDFRL with Variation of the Amplitude	139
4.4	Summary	141
5.	LOSS MODULATION OF THE EDFLL AND EDFRL	144
5.1	Experimental and Theoretical Results of the Loss-modulated EDFLL	147
5.2	Experimental and Theoretical Results of the Loss-Modulated EDFRL	155
5.3	Summary	170
6.	CONCLUSION AND FUTURE WORK	173
6.1	Conclusion	173
6.2	Recommendation for Future Works	176
	REFERENCES	177
	APPENDICES	
	A. DATASHEET FOR ERBIUM DOPED-FIBER ISOGAIN	187
	B. PUBLICATION 1	189
	C. PUBLICATION 2	190
	D. PUBLICATION 3	191
	E. PUBLICATION 4	192
	F. PUBLICATION 5	194

LIST OF TABLES

Table		Page
2.1	Symbols from the rate equations and their definition	17
2.2	Summary of literature on EDFL under pump modulation describing their laser configurations and behaviors observed.	42
2.3	Summary of literature on EDFL under loss modulation describing their laser configurations and behaviors observed	49
3.1	Results obtained from the field test experiments	62
3.2	Input parameters used when pump-modulating the EDFLL from 1kHz to 60 kHz	69
3.3	Input parameters used when pump-modulating the EDFRL from 1kHz to 30 kHz	73
3.4	Input Parameters used when loss-modulating the EDFLL from 1kHz to 20 kHz	76
3.5	Input Parameters used when loss-modulating the EDFRL from 1kHz to 20 kHz	77
3.6	Input parameters used for amplitude modulation of the EDFRL	78
3.7	Variables and input parameters employed in the theoretical analysis of the pump-modulated and loss-modulated EDFLL and EDFRL (Variables and input conditions/parameters without units are non-dimensional) (Onubogu, et al., 2022)	86
4.1	Initial conditions used for the experimental and numerical pump modulation of the EDFLL and the resonance peaks observed experimentally and numerically	92
4.2	Quantitative analysis of the bifurcation results obtained for all four pump modulation experiments of the EDFLL1, 2, 3, and 4 in terms of resonance frequency peak.	93

4.3	Quantitative analysis of the bifurcation results obtained for all four pump modulation experiments of the EDFLL1, 2, 3, and 4 in terms of the saturation frequency in the bifurcation diagram.	94
4.4	Quantitative analysis of the bifurcation results obtained for all four pump modulation experiments of the EDFLL1, 2, 3, and 4 in terms of the width of OB regions in the bifurcation diagram	94
4.5	Detailed description of the linear to non-linear behaviors observed when the EDFLL4 was subjected to pump modulation at MA of 0.4 V and 19 kHz ω_r	111
4.6	Initial conditions used for the experimental and numerical pump modulation of the EDFRL	114
4.7	Quantitative analysis of the bifurcation results obtained for all six pump modulation experiments of the EDFRL1 to 6 in terms of resonance frequency peak.	115
4.8	Quantitative analysis of the bifurcation results obtained for all six pump modulation experiments of the EDFRL1 to 6 in terms of the saturation frequency in the bifurcation diagram.	116
4.9	Detailed description of the linear to non-linear behaviors observed when the EDFRL1 was subjected to experimental pump modulation at MA of 0.4 V and 2 kHz ω_r	120
5.1	Initial conditions/parameters used for the experimental and theoretical loss modulations of the EDFLL and EDFRL	145
5.2	Quantitative analysis of the bifurcation results obtained for all four cavity-loss modulation experiments of the EDFLL in terms of resonance frequency peak.	146
5.3	Quantitative Analysis of the Bifurcation Results Obtained for All Four Cavity-Loss Modulation Experiments of the EDFLL in Terms of the Saturation Frequency in the Bifurcation Diagram.	147
5.4	Quantitative analysis of the bifurcation results obtained for all four cavity-loss modulation experiments of the EDFRL in terms of resonance frequency peak.	157

5.5	Quantitative analysis of the bifurcation results obtained for all four cavity-loss modulation experiments of the EDFRL in terms of the saturation frequency in the bifurcation diagram.	157
-----	---	-----

LIST OF FIGURES

Figure		Page
2.1	(a) Schematic diagram of an optical fiber laser having a (a) linear cavity; (b) ring cavity (Liu, et al., 2022)	14
2.2	Illustration of the energy levels of the Erbium ions inside the EDFL system	16
2.3	Experimental configuration of the FPFL (Pua, et al., 2012a)	19
2.4	(a) Optical output of the FPFL after being subjected to vibration; (b) Arrangement of the piezoelectric source emanating acoustic waves to the SMF (Pua, et al., 2012b)	20
2.5	Optical output response of the EDFL after an impact indicating acoustic wave detection (Pua, Chong and Ahmad, 2013)	22
2.6	(a) Sensor configuration to locate the vibration source; (b) EDFL 1 and EDFL 2 output power measurements from the photodetector at 45 cm separation distance between both sensor fiber lengths (Pua, Chong and Ahmad, 2013)	23
2.7	(a) EDFL set-up; (b) Perimeter sensing EDFL sensor configuration (Woon, et al., 2017)	24
2.8	Experimental EDFRL set-up under pump modulation (Sola, Martin and Alvarez, 2002)	28
2.9	Figure 2.9: (a) Experimental pump-modulated EDFRL bifurcation diagrams for modulation index of (i) 0.05, (ii) 0.16, and (iii) 0.22; (b) theoretical pump-modulated EDFRL bifurcation diagrams for modulation index of (i) 0.22 (using Equation 2.3 and 2.5), (ii) 0.22 (using Equation 2.6 and 2.7), and (c) 0.22 (using a combination of both procedures) (Sola, Martin and Alvarez, 2002).	31
2.10	Experimental configuration of the EDFL subjected to pump modulation (Pisarchik, Barmenkov and Kir'yanov, 2003)	32

2.11	Bifurcation diagram of the pump-modulated EDFL where the fundamental laser frequency is indicated by dashed lines and the frequency locked is bounded by the dotted line (Pisarchik, Barmenkov and Kir'yanov, 2003)	33
2.12	Experimental setup of the EDFL (Pisarchik, Kir'yanov and Barmenkov, 2005)	34
2.13	(a) Experimental and (b) theoretical bifurcation diagram of the EDFL under pump modulation at 50 % modulation depth (Pisarchik, Kir'yanov and Barmenkov, 2005)	35
2.14	Experimental setup of the EDFL (Luo, Tee and Chu, 1998)	37
2.15	(a) Experimental; (b) Theoretical bifurcation diagrams of the EDFL indicating the presence of chaos, bifurcation and optical bistability (Luo, Tee and Chu, 1998)	39
2.16	Experimental set-up of the EDFL (Delgado, et al., 2022; Delgado, et al., 2023).	40
2.17	(a) Numerical, (b) Experimental bifurcation diagram of the pump-modulated EDFL (Delgado, et al., 2022; Delgado, et al., 2023)	41
2.18	Experimental configuration of the Erbium-doped fiber ring laser under loss modulation (Ghosh, Goswami and Vijaya, 2010)	43
2.19	Optical output variation with modulation frequency at 10 mV driving amplitude at four pump power values (left); Optical output variation with modulation frequency at 57.2 mW fixed pump power and other driving amplitudes of 10 mV, 50 mV, and 75 mV (right) (Ghosh and Vijaya, 2014)	45
2.20	Experimental set-up of the EDFL under loss modulation (Kumar and Vijaya, 2017a)	46
2.21	(a) Experimental bifurcation diagram obtained at a set modulation amplitude of $m = 0.0018$ (b) Theoretical bifurcation diagram at a set modulation amplitude of $m = 0.00022$. (Kumar and Vijaya, 2015a; Kumar and Vijaya, 2017a)	48

2.22	(a.) Experimental (b.) Theoretical non-linear responses of the loss-modulated EDFRL for a range of modulation indices when varying the modulation frequency (Kumar and Vijaya, 2015a)	48
3.1	Flow diagram of the methodology utilized in executing the research	54
3.2	Erbium-doped fiber linear laser (EDFLL) set-up for field test on the pipeline	55
3.3	Field test pipeline showing dimensions and different views of the pipeline setup	58
3.4	(a) Real photo of the test pipeline used for field experiments; (b) Illustration of the anticipated application of the EDFL for pipe leakage detection and location; (c) real photo of one EDFL sensor placed on the test pipeline; (d) close photo of the sensor showing its flexibility	59
3.5	Waveform of the signal from (a) sensor 1 placed on the pipeline with water flowing at a pressure of 1 bar (without leakage and with leakage) (b) sensors 1 and 2 placed 3 m apart on the pipeline with water flowing at a pressure of 2 bar.	62
3.6	Experimental configuration of the (a) EDFLL under pump modulation; (b) EDFLL under loss modulation	66
3.7	Experimental configuration of the (a) EDFRL under pump modulation; (b) EDFRL under loss modulation	67
3.8	Optical spectrum of the EDFLL	68
3.9	Optical spectrum of the EDFRL	71
3.10	Graph of the resonance frequency (ω_r) vs the laser pump power of the EDFRL (Onubogu, et al., 2020). (The two insets show the time domain of the laser output acquired at pump powers of 125.5 mW and 218.2 mW)	72
4.1	(a) Experimental (Onubogu, et al., 2019) and (b) theoretical (Onubogu, et al., 2022) bifurcation diagrams displaying the dynamical behaviors of the EDFLL1 when subjected to pump modulation at MA of 0.2 V and 7 kHz ω_r obtained by frequency variation from 1 kHz to 60 kHz and from 60 kHz to 1 kHz.	96

4.2	Time domain of the EDFLL1 sensor displaying its routes to chaos (Onubogu, et al., 2019).	98
4.3	(a) Experimental and (b) theoretical bifurcation diagrams describing the dynamic behaviors of the EDFLL2 subjected to pump modulation at MA of 0.4 V and 7 kHz ω_r gotten by frequency variation from 1 kHz to 60 kHz and from 60 kHz to 1 kHz (Onubogu, et al., 2022).	102
4.4	(a) Experimental and (b) theoretical bifurcation diagrams describing the EDFLL3's dynamic behaviors when subjected to pump modulation at MA of 0.1 V and 13 kHz ω_r gotten by frequency variation from 1 kHz to 60 kHz and from 60 kHz to 1 kHz (Onubogu, et al., 2022).	105
4.5	(a) Experimental and (b) theoretical bifurcation diagrams describing the EDFLL4's dynamic behaviors when subjected to pump modulation at MA of 0.4 V and 19 kHz ω_r gotten by frequency variation from 1 kHz to 45 kHz and from 45 kHz to 1 kHz (Onubogu, and Pua, 2022).	108
4.6	Time domain plots for some selected MFs of the pump-modulated EDFLL4 at MA of 0.4 V and 19 kHz ω_r (Onubogu and Pua, 2022).	110
4.7	(a) Experimental and (b) theoretical bifurcation diagrams displaying the EDFRL1's dynamic behaviors obtained by modulating the frequency from 1kHz MF to 30 kHz MF and from 30 kHz to 1 kHz at MA of 0.4 V and 2 kHz ω_r (Onubogu, et al., 2020; Onubogu, et al., 2022).	118
4.8	(a) Experimental (Onubogu, et al., 2020) and (b) theoretical (Onubogu, et al., 2022) bifurcation figures displaying the EDFRL2 dynamic behaviors obtained by modulating the frequency from 1kHz to 30 kHz MF and from 30 kHz to 1 kHz at MA of 0.4 V and 3 kHz ω_r .	125
4.9	(a) Experimental (Onubogu, et al., 2020) and (b) theoretical (Onubogu, et al., 2022) bifurcation diagrams displaying the EDFRL3 dynamic behaviors gotten via frequency variation from 1kHz to 30 kHz MF and from 30 kHz to 1 kHz at 0.4 V MA and 5 kHz ω_r (c) Time domain (left) and frequency domain (right) gotten during experimental pump modulation.	127

4.10	(a) Experimental (Onubogu, et al., 2020) and (b) theoretical (Onubogu, et al., 2022) bifurcation figures displaying the dynamic behaviors of the EDFRL4 gotten by frequency variation from 1kHz MF to 30 kHz MF and vice versa at MA of 0.4 V and 7 kHz ω_r (c) Time domain (left) and frequency domain (right) obtained during experimental pump modulation.	130
4.11	(a) Experimental (Onubogu, et al., 2020) and (b) theoretical (Onubogu, et al., 2022) bifurcation figures displaying the dynamic behaviors of the EDFRL5 gotten by modulating the frequency from 1kHz to 30 kHz MF and vice versa at MA of 0.4 V and 10 kHz ω_r (c) Time domain (left) and frequency domain (right) obtained during experimental pump modulation.	133
4.12	(a) Experimental and (b) theoretical bifurcation figures displaying the dynamic behaviors of the EDFRL6 obtained by modulating the frequency from 1kHz to 60 kHz MF and from 60 kHz to 1 kHz at MA of 0.4 V and 10 kHz ω_r	137
4.13	Dynamic behavior of the EDFRL subjected to amplitude modulation ranging from 400 mV to 5000 mV MA at 2 kHz MF and 2 kHz ω_r ; 3 kHz MF and 3 kHz ω_r ; 5 kHz MF and 5 kHz ω_r ; 7 kHz MF and 7 kHz ω_r , and 10 kHz MF and 10 kHz ω_r respectively (Onubogu, et al., 2019)	140
5.1	(a) Experimental and (b) Theoretical bifurcation diagrams obtained at a fixed MA of 800 mV displaying the dynamic behavior of the EDFLL subjected to external cavity-loss modulation gotten by sweeping the loudspeakers' frequency ranging from 1kHz to 20 kHz and back again for ω_r values of (4, 8, 10 and 16) kHz.	149
5.2	Bifurcation diagram obtained at a fixed ω_r of 14 kHz displaying the EDFRL's reaction to external loss modulation gotten by variation of the loudspeaker's frequency from 1 kHz to 20 kHz for MA of (a) 200 mV (experimental result); (b) 500 mV (experimental result); (c) 900 mV (experimental result); (d) 1000 mV (experimental result); (e) 200 mV (theoretical result) and (f) 500 mV, 900 mV, and 1000 mV (theoretical results). (Onubogu, Pua and Faidz, 2021)	159
5.3	(a) Time domain response obtained from experimental loss modulated EDFRL with 14 kHz ω_r and 200 mV MA at (7, 14, and 20) kHz MF; (b) Corresponding	164

frequency domain responses (Onubogu, Pua and Faidz, 2021)

- | | | |
|-----|---|-----|
| 5.4 | (a) Time domain response obtained from experimental loss modulated EDFRL with 14 kHz ω_r and 500 mV MA at (3, 7, 14, and 18) kHz MF; (b) Corresponding frequency domain response (Onubogu, Pua and Faidz, 2021) (c) Theoretical time domain response (d) Theoretical frequency domain response | 166 |
| 5.5 | (a) Time domain response obtained from experimental loss modulated EDFRL with 14 kHz ω_r and 900 mV MA at MF of 3 kHz; 6.8 kHz; 10 kHz and 13.6 kHz; (b) Corresponding frequency domain (Onubogu, Pua and Faidz, 2021) | 168 |
| 5.6 | (a) Time domain response obtained from experimental loss modulated EDFRL with 14 kHz ω_r and 1000 mV MA at (1, 2, 6.7 and 13.5) kHz MF; (b) Corresponding frequency domain (Onubogu, Pua and Faidz, 2021) | 170 |

LIST OF ABBREVIATIONS

AE	Acoustic emission
ASE	Amplified spontaneous emission
EDF	Erbium-doped fiber
EDFL	Erbium-doped fiber laser
EDFLL	Erbium-doped fiber linear laser
EDFRL	Erbium-doped fiber ring laser
ESA	Excited state absorption
FBG	Fiber Bragg Grating
FPFL	Fabry-Perot fiber laser
MA	Modulation amplitude
MF	Modulation frequency
MZM	Mach–Zehnder modulator (MZM)
NA	Numerical Aperture
OB	Optical bi-stability
OSA	Optical Spectrum Analyzer
ω_r	Resonance frequency
ω_{ro}	Relaxation Oscillation Frequency
SHM	Structural health monitoring
SMF	Single Mode Fiber
WDM	Wavelength Division Multiplexer

LIST OF PUBLICATIONS

The findings from this research have led to the publication of several papers in peer-reviewed international journals and some conference proceedings as shown below:

Appendix	Paper authors, title and doi	Journal/Conference	Year published	Impact Factor
B	<p>N.O. Onubogu, C.H. Pua, H.S. Lin, A. Faidz, The dynamic behavior of non-polarized erbium-doped fiber ring laser under experimental pump modulation.</p> <p>https://doi.org/10.1016/j.ijleo.2020.164442</p>	Optik	2020	2.443
C	<p>N.O. Onubogu, C.H. Pua, A. Faidz, Dynamic features of a non-polarized Erbium-doped fiber ring laser subjected to external cavity-loss modulation.</p> <p>https://doi.org/10.1016/j.ijleo.2020.165846</p>	Optik	2021	2.443
D	<p>N.O. Onubogu, C.H. Pua, A. Faidz, W.C. Rose, Numerical analysis of the behavioral response of pump-modulated linear and ring erbium-doped fiber lasers.</p> <p>https://doi.org/10.1016/j.ijleo.2022.169519</p>	Optik	2022	2.443

- E** **N.O. Onubogu, C.H. Pua, H.S. Lin, A. Faidz, Dynamics of a highly sensitive erbium-doped Fabry-Perot fiber (EDFPF) laser sensor under pump modulation.** 24th Microoptics Conference (MOC); IEEE Xplore 2019
- doi:10.23919/MOC46630.2019.8982878
- F** **N.O. Onubogu, C.H. Pua, Dynamic behavior of a pump-modulated erbium-doped fiber linear laser with single fiber Bragg grating.** In A. Sivasubramanian, P.N. Shastry, P.C. Hong (Eds.), Futuristic Communication and Network Technologies, Lecture Notes in Electrical Engineering, vol 792, Springer, Singapore 2022
- https://doi.org/10.1007/978-981-16-4625-6_28.

CHAPTER 1

INTRODUCTION

1.1 Research Background

Structures such as ships, airplanes, bridges, and buildings, including water, oil, or gas pipelines will undergo deformation due to the large distortion of their structural components over time. Apart from that, these structures also go through constant changes triggered by environmental influence, aging processes, and possible unpredicted natural disasters such as earthquakes. Hence, it is of great importance to develop a structural health monitoring (SHM) system to observe these structures throughout their lifetime for signs of deformation and also measure the seriousness of the deformation of these structural components in real time.

1.1.1 Conventional methods of SHM

Various conventional methods of SHM have been explored in the past such as vision-based systems (Canavese, et al., 2015), electro-mechanical impedance (Moura and Steffen, 2005), comparative vacuum monitoring (Roach, 2018), acoustic emission (AE) detection (Paget, Atherton and O'Brien, 2004; Liu, et al., 2015) and others. Each of these technologies has its features, merits, and demerits. Also, these methods have preferred applications; so, they are not versatile. AE detection is a very common method that is widely

used. It is achieved by using piezoelectric-based sensors made of solid ceramic material which obstructs the contact area between the structures and the sensors. This limits the coverage and sensitivity for large or long structures such as pipelines. For these large or long structures, numerous sensors are required which makes the acoustic emission method very expensive and not practical.

1.1.2 Fiber Optics Technologies for SHM

To solve the problem of AE sensors, fiber optics technologies for SHM emerged many years ago and have become a popular sensing technology with many applications due to their vital advantages such as high sensitivity, low maintenance cost, simplicity, applicability in harsh environments, immunity to electromagnetic waves, etc. (Allwood, Hinckley and Wild, 2012; Fu, Chen and Cai, 2012). Optical fiber sensing technology development has reached a point where its impact is evident and has been applied in various fields of science and technology successfully. Fiber optic cables are long. Therefore, they can be installed in structures as distributed sensors over long distances to sense deformations by measuring either strain or temperature, dynamic magnetic fields, and even vibrations in the structure.

Four popular optical fiber-based methods that have been used in the past to detect or measure acoustic waves or vibration are Fiber Bragg Grating (FBG) distributed sensing method; Raman scattering optical fiber sensing method, the Brillouin scattering optical fiber sensing method, and the Rayleigh

scattering optical fiber sensing method. For the FBG sensing method, the central wavelength of the FBG fluctuates with respect to the variation of the parameters (strain, temperature, pressure, etc.) experienced by the fiber and the corresponding wavelength shifts (Rao, 1997). To measure acoustic signals using FBG, strain is applied to the measurand (Hinckley and Wild, 2010). Brillouin optical fiber sensing method measures the distribution of strain and temperature from one end of the optical fiber to the other. For long distances, it can also attain a high spatial resolution meaning that more detailed information can be obtained. One important merit of the Raman optical fiber sensing method is that it can monitor temperature distribution on a large scale. In comparison to the Brillouin optical fiber sensing method, the Raman optical fiber sensing method is unresponsive to strain. Hence, it does not provide information on the cross-sensitivity of strain and temperature. On the other hand, Rayleigh optical fiber sensing method is generally used to sense the acoustic vibrations and attenuation characteristics of the optical fiber (Zhang and Li, 2022). One key benefit of this sensing method is that it is very efficient leading to higher signal-to-noise ratio (SNR) measurements. As a result, it is possible to acquire long-range measurements with higher spatial resolution and high measurement rates. This is in contrast with Raman and Brillouin scattering methods which usually have low SNR leading to prolonged measurement times (Palmieri, et al., 2022).

Research projects where the aforementioned optical fiber sensing methods have been successfully employed include perimeter sensing (Bush, et al., 1999; Wooler and Crickmore, 2005; Kumagai, Sato and Nakamura, 2012;

Wu, et al., 2013; Catalano, et al., 2014; Lu, et al., 2019; Violakis, et al., 2020); pipeline leakage sensing (Yan, Shi-jiu and Zhi-gang, 2006; Yan and Chyan, 2010; Rajeev, et al., 2013; Frings and Walk, 2010; Fu, Wan and Qiu, 2010; Inaudi and Glisic, 2010; Fu, et al., 2020); building SHM (Wu, Peng and Xu, 2010, Pendão and Silva, 2022., Li and Zhang, 2022; Galindez-Jamioy and López-Higuera, 2012, Hi and Liu, 2021; Gorshkov et al., 2022), etc., However, the general problem with the FBG method, Raman, and Brillouin scattering methods is that they involve monitoring of wavelength scattering. This generally requires a complicated set-up including expensive instruments such as interrogators, and their response time is comparatively slow. Rayleigh optical fiber sensing method is not commonly applied in sensing because, in mostly single-mode fibers, the light frequency of Rayleigh scattering is equivalent to that of the incident light and extremely weak (Pendão and Silva, 2022).

In contrast, fiber laser dynamics behavior-based sensors involve monitoring of optical power fluctuation where the fluctuation ranges from 100 Hz to 100 kHz operating bandwidth with a high sensitivity of about -60 dBA (Pua, et al., 2012a). The optical fibers are very flexible to be bent into any shape as they possess an extremely small diameter of about 80 μm . Also, the photodetector used in the sensor can reach up to a maximum speed of approximately 20 GHz. Since the dynamic behavior of the laser is sensed as a great optical intensity fluctuation, the only instruments required in the monitoring system are a laser source, a conventional photodetector, and a digital oscilloscope. This makes the system very simple and cost-effective. The

full capability of optical fiber sensing technology is not yet fully developed, especially in the area of optical fiber laser dynamics behavior-based sensors.

In this research project, the fiber laser dynamics behavior-based sensor, specifically the erbium-doped fiber laser sensor is proposed for pipe leakage monitoring to detect both leakage and the location of the leakage. Pipeline leak incidents occurring around the world have revealed that the damages caused can endanger human lives and lead to additional downtime and clean-up expenses for the companies involved. Hence, an economical, highly sensitive, and reliable pipeline leak detection system is seriously in demand. Erbium-doped fiber is the best option for constructing a laser as a result of its ability to aid the build-up and magnification of small optical pulses in the C-band region. Erbium-doped fiber laser (EDFL) is called a class B laser for two reasons. Firstly, its polarization may be eliminated in the absence of heat transfer. Secondly, its dynamics are mainly governed by rate equations for field and population inversion (Pisarchik, Barmenkov and Kir'yanov, 2003). EDFLs have numerous advantages over other fiber lasers that have led to an increase in their popularity in areas such as medicine (Moren et al., 2009; Gursel, 2018), long-distance secure optical communication (Thalangunam, 2015; Ke, et al., 2018), industrial processes (Selleri and Poli, 2008; Kraus et al., 2010), LIDAR technology (Sharma, Kim and Kang, 2004; Philippov and Codemard, 2004), sensing (Ronghua, Hangtao and Liya, 2018; Wu, Okabe and Sun, 2014), spectral interferometry (Keren and Horowitz, 2001), etc. These advantages consist of their simplicity, flexibility, resistance to electromagnetic interference, extreme resistance to heavy environments, single-mode

operation, wide tuning range, and elongated length of the fiber to allow more interaction between the active erbium ions and the pumped laser light leading to high gain, etc. (Digonnet, 2001). This implies that an EDFL dynamics behavior-based sensor could have all these advantages and most importantly EDFLs are very economical and easy to manufacture and also compact, making them applicable in hand-held sensors (Sharma, Kim and Kang, 2004).

In this research, the proposed EDFL sensor was designed and successfully tested on a real water pipeline by directly placing the sensor on the surface of the pipe to detect and locate a leakage. However, some intensity fluctuation instabilities due to the chaotic condition present in the sensor were observed that needed further study. This is the research gap that led to further research and analysis to determine the cause of the instabilities for improvement of the sensor in the future. Therefore, the EDFL was experimentally and theoretically pump-modulated and loss-modulated respectively to trigger its laser dynamics and study its behavior. Pump modulation is a direct way to regulate the intensity of the optical fiber laser using a pump laser diode. Loss modulation is achieved by directly using acoustic waves in the form of mechanical vibration (external cavity loss modulation). During loss modulation, chaotic features can be easily generated at low modulation amplitudes compared to pump modulation where large modulation amplitudes are needed to display chaotic features.

Most of the existing studies on EDFL pump and loss modulations (Sola et al., 2002; Pisarchik, Barmenkov and Kir'yanov, 2003; Pisarchik et al., 2005;

Reategui et al., 2004., etc.) developed a theoretical model to describe the laser dynamics of their EDFL configuration. The theoretical model predicted their experimental results accurately. The EDFL configuration in this research is different from those studied by other authors and their theoretical models cannot exactly describe the laser dynamics of the EDFL here. Therefore, a modified theoretical model (closely related to that of Pisarchik et al., (2005)) that considers the resonance frequency of the EDFL at a particular time is presented. This is crucial for the characterization of the EDFL's sensitivity to acoustic waves, which can help in designing an improved and more efficient EDFL sensor. The model can envisage the bifurcations including linear and chaotic behaviors exhibited under certain pump and loss modulation input conditions. It is important to highlight that during loss modulation, the bifurcation of the EDFL configuration was modeled when the EDFL is externally modulated by acoustic waves between 1 kHz to 20 kHz frequency to emulate vibrations from a pipeline leakage. This is one of the novelties of this research. External cavity-loss modulation by acoustic waves was the chosen method of modulation to emulate the vibrations emanating from the leakage of a water pipeline at ground level as this is the main proposed application of the EDFL sensor. The significant contribution of this study is the modified theoretical model which can be used to quickly predict the output of the sensor for further improvement in the future.

1.2 Problem Statement

Deformation occurs over time in structures. Hence, SHM is essential to monitor the condition of these structures at every moment in their lifetime. The structures that are of concern in this research are pipelines which can have leakages many times in their lifetime due to metal corrosion, metal failure, excavation operations, pipeline vandalism, etc. Pipeline leakage can endanger human lives and lead to additional downtime and clean-up expenses for the companies involved. Therefore, there is a demand for economical and reliable pipeline leak detection systems. Several methods including optical fiber-based methods exist for sensing or detection purposes. However, most of them are not economical, effective, and always reliable for sensing in mainly big or long structures such as pipelines. This is the first motivation for this study, to design an economical optical fiber-based sensor that can detect pipeline leakage and also the location of the leakage.

A few UTAR researchers have designed similar EDFL sensors for various purposes. Pua, et al., (2012a) and Pua, Chong and Ahmad, (2013) designed an EDFL sensor that could instantaneously sense acoustic waves. Woon, et al. (2017), designed an EDFL sensor for perimeter sensing that could detect physical intrusion. Woon et al., (2018) designed another EDFL sensor for pipeline leak monitoring of a small water circulation system in the lab. In all these studies, some instabilities related to intensity fluctuations were observed in the sensor and the cause of this is unknown. It is presumed that the bifurcation occurring in the EDFL is the major cause of the instabilities

observed. It is important to confirm how true this presumption is by understanding the dynamic behavior of the EDFL sensor. This is the second motivation for this study.

To understand the behavior of the EDFL sensor, it is necessary to carry out experimental and theoretical analysis to see if the bifurcation happening in the EDFL as experienced by other researchers is the root cause of the instabilities. Understanding the cause of the instabilities and how to control them can aid in the improvement of the sensor in the future. To trigger bifurcation and the chaotic condition of the EDFL, the EDFL would have to be subjected to experimental pump and loss modulations. It is also important to theoretically model the bifurcations of the EDFL under pump and loss modulations for quicker and easier analysis of the sensor behavior.

1.3 Research Questions

From the problem statement, three questions arose which are as follows:

1. Can an EDFL-based sensor be used as a highly sensitive (≤ -60 dBA) and effective sensor in pipe leakage monitoring?
2. Do bifurcations occur in the linear and ring EDFLs under pump and external cavity-loss modulations?
3. Can the bifurcations of the EDFLs under pump and loss modulations be theoretically modeled using basic rate equations?

1.4 Research Objectives

To solve the above-mentioned problems in the problem statement, this research aims to design a highly sensitive EDFL-based sensor for pipe leakage monitoring and to experimentally and theoretically study the dynamic behavior of the sensor in response to acoustic vibrations so as to find out the cause of the instabilities observed in the sensor. To achieve this aim, the objectives of this research include:

1. to design an erbium-doped fiber laser (EDFL) sensor and test its effectiveness in pipeline leakage monitoring.
2. to experimentally study the behavior of the erbium-doped fiber linear laser (EDFLL) and the erbium-doped fiber ring laser (EDFRL) to confirm whether bifurcations occur during pump modulation and external loss modulation.
3. to develop an improved theoretical model of the EDFLL and the EDFRL based on rate equations to quickly simulate the laser output (bifurcation) with pump modulation and external loss modulation.

1.5 Thesis Outline

This thesis is organized into six chapters. The content of each chapter is described below:

- Chapter 1 consists of the introduction to the research and the motivation behind it. It also covers the problem under study, the research questions, the aims or objectives of the research, and the outline of the thesis.
- Chapter 2 explains the working principle of the EDFL, followed by a review of existing literature on the use of EDFL for the detection of acoustic waves; followed by a review of some literature on the laser dynamics (bifurcation, chaotic condition, optical bistability, etc.) of the EDFL triggered by pump and loss modulations.
- Chapter 3 is the methodology in which all the methods used to achieve the main aim of this study are presented. Areas covered comprise the design of the EDFL sensor used for field test on a water pipeline to detect leakage and the location of the leak; a breakdown of the analysis to be performed to understand the sensor's behavior; description of the experimental configurations of the EDFLL and EDFRL and their working principle when used for sensing; description of the pump and external cavity-loss modulations to be carried out experimentally on the EDFLL and EDFRL respectively; the derivation of the equations used for theoretical pump and loss modulations and all parameters used in the calculations.
- Chapter 4 is the first results and discussion section that explains in detail the results gotten from pump modulating the EDFLL and

EDFRL experimentally and theoretically. It also discusses the dynamic behaviors observed.

- Chapter 5 is the second results and discussion section which presents in detail the results gotten from the experimental and theoretical external cavity loss modulation of the EDFLL and EDFRL and discusses the dynamic behaviors observed.
- Chapter 6 is the conclusion and future works section which highlights the main findings of the research and a summary of the entire research outcome, significance and application of the research, and future works/further studies to be carried out to improve the EDFL sensor.

CHAPTER 2

LITERATURE REVIEW

2.1 Introduction

This chapter consists of the fundamental concept and working principle of the EDFL; a review of the literature on the use of EDFL for acoustic wave detection and a review of the laser dynamics of pump-modulated and loss-modulated EDFL. A table showing a summary of the reviewed literature on pump-modulated and loss-modulated EDFLs is presented at the end of their respective sections.

2.1 Erbium-Doped Fiber Laser (EDFL) and its Working Principle

Generally, a fiber laser comprises a pump source, a laser resonator or cavity, and an amplification medium doped with rare earth elements. An EDFL can be described as a fiber laser having a gain medium doped with erbium ions (Pua, Chong and Ahmad, 2013). The EDFL system is a class B three-level laser system having a degree of polarization decay of 10^{11} s^{-1} . However, the degree of decay of the population from the level of lasing is 10^2 s^{-1} while that of the lasing field is 10^7 s^{-1} . Since the degree of polarization decay is significantly higher compared to the polarization decay of its population inversion and its lasing field (Reátegui, 2004), the polarization variable is insignificant (Luo, Tee and Chu, 1998; Luo and Chu, 1998).

A typical EDFL setup consists of a 980 nm or 1480 nm pump source, 980/1550 nm wavelength division multiplexer (WDM), and an erbium-doped fibre (EDF). The pump source generates the seed light which enters the EDF via the WDM to generate stimulated emission (Liu et al., 2022). EDFL supports laser generation and amplification around the 1550 nm region. EDFLs are typically realized in either linear/Fabry-Perot/standing-wave resonator or ring/traveling wave resonator configurations as shown in Figure 2.1.

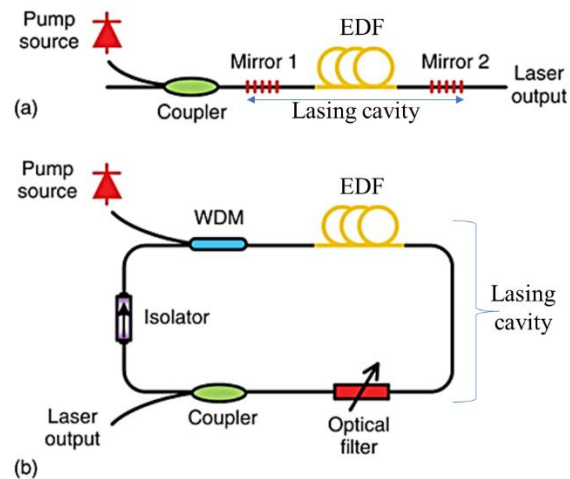


Figure 2.1(a) Schematic diagram of an optical fiber laser having a (a) linear cavity; (b) ring cavity (Liu, et al., 2022)

The linear resonator consists of mirrors having different reflectivity at both ends of the EDF (Liu, et al., 2022). These mirrors can be FBGs or flatly cleaved fiber ends that can send feedback to the laser system via Fresnel reflection. In this kind of resonator, light bounces back and forth between the two end mirrors so the laser will go through an amplification process every time. After the amplified light reaches mirror 2 as shown in Figure 2.1, most

of the amplified light is reflected to the EDF where stimulated emission amplification occurs again. Mirror 1 has a higher reflectivity compared to mirror 2 such that the light is reflected and magnified again. This process continues until the intensity of the light attains the laser oscillation threshold. At this point, a little portion of the laser is collected via mirror 2 while about 95 % of the light is reflected for continuous light amplification (Liu, et al., 2022).

In the ring resonator, light waves travel one round trip in two opposite directions of the closed fiber ends of the resonator. In this way, multiple amplification and laser oscillation are possible. To obtain precise wavelength, an optical filter is sometimes inserted into the resonator. For the unidirectional operation of the light waves in the ring, an isolator is usually inserted into the resonator (Liu, et al., 2022).

The generation of EDFL can be described with a three-level model. Figure 2.2 illustrates the energy levels of the Erbium ions inside the EDFL.

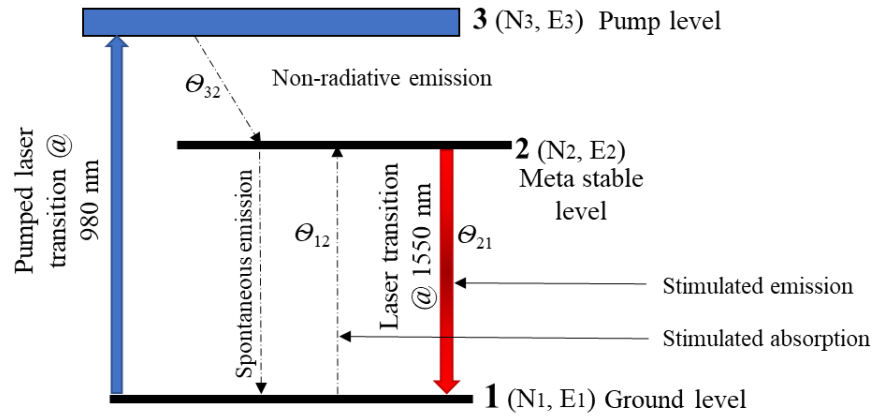


Figure 2.2: Illustration of the energy levels of the Erbium ions inside the EDFL system

In a three-level EDFL system, the number of electrons in energy level 2 (N_2) must be greater than the number of electrons within energy level 1 (N_1) to achieve population inversion. This is required for lasing to occur. The number of electrons in energy level 1 (N_1) is always greater than the number of electrons in energy level 3 (N_3) as electrons decay to E_2 right after reaching E_3 . Immediately after the 980 nm laser pump is switched on, the 980 nm photons get absorbed by the electrons at level 1. The electrons will then get excited to an upper energy level, E_3 . The lifespan of the electrons at E_3 is very brief. Therefore, the electrons drop almost instantly to level E_2 via non-radiative emission (Θ_{32}). The lifespan of level 2 electrons is prolonged compared to that of level 3 electrons instigating the accumulation of a great number of electrons at level 2 compared to level 3 and level 1. When this happens, population inversion is said to have occurred which gives rise to laser generation. After the lifespan of the electrons at level 2 is finished, they fall to level 1 releasing a photon via spontaneous emission (Θ_{21}). The released photon reacts with the other electrons at level 2. This stimulates another electron to

descend to level 1 and emit another coherent photon by stimulated emission. With continuous pumping of the laser medium, the process continues and more and more coherent photons will be released.

When the pump power is low, the lasing condition becomes unstable leading to continuous sudden jumps of optical frequency related to transitions between different resonator modes. This is exactly what happens when the EDFL system is exposed to external disturbances such as vibrations.

The intracavity laser output power (P) and population inversion (N) at level 2 are governed by two rate equations (Pisarchik, et al., 2005).

$$\frac{dP}{dt} = \frac{2L}{T_r} P \{ r_w \alpha_0 [N(\xi_1 - \xi_2) - 1] - \alpha_{th} \} + P_{sp} \quad (2.1)$$

$$\frac{dN}{dt} = -\frac{\sigma_{12} \Gamma_s r_w P}{\pi r_0^2} (N \xi_1 - 1) - \frac{N}{\tau} + P_{pump} \quad (2.2)$$

Where the symbols in the equations are as defined in Table 2.1.

Table 2.1: Symbols from the rate equations and their definition

Symbol	Definition
N	The population of upper laser level 2
L	The length of the fiber
T_r	The time taken for the photon to travel around the resonator
P_{pump}	The laser pump power
P_{sp}	The spontaneous emission of photons into the fundamental laser mode
r_w	The factor representing a match between the fundamental laser mode and core volumes inside the erbium-doped fiber
τ	The life span of erbium ions existing in the excited state
σ_{12}	The cross-section of the return stimulated transition from the ground state to the excited state

α_0	The signal absorption of the erbium fiber at the lasing wavelength
Γ_s	The factor representing the EDFL radiation
r_o	The radius of the core of the EDF
α_{th}	Intra-cavity threshold loss
ξ_1 and ξ_2	Coefficients signifying the ratio between the excited state absorption and ground state absorption cross-sections at the laser wavelength

The losses (α_{th} , α_0 and r_w) are the main parameters equivalent to the resonator loss due to external modulation. When the EDFL is subjected to external modulation such as vibration from the leakage in a pipeline, it leads to losses in the laser resonator since the photon emission is suppressed and a large pulsing effect is seen. When this happens, the non-linear dynamic behavior of the EDFL is activated. The proposed EDFL sensor in this thesis makes use of this dynamic behavior for pipeline leakage monitoring and detection. Therefore, a review of the literature on the application of the EDFL for sensing is necessary.

Four major research studies on the use of the EDFL for sensing have been carried out which confirm its practicability in the detection of acoustic waves. The four of them are discussed in Chapter 2.1.

2.1 Erbium-Doped Fiber Laser Dynamic Behaviour for Sensing

A linear laser set-up called a Fabry-Perot fiber laser (FPFL) was proposed as an acoustic sensing medium in the absence of a diaphragm as a transducer (Pua, et al., 2012a). The FPFL setup is very simple, flexible, and

compact, consisting of only a 980 nm laser diode pump, a 980/1500 nm wavelength division multiplexer (WDM) coupler, and a 3 m EDF of 80 μm clad as illustrated in Figure 2.3.

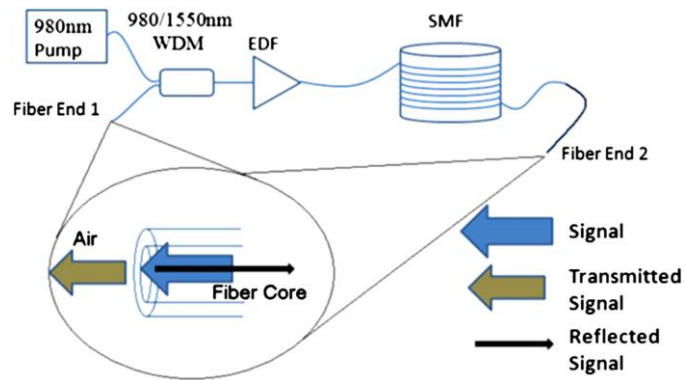


Figure 2.3: Experimental configuration of the FPFL (Pua, et al., 2012a)

A special single-mode fiber (SMF) of 10 m length is connected to the EDF to achieve high sensitivity. To create a strong interaction between the surface of the SMF and the acoustic waves, the SMF was wound around the center rim of a compact disc holder forming a very flat circular shape. The 20 m linear resonator was formed by Fresnel reflection (approximately 4 %) from the cleaved ends of the fiber which are exposed to air as shown in Figure 2.3. The optical output power was measured with the help of an oscilloscope and photodetector. It was observed that under pump power of 17.5 mW, the output power fluctuation (photo-detector voltage) of less than 22.5 mW is 7 % of the 320 mV average output power. Also, a bulk noise spectral peak was observed at about 27 kHz and recognized as the resonance frequency of the system. A test was carried out to observe the output optical power when there is an impact on the FPFL. The FPFL was placed on a flat table while a 253 gm metal piece was dropped from 1 cm height above the same table. An immediate

drop in output power was observed immediately after the impact Figure 2.4 (a). This is as a result of cavity loss and destructive interference in the resonator leading to pulse generation (Pua, et al., 2012b).

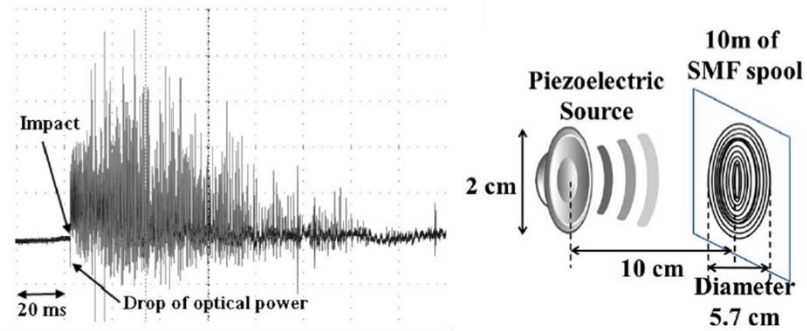


Figure 2.4: (a) Optical output of the FPFL after being subjected to vibration; (b) Arrangement of the piezoelectric source emanating acoustic waves to the SMF (Pua, et al., 2012b)

The response of the FPFL to acoustic waves was then tested in a free-running condition creating an unstable laser condition. Single-tone acoustic waves were generated as shown in Figure 2.4 (b) to observe their direct interaction with the FPFL. Results of the experiment showed that the interaction of the FPFL with the acoustic waves gave rise to a generation of pulses (seen as multiple longitudinal modes via an optical spectrum analyzer (OSA)) by the FPFL symbolizing its response to acoustic waves and vibrations. The tunability of the resonant frequency of the FPFL system from 5 kHz – 85 kHz allowed acoustic wave detection ranging from 100 Hz – 100 kHz frequency. Resonant frequency tuning was achieved by tuning the pump power from as low as 10 – 68.5 mW. In conclusion, it was proven that the FPFL is capable of detecting airborne acoustic waves or vibrations

implying that it can be used for small and large-area sensing with “unlimited” sensing points (Pua, et al., 2012b).

Pua, Chong and Ahmad, 2013 further demonstrated the possibility of using the laser dynamics behavior of the EDFL to sense acoustic waves for wide-area intrusion sensing. The EDFL setup is similar to that of Pua, et al., 2012a except that the lengths of the EDF and the SMF are 5 m and 25 km respectively. They utilized the laser transient effect induced by acoustic waves to design the EDFL intrusion sensor.

The output response of the EDFL sensor after an induced impact was demonstrated. It was observed that before the impact is induced, the laser output power is stable. After the impact, the optical output power fluctuated until large power spikes were generated rapidly as illustrated in Figure 2.5. After some time, a stable state was again observed. It was also confirmed that with a larger acoustic energy, the EDFL sensor takes a longer time to recover but eventually returns to a steady state.

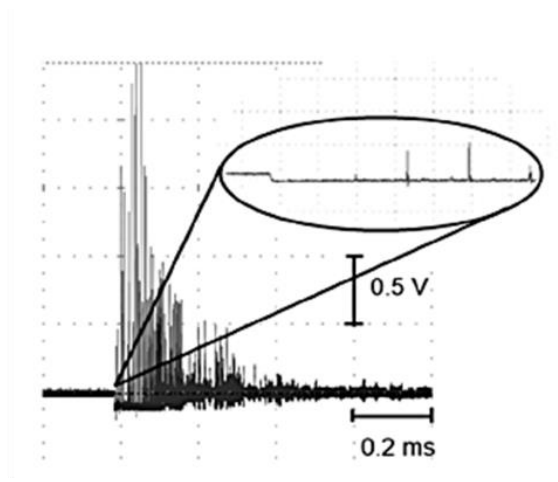


Figure 2.5: Optical output response of the EDFL after an impact indicating acoustic wave detection (Pua, Chong and Ahmad, 2013)

An experiment to test the application of the EDFL sensor for sensing was carried out, where 5 m of the SMF was pulled out of the spool and stuck on the floor. Acoustic energy of different intensities was induced by dropping a metal of 100 g weight from various heights at a 10 cm distance away from the EDF. It was noticed that the higher the height from which the metal is dropped, the stronger the vibration energy. From this experiment, it was confirmed that the EDFL intrusion sensor quickly responded to vibration activities around it (Pua, Chong and Ahmad, 2013).

Another experiment was carried out to test the sensors' capability to pinpoint the acoustic wave location. Two independent EDFL sensors were constructed such that a part of their fiber length was firmly positioned side by side with a distance separating them. A vibration source is placed near the sensors as displayed in Figure 2.6. For various distances between the two sensors, the difference in the time at which the acoustic wave is detected

simultaneously by both sensors was calculated for the estimation of the location of the vibration. In Figure 2.6 (a), the vibration source (a metal piece of block dropped from a height to the ground) was placed 45 cm away from the 1st sensor (EDFL1). The results of the experiments showed that two fluctuation packets appeared on the EDFL2 signal as a result of the second effect of the metal block piece bouncing on the floor. Secondly, one fluctuation packet appeared on the EDFL1 signal as illustrated in Figure 2.6 (b) because it was nearer to the impact location compared to EDFL 2, thus experiencing a larger vibration (Pua, Chong and Ahmad, 2013).

Also, an obvious delay in time was observed between the responses of both EDFLs, and different amplitude fluctuations were observed for both EDFLs. A few drawbacks were identified in their sensor design, however; the EDFL sensor gives a good foundation for intrusion sensor development reliant on the laser dynamic behavior.

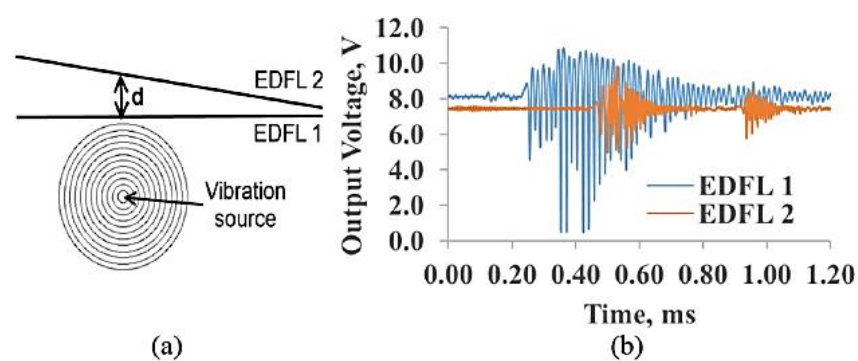


Figure 2.6 (a) Sensor configuration to locate the vibration source; (b) EDFL 1 and EDFL 2 output power measurements from the photodetector at 45 cm separation distance between both sensor fiber lengths (Pua, Chong and Ahmad, 2013)

In another study, a cost-effective and simple acoustic EDFL sensor having linear configuration showed its capability in detecting and responding to external perturbations (such as acoustic waves) instantaneously while being implemented for perimeter sensing for physical intrusion detection (Woon, et al., 2017). Similar to Pua, et al., 2012a; the EDFL set-up consists of a laser pump source with 980 nm wavelength and a 980/1550 nm WDM coupler which is connected to the EDF as the gain medium. For maximum reflection, the fiber ends have a 90 degrees cleaved angle and a reflectivity of about 4 %. A 10 m length SMF is connected to point B of the EDFL set-up in Figure 2.7 as a sensing medium for zone identification purposes as it will be placed around an area as a perimeter sensor.

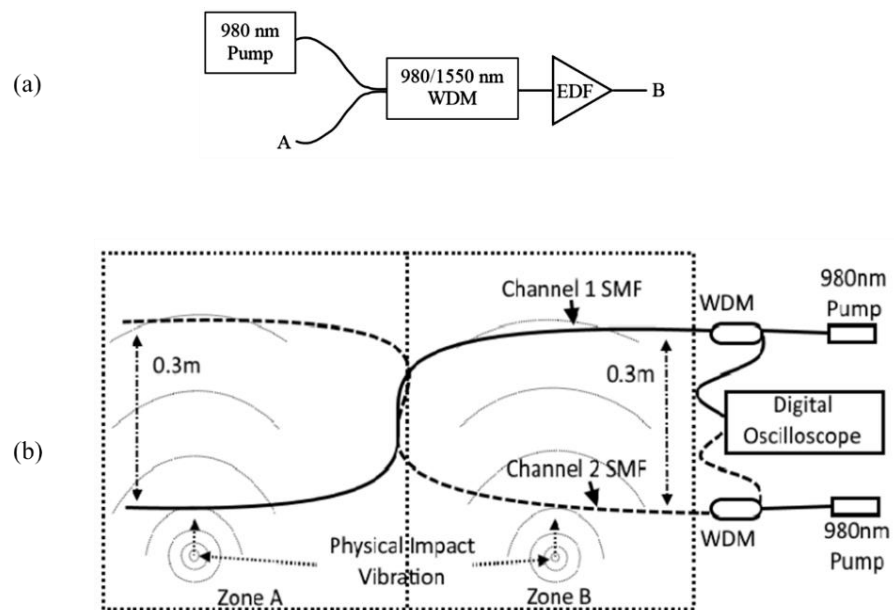


Figure 2.7 (a) EDFL set-up; (b) Perimeter sensing EDFL sensor configuration (Woon, et al., 2017)

The capability of the sensor to identify intrusion location was demonstrated with the use of two identical EDFL sensors (inclusive of the 10 m SMF as the sensing element) separated by a distance of 0.3 m. The fibers are interchanged from zone A to zone B as illustrated in Figure 2.7 so that the zones can be distinguished. To observe the optical output changes, an impact was generated by releasing a metal block piece from a height of 2 cm at a 5 cm distance away from one of the sensor channels and 35 cm away from the second sensor channel. This experiment was repeated 10 times with various distances between both sensors and metal drop heights. It was noticed that the nearer the sensor is to the acoustic source, the more the fluctuation of the amplitude of optical output power and vice versa. The EDFL sensor sensing technique is by loss modulation whereby loss occurs in the laser cavity if there is an acoustic impact on the sensor (Pua, Chong and Ahmad, 2013). Outputs of both sensors were measured from photo-detectors connected to each sensor from which zone sensing was achieved by calculating the delay in the detection of acoustic waves between sensors 1 and 2.

Furthermore, Woon, et al., 2018 designed a low-cost and highly sensitive EDFL sensor (a similar set-up to Woon, et al., 2017) for pipeline leak monitoring. The experimental set-up consisted of a small water circulation system having mainly a tank and a hose made of Polyvinyl chloride (PVC) to guide water to and from the tank. To simulate leakage conditions, a hole was drilled at the center of a 3 m length water pipe. For non-leakage conditions, the hole was closed with the help of a bolt screwed through the hole. The first experiment carried out was to detect leak and no-leak conditions using the

EDFL. When a leak was detected, high-amplitude sharp peaks were observed confirming the presence of a leak. The opposite was the case for the no-leak condition. To detect the location of a leak, two similar EDFL sensors were positioned on top of the pipe before and after the leakage hole. By calculating the difference in the time when the signal got to both sensors, the leak location was found for all experiments carried out (at 10 kPa and 20 kPa water pressures) with an error of 4.6 % (Woon, et al., 2018).

In all these studies, the 4 % Fresnel reflection of the linear laser gave low feedback that created the unstable lasing condition of the EDFL to effortlessly trigger its laser dynamics. In the laser dynamics behavior of the EDFL for all the studies discussed, a non-linear effect (chaotic condition) leading to instability in the EDFL was observed. This is an interesting behavior that has led several researchers to study the bifurcation of their EDFL configurations, particularly under modulation because it presently has a wide range of applications and countless developing prospective applications. The EDFL is modulated to disturb the normal operation of the laser by activating its laser dynamics. Modulation of the EDFL can be accomplished by three well-recognized methods: pump modulation, internal or external cavity-loss modulation, and controlled feedback methods (Kumar, and Vijaya, 2015a). Pump modulation is a technique used to regulate the fiber laser intensity using a pump laser diode. Loss modulation is attained by employing a modulator, either acousto-optic or electro-optic within the linear resonator or cavity (for internal cavity-loss modulation) or by employing acoustic waves from mechanical vibration (external cavity-loss modulation) to induce loss in the

cavity. This research focuses on the pump and external cavity-loss modulations only. The difference between the two is that during loss modulation with low modulation amplitudes, there is a high chance of obtaining chaotic features effortlessly. In comparison, large modulations are needed during pump modulation in order to obtain chaotic features (Kumar, and Vijaya, 2015a). However, the dynamics of the pump-modulated laser are unlike that of the loss-modulated laser, but both modulations share some features in common (Pisarchik, Barmenkov and Kir'yakov, 2003). Chapters 2.2 and 2.3 are a review of some of the studies that have been carried out on the laser dynamics of the EDFL observed during pump modulation and loss modulation respectively. With a major understanding of the laser dynamics of the fiber laser, a higher stage of research involving harnessing the laser dynamics behavior for useful applications can be implemented. Also, to explore the possibility of the fiber laser in real pipeline monitoring applications, a study on the fundamental operation and behavior of the fiber laser, especially its chaotic condition (irregular intensity fluctuations) is of significance. By controlling the operating condition of the fiber laser, its chaotic condition or behavior can be activated easily.

2.2 Laser Dynamics of the Erbium-doped Fiber Laser Triggered by Pump Modulation

Sola, Martin and Alvarez (2002) experimentally and theoretically analyzed the responses of an erbium-doped fiber ring laser (EDFRL) that was

placed under sinusoidal pump modulation for its laser dynamics including chaotic conditions. The setup of the EDFRL is presented in Figure 2.8.

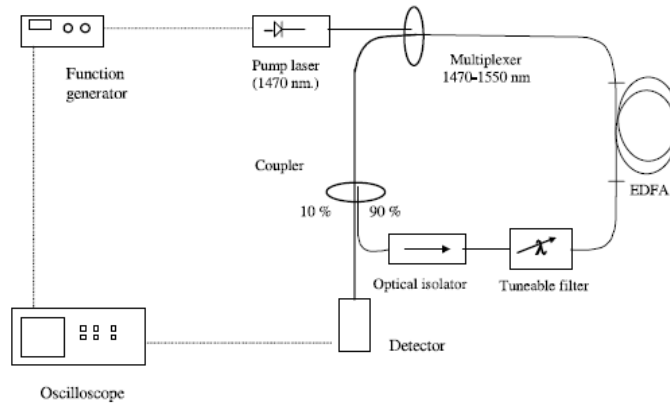


Figure 2.8: Experimental EDFRL set-up under pump modulation (Sola, Martin and Alvarez, 2002)

During experimental pump modulation, the laser was pumped to the multiplexer via the laser diode pump of 1470 nm wavelength. The current driving the laser pump was modulated using a signal generated by the function generator and the output signal of the pump-modulated EDFRL was detected by a photo-detector connected to the oscilloscope for observation. The modulated parameters consisted of the optical modulation index and frequency. For the pump-modulated frequency, the EDFRL signal response was measured for different modulation index values. Results obtained (Figure 2.9 (a)) showed several resonance peaks including optical bi-stability (OB) regions within some frequency ranges as the modulation index increases. Increasing the modulation index led to wider resonance peaks, and more bistable regions were seen. Also, chaos was observed for some pump modulation conditions. It was also observed that the mean output laser power

remained constant when the average pump power is kept constant irrespective of the pump frequency or modulation index. A model formulated from the rate equations and the basic laser theory was presented. Equation 2.3 provides the development of the top/upper laser level population which is normalized to the entire concentration of erbium ions ($N_{2r}(t)$). Equation 2.5 provides the development of the average laser power signal ($P_1(t)$) in the ring (Sola, Martin and Alvarez, 2002).

$$\begin{aligned} \frac{dN_{2r}(t)}{dt} = & \frac{\gamma_a(\nu_p)P_p(t)}{h\nu_p N_T} + \frac{\gamma_a(\nu_1)P_1(t)}{h\nu_1 N_T} - \left[\frac{(\gamma_a(\nu_p) + \gamma_e(\nu_p))P_p(t)}{h\nu_p N_T} + \frac{1}{\tau} \right] \\ & - \frac{\gamma_a(\nu_1) + (\gamma_e(\nu_1))}{h\nu_1 N_T} P_1(t)N_{2r}(t) \end{aligned} \quad (2.3)$$

$$\text{Where } P_p(t) = P_{av}[1 + m\cos(2\pi f_e t)] \quad (2.4)$$

and P_{av} is the average pump power

$$\begin{aligned} P_1(t + \Delta t) = & P_1(t) \{ \text{Texp} [[(\gamma_a(\nu_1) + (\gamma_e(\nu_1))N_{2r}(t) \\ & - \gamma_a(\nu_1))L] \}^{(c\Delta t)/D} \end{aligned} \quad (2.5)$$

With this model, the response of the laser was obtained for specific modulation and preliminary conditions as shown in Figure 2.9 (b)(i). However, the results obtained when the frequency was varied either during ascending or descending chirp (represented as dots and triangles in Figure 2.9) differed in most cases since the preliminary conditions taken were not exactly alike. In this way, the theoretical results did not quite match the experimental results. To solve this problem; Sola, Martin and Alvarez (2002) revised the model to include the variations of power and concentration of erbium ions along the fiber such that

Equations (2.3) and (2.5) became Equations (2.6) and (2.7). With the revised model, the accuracy of the laser response was improved and had a closer match with the experimental result as shown in Figure 2.9 (b)(ii).

$$\begin{aligned} \frac{dN_{2r}(z, t)}{dt} = & \frac{\gamma_a(v_p)P_p(z, t)}{hv_p N_T} + \frac{\gamma_a(v_1)P_1(z, t)}{hv_1 N_T} \\ & - \left[\frac{(\gamma_a(v_p) + \gamma_e(v_p))P_p(z, t)}{hv_p N_T} + \frac{1}{\tau} \right] \times N_{2r}(z, t) \\ & - \frac{\gamma_a(v_1) + \gamma_e(v_1)}{hv_1 N_T} P_1(z, t) \times N_{2r}(z, t) \end{aligned} \quad (2.6)$$

$$P_1(z, t + \Delta t) = P_1(z, t) [Texp [I_1(z, t)]]^{\frac{c\Delta t}{D}} \quad (2.7)$$

Sola, Martin and Alvarez (2002) went further to combine both calculation methods to obtain the most accurate laser response presented in Figure 2.9 (b)(iii). Very good agreements were observed experimentally and theoretically for a modulation index of 0.22, with all the laser dynamics behaviors seen including chaotic conditions.

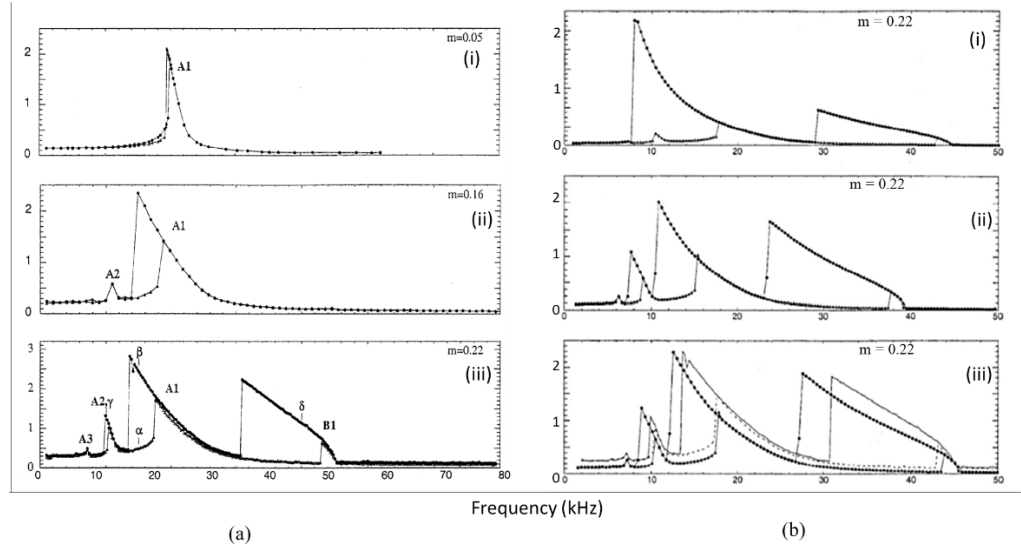


Figure 2.9: (a) Experimental pump-modulated EDFRL bifurcation diagrams for modulation index of (i) 0.05, (ii) 0.16, and (iii) 0.22; (b) theoretical pump-modulated EDFRL bifurcation diagrams for modulation index of (i) 0.22 (using equation 2.3 and 2.5), (ii) 0.22 (using equation 2.6 and 2.7), and (c) 0.22 (using a combination of both procedures) (Sola, Martin and Alvarez, 2002).

The bifurcation structure of a heavily doped EDFL (SCL110–01 from IPHT) under experimental pump modulation was characterized by Pisarchik, Barmenkov and Kir’yanov, 2003. The experimental configuration is displayed in Figure 2.10. The 1.5 m length EDFL linear cavity consisted of a laser diode (976 nm wavelength, 300 mW maximum pump power); wavelength division multiplexer (WDM), EDF (70 cm length, 2.7 μm core diameter, numerical aperture of 0.27); a polarizer and two Fiber Bragg Gratings (91 % and 95 % reflectivity at 1560 nm).

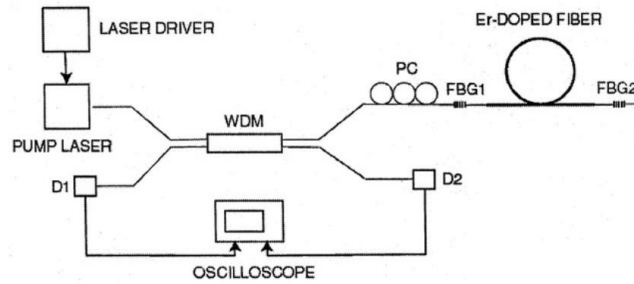


Figure 2.10. Experimental configuration of the EDFA subjected to pump modulation (Pisarchik, Barmenkov and Kir'yanov, 2003)

A signal generator controlling the drive current was used in modulating the output power produced by the laser diode pump of which its signals were recorded with a photodetector. The photodetector converted the light signals to electrical signals which were visualized via an oscilloscope and analyzed with a Fourier Spectrum Analyzer. The output signal of the EDFA was also recorded with another photodetector. It was noted that when there was no modulation, periodic oscillations were generated by the EDFA with the fundamental laser frequency because of the saturable loss in the EDF. While during pump modulation, self-oscillations and external modulation were the two processes involved in the laser dynamics of the EDFA (Pisarchik, Barmenkov and Kir'yanov, 2003).

During pump modulation, the frequency was the control parameter while the modulation depth was fixed at 50 %. In all their experiments, the fundamental laser frequency was fixed at 30 kHz (equivalent to a pump power of 15 mW). The bifurcation diagram was then obtained by measuring the peak-to-peak laser output at every modulation frequency. The bifurcation diagram

as shown in Figure 2.11 (similar to that of Sola, Martin and Alvarez, 2002) showed periodic routes to chaos, a series of bifurcations, and the co-existence of many attractors which appeared in the primary saddle-node bifurcations. It was also noticed that the laser dynamic behavior is principally governed by the ratio of the modulation frequency to the fundamental laser frequency of the EDFL. From the bifurcation diagram in Figure 2.11, f is the modulation frequency and f_0 is the fundamental laser frequency. It was observed that when $f < f_0/2$, a powerful interaction of the two parameters will cause frequency and phase locking of self-pulsations to the external modulation, and a transition from period-doubling to chaos is seen (Pisarchik, Barmenkov and Kir'yanov, 2003). When $f \geq f_0/2$, an increase in f leads to the appearance of bistability and multistability.

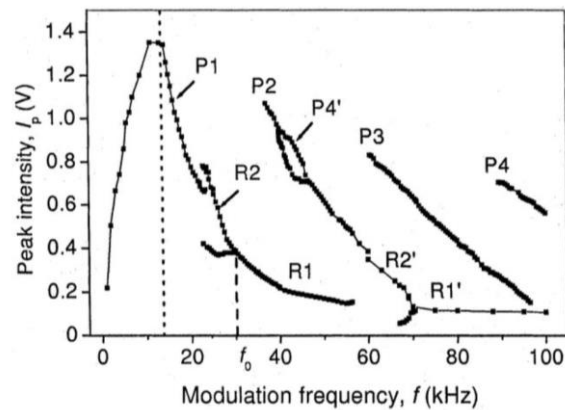


Figure 2.11: Bifurcation diagram of the pump-modulated EDFL where the fundamental laser frequency is indicated by dashed lines and the frequency locked is bounded by the dotted line (Pisarchik, Barmenkov and Kir'yanov, 2003)

In another study by Pisarchik, et al., 2005 and Reategui, et al., 2003; the complex dynamics of an EDFL with a Fabry-Perot cavity under pump modulation were analyzed experimentally and theoretically. The experimental configuration of the EDFL with a resonator length of 1.5 m is shown in Figure 2.12. The resonator consists of the 976 nm laser pump with 300 mW maximum pump power; 70 cm length EDF (2.7 μm core diameter) and two Fiber Bragg Gratings (91 % and 95 % reflectivity at 1560 nm). In their experiments, the average diode current was set to 40 mA with the signal having a modulation amplitude of 800 mV with a 100 % modulation depth of the pump power.

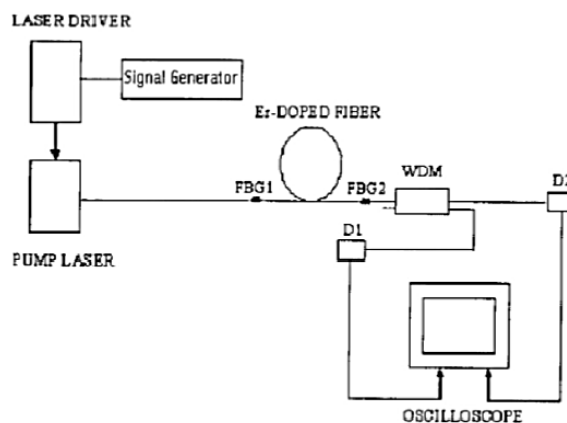


Figure 2.12: Experimental setup of the EDFL (Pisarchik, et al., 2005)

Their study was focused on low average pump powers wherein the amplitude of self-modulation of the EDFL when there is no external pump modulation is very small and negligible. Experimental results were presented for low modulation frequencies where the modulation frequency is lower than the fundamental resonance frequency and the fundamental resonance frequency of 50 kHz occurs at 40 mA current of the laser diode pump. For

various modulation amplitudes, the laser intensity was measured from peak-to-peak and the phase difference was experimentally measured versus the modulation frequency. The experimental bifurcation diagram obtained when the modulation parameter was 0.5 is shown in Figure 2.13 (a). Generalized bistability was observed for some modulation frequency values. Results of their experiments showed bistability in the lower frequency range; a variety of bifurcations; chaotic regimes with an increment in the modulation amplitude; the presence of the phase-locked states and co-occurrence of attractors in the main saddle-node bifurcations (Pisarchik, et al., 2005).

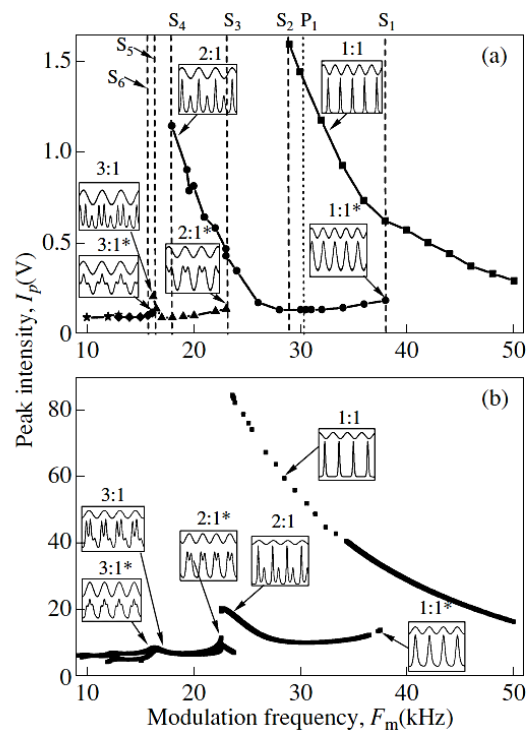


Figure 2.13: (a) Experimental and (b) theoretical bifurcation diagram of the EDFL under pump modulation at 50 % modulation depth (Pisarchik, et al., 2005)

Theoretically, the laser dynamics behavior of the EDFL was also analyzed over a range of modulation frequencies and pump modulation amplitudes with a novel laser model derived based on rate equations. Equation 2.8 is used to calculate the sum of the laser power in the laser resonator while Equation 2.9 is used to calculate the averaged population of the higher level two over the active length of the fiber. The two equations described the dynamics of the EDFL in the absence of external modulation. P_{pump} (Equation 2.10) is the pump power and P_p (Equation 2.11) is the pump power at the entrance of the EDF introduced as the harmonic pump modulation (Pisarchik, et al., 2005).

$$\frac{dP}{dt} = \frac{2L}{T_r} P \{ r_w \alpha_0 [N(\xi_1 - \xi_2) - 1] - \alpha_{th} \} + P_{sp}(t) \quad (2.8)$$

$$\frac{dN}{dt} = -\frac{\sigma_{12} \Gamma_s r_w P}{\pi r_0^2} (N \xi_1 - 1) - \frac{N}{\tau} + P_{pump}(t) \quad (2.9)$$

$$\text{Where } P_{pump}(t) = \left(\frac{P_p}{N_0 \pi r_0^2} L \right) \{ 1 - \exp[-\alpha_p L(1 - N)] \} \quad (2.10)$$

$$P_p(t) = P_p^0 (1 + m \sin(2\pi F_m t)) \quad (2.11)$$

For simplification of the laser model, Equations (2.8) and (2.9) were converted to a normalized form to Equation (2.12) and Equation (2.13).

$$\frac{dx}{d\theta} = xy - a_1 x + a_2 y + a_3 \quad (2.12)$$

$$\frac{dy}{d\theta} = -xy - b_1 y - b_2 + P_0(\theta) \cdot (1 - b_3 \exp y) \quad (2.13)$$

With Equation (2.12) and Equation (2.13), the laser dynamics behavior of the EDFL was simulated when the modulation frequency is greater than the relaxation oscillation frequency (ω_{ro}) of 30 kHz (high-frequency range) and vice versa (with a low-frequency range where the ω_{ro} is 50 kHz). With different initial conditions of laser power and averaged population over the fiber length, it was possible to plot the theoretical bifurcation diagram when the modulation parameter was 0.5 as shown in Figure 2.8 (b). Similar laser dynamics behavior as observed experimentally were seen in the bifurcation diagram obtained theoretically. Hence, it was concluded that their novel laser model perfectly described all the dynamic features observed experimentally as illustrated in Figure 2.8.

An experimental and theoretical study on the chaotic behavior of an EDFL with one polarized mode has been reported by Luo, Tee and Chu, 1998. The experimental configuration of the EDFL under pump modulation is shown in Figure 2.14 consisting of a 980 nm laser pump, WDM coupler, 4.2 m length EDF with a core diameter of 2 μm , manual polarizer, and a crystal polarizer. The total length of the EDFL cavity is 9.3 m.

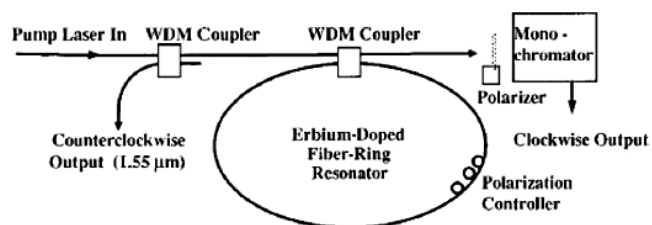


Figure 2.14: Experimental setup of the EDFL (Luo, Tee and Chu, 1998)

It was realized that with a small modulation index, a resonant peak was seen at a particular modulation frequency such that an increase in the modulation index produced two optical bistable regions. Chaos was observed at some pump modulation frequencies when the modulation index was greater than 0.85. During experimental pump modulation; bifurcation, optical bistability, chaos as well as concurrent and intermittent scenarios of the period doubling routes to chaos were all observed (Figure 2.15 (a)).

A simple theoretical model generated from the rate equations and the semi-classical laser theory was also developed. Equation 2.14 is used to calculate the laser intensity and Equation 2.15 is used to calculate the population inversion along the fiber length.

$$\dot{I}_L = -kI_L + gI_L D \quad (2.14)$$

$$\dot{D} = -(1 + I_p + I_L) + I_p - 1 \quad (2.15)$$

During sinusoidal pump modulation, the laser intensity (I_p) becomes:

$$I_p = \bar{I}_p (1 + m \cos \omega_p \tau) \quad (2.16)$$

With the above laser model; Luo, Tee and Chu (1998) simulated the dynamical behavior of the EDFL using equivalent data from the experiment which produced almost all the dynamical behaviors observed experimentally (Figure 2.15).

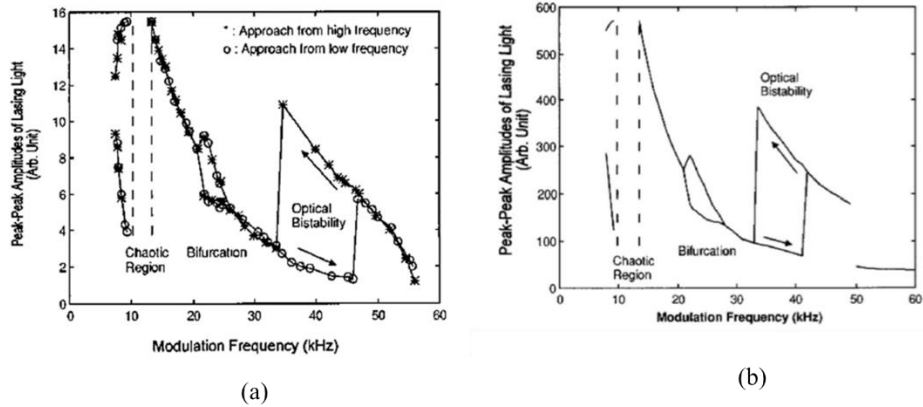


Figure 2.15: (a) Experimental; (b) Theoretical bifurcation diagrams of the EDFL indicating the presence of chaos, bifurcation, and optical bistability (Luo, Tee and Chu, 1998)

Another study that presented the numerical and experimental data of the implementation of logic gates in an EDFL showed that the numerical results and experimental observations obtained when the EDFL is pump-modulated are in good agreement with each other (Delgado, et al., 2023). The main aim of their study was to observe the laser response when the EDFL is controlled by the intensity of a digital signal added to the modulation so that various logical operations can be made possible (Delgado, et al., 2022; Delgado, et al., 2023). The laser resonator as displayed in Figure 2.16 consisted of an 88 cm length EDF (2.7 μ m core diameter) pumped by a 977 nm laser diode and two FBGs (100 % and 95.88 % respective reflectivity).

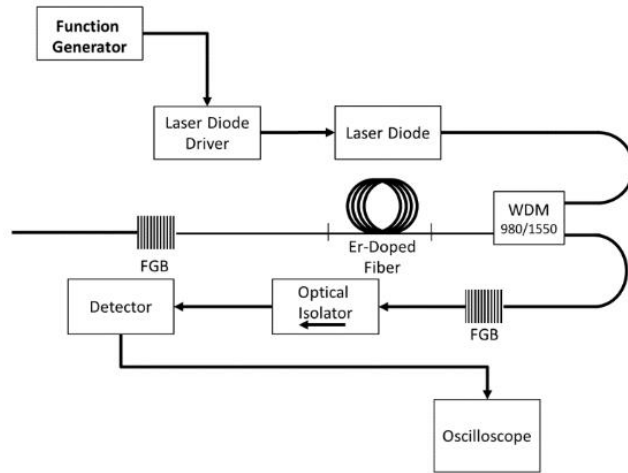


Figure 2.16: Experimental set-up of the EDFL (Delgado, et al., 2022; Delgado, et al., 2023).

The pump current was set at 145.5 mA (20 nW) for all experiments to achieve about 30 kHz ω_{r0} . The dynamics of the EDFL were controlled by injecting the harmonic modulation together with the bias signal into the pump diode. For the numerical analysis, normalized rate equations similar to that derived by Pisarchik et al., 2005 were employed to run the simulations from which the peak-to-peak amplitude of the laser intensity was plotted as a function of the pump modulation frequency (Figure 2.17 (a)). It was observed that when the modulation amplitude is 1, a dynamic-rich behavior (bifurcation, chaos, and optical bi-stability) is exhibited with a variation of the modulation frequency. In Figure 2.17, the experimental and numerical estimates showed good agreement (Delgado et al., 2022; Delgado et al., 2023).

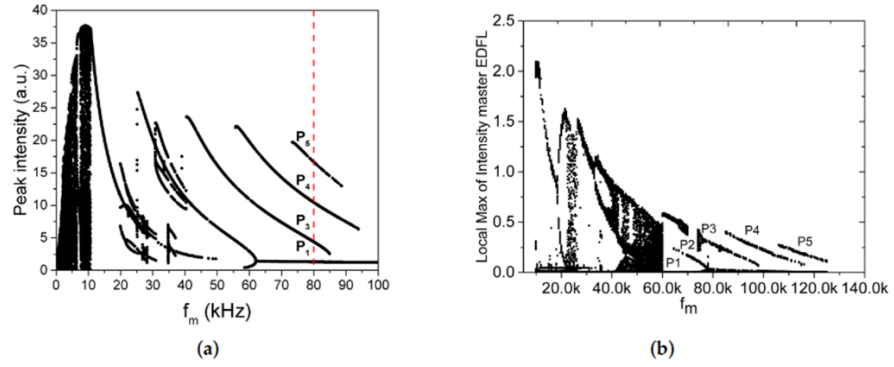


Figure 2.17: (a) Numerical, (b) Experimental bifurcation diagram of the pump-modulated EDFL (Delgado, et al., 2022; Delgado, et al., 2023)

More so, Pisarchik, and Barmenkov, 2005 experimentally studied the frequency locking of self-oscillations in an EDFL under pump modulation. The EDFL configuration is the same as in Pisarchik, et al., 2005. Dynamic features such as optical bi-stability, locking and unlocking regimes, and chaos were observed. Lacot, Stoeckel and Chenevier, 1994 also analyzed the dynamics of an EDFL under continuous pump modulation both experimentally and theoretically. Interesting modes of dynamic behavior including chaos were discovered. A theoretical model generated from two coupled lasers pumped consistently was developed and the results obtained numerically described the experimental results well. There are various other studies on EDFLs under pump modulation showing the laser dynamics behavior such as (Kumar, and Vijaya, 2015; Arellano-Sotelo et al., 2011, Pisarchik, Barmenkov and Kir'yanov, 2003; García-López et al., 2014; García-López et al., 2018; Jaimes-Reategui et al., 2014; Esqueda De La Torre et al., 2022, etc). Table 2.2 summarizes the already explained studies carried out on pump modulation of the EDFL and the dynamic features observed.

Table 2.2: Summary of literature on EDFL under pump modulation describing their laser configurations and behaviors observed.

PUMP MODULATION			
Paper authors	Laser configuration	Type of analysis	Dynamic behaviors observed
Sola, Martin and Alvarez, 2002	EDF ring laser, excited by a sinusoidally modulated pump power	Experimental and theoretical analysis with good agreement	Several resonance peaks Various frequency ranges exhibit bistable behavior.
Pisarchik, Barmenkov and Kir'yanov, 2003	Heavily-doped Erbium fiber laser with linear configuration excited by harmonic pump modulation	Experimental	Great variation of bifurcations and attractors Frequency-locked states
Pisarchik, Kir'yanov and Barmenkov, 2005		Experimental and theoretical analysis with good agreement	Two scenarios to chaos via period doubling and quasiperiodicity
Reategui, et al., 2004			
Luo, Tee and Chu, 1998	EDF ring laser under harmonic pump modulation	Experimental and theoretical analysis with good agreement	Optical bistability Period-doubling bifurcation Sporadically irregular routes to chaos Chaos
Pisarchik, and Barmenkov, 2005	Heavily-doped Erbium fiber laser with linear configuration excited by harmonic pump modulation	Experimental	Optical bistability in the frequency locking region. Chaos
Lacot, Stoeckel, and Chenevier, 1994	Erbium-doped fiber linear laser pump modulated with krypton ion pump laser.	Experimental and theoretical analysis with good agreement	Relaxation oscillations Self-pulsed working mode to deterministic chaos Linear and non-linear bifurcation Period doubling leading to chaos
Delgado et al., 2023; Delgado et al., 2022	EDF linear laser, excited by a sinusoidally modulated pump power	Experimental and theoretical analysis with good agreement	Bifurcation, chaos, and optical bistability

2.3 Laser Dynamics of Erbium-doped Fiber Laser Triggered by Loss Modulation

Experimental analysis involving a cavity-loss modulated EDFRL demonstrating non-linear phenomena has been carried out by Ghosh, Goswami and Vijaya, 2010. The EDFL was subjected to intracavity loss with a LiNbO₃ electro-optic modulator. Figure 2.18 illustrates the experimental configuration consisting mainly of the laser diode pump, EDF, WDM, and Mach–Zehnder modulator (MZM). Throughout the experiments, the laser pump power was adjusted to approximately 57.8 mW. The ω_{ro} of the EDFRL was predicted to be 35 kHz. During loss modulation, the laser diode current was fixed at 200 mA and the driving frequency was modulated in the range of 5 kHz to 105 kHz at a constant driving amplitude of 75 mW. Behaviors such as harmonic period and sub-harmonic resonances leading to optical bistability and chaos were exhibited.

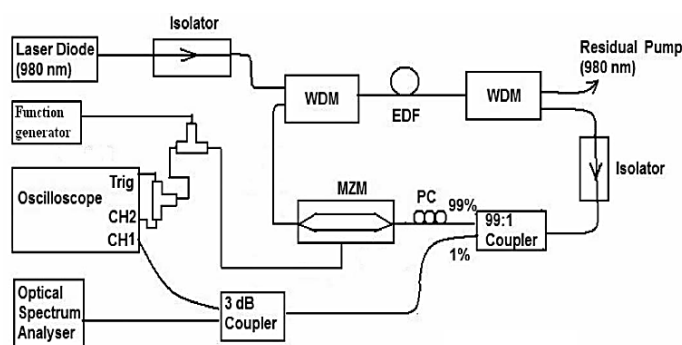


Figure 2.18: Experimental configuration of the Erbium-doped fiber ring laser under loss modulation (Ghosh, Goswami and Vijaya, 2010)

Ghosh and Vijaya, 2014 demonstrated that the behavior of an EDFRL exposed to cavity-loss modulation can change from linear to irregular dynamic resonance features. The experimental setup is the same as that of Ghosh, Goswami and Vijaya, 2010 in Figure 2.18 with a 13 m ring cavity length. Loss modulation is achieved in the laser cavity with the use of a LiNbO₃ Mach–Zehnder modulator (MZM). The lasing wavelength was obtained at 1555.1 nm.

For pump powers ranging from 30 mW to 92 mW and a driving amplitude of 10 mV, the frequency was modulated from 1 kHz to 100 kHz to determine the ω_{ro} of the EDFRL. The experiments were repeated for various levels of pump power and higher driving amplitudes. With the help of simple Fourier transform techniques and phase portraits, the experimental results were analyzed. Results of the experiments showed that non-linearity exists in the EDFRL system. It was also observed that at low driving amplitudes, the laser system acted like a linear damped oscillator, while at higher driving amplitudes, the system acted in a manner similar to that of a non-linear damped oscillator as more complicated behaviors were exhibited (Figure 2.19). These irregular dynamical features, as well as harmonic and subharmonic resonances, were further analyzed using time domain and frequency domain signals. Narrow optical bi-stable regions were also seen near the main resonance frequency at 75 mV amplitude.

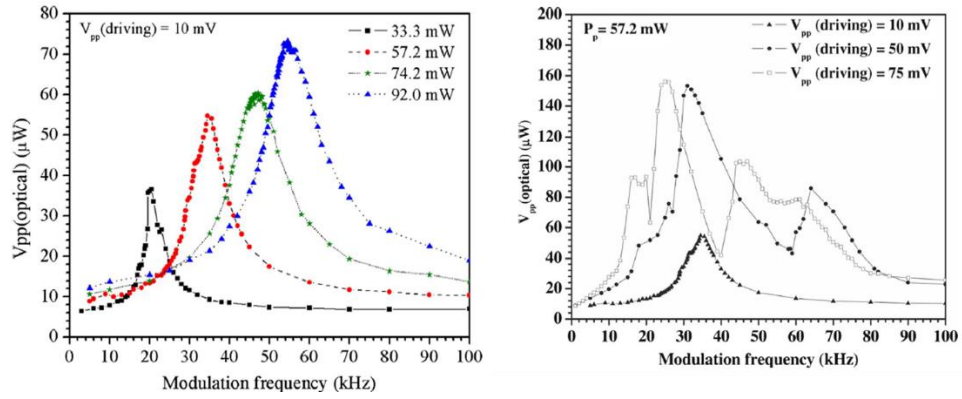


Figure 2.19: Optical output variation with modulation frequency at 10 mV driving amplitude at four pump power values (left); Optical output variation with modulation frequency at 57.2 mW fixed pump power and other driving amplitudes of 10 mV, 50 mV, and 75 mV (right) (Ghosh and Vijaya, 2014)

In addition, another experimental and theoretical study on the optical bistability observed in a cavity loss-modulated EDFL was carried out by Kumar and Vijaya, 2017a. The experimental setup is shown in Figure 2.20. The resonator length is about 13 m consisting of 8 m EDF, 980/1550 nm wavelength WDM, 1550 nm isolator, 99:1 coupler, 80:20 coupler, a polarizer, and a Mach–Zehnder modulator. The lasing wavelength of the EDFRL was obtained at 1570 nm and a pump power of 39.5 mW was used for all experiments.

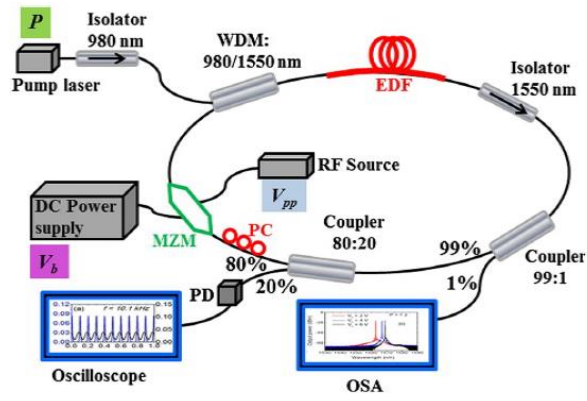


Figure 2.20: Experimental set-up of the EDFA under loss modulation (Kumar and Vijaya, 2017a)

Intra-cavity loss modulation was performed both experimentally and theoretically respectively modulating the frequency (from 1 – 35 kHz and vice versa) and amplitude (10 – 100 mV and vice versa at 10 kHz modulation frequency). While varying the modulation frequency, the laser response observed was unidentical when increasing and decreasing the frequency, giving rise to a bistable response at some frequencies. Likewise, while varying the modulation index, the laser response seen was also different, giving rise to a bistable response. It was also noticed that when the modulation frequency is decreased, the cavity loss drops leading to an increase in the cavity lifetime for the field (Kumar and Vijaya, 2015a; Kumar and Vijaya, 2017b).

For theoretical loss modulation, the scaled rate equations of population inversion and laser intensity (Equations (2.17) and (2.18)) were used (Kumar and Vijaya, 2015a; Kumar and Vijaya, 2017a).

$$\frac{dx}{d\theta} = s + gx(y - \alpha) \quad (2.17)$$

$$\frac{dy}{d\theta} = a - y(x + 1 + d) \quad (2.18)$$

Where α is the cavity loss given as:

$$\alpha = \alpha_o[1 + m \sin(2\pi v\theta)] \quad (2.19)$$

With these equations, parameters that are appropriate to the input conditions used in the experiments were used in the theoretical analysis. For frequency modulation, similar to the experimental bifurcation result (Figure 2.21 (a)), the theoretical bifurcation diagram (Figure 2.21 (b)) showed two optical bistable regions around 2.4 kHz and 7.5 kHz frequency spread. For modulation index variation, similar trends between the experimental and theoretical results were identified particularly in the resonance frequency range as shown in Figure 2.22. Also, more complex behavior was exhibited at higher modulation amplitudes with an increase in the extent of nonlinearity (Kumar and Vijaya, 2015b). A hysteresis loop was also formed. It was then concluded that the experimental and theoretical results showed good agreement qualitatively in terms of trend; however, a quantitative accurate matching is beyond their theoretical model. This is due to the fact that some parameters used in the calculation were not exactly the same as the parameters in the experiment, but were mere estimates. There were also numerous hidden losses from the several components in the experiments that were not considered in the calculations.

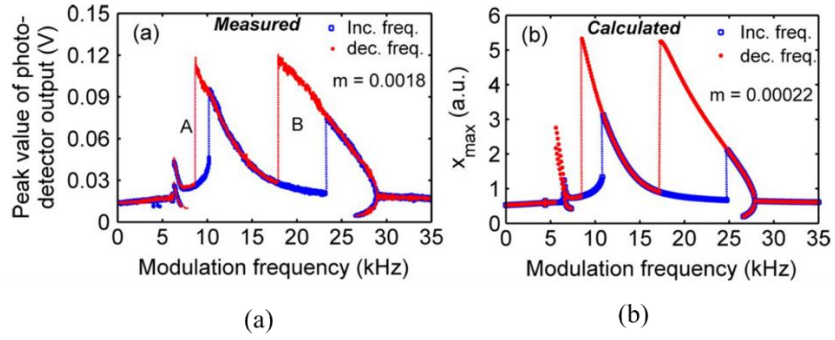


Figure 2.21: (a) Experimental bifurcation diagram obtained at a set modulation amplitude of $m = 0.0018$ (b) Theoretical bifurcation diagram at a set modulation amplitude of $m = 0.00022$. (Kumar and Vijaya, 2015a; Kumar and Vijaya, 2017a)

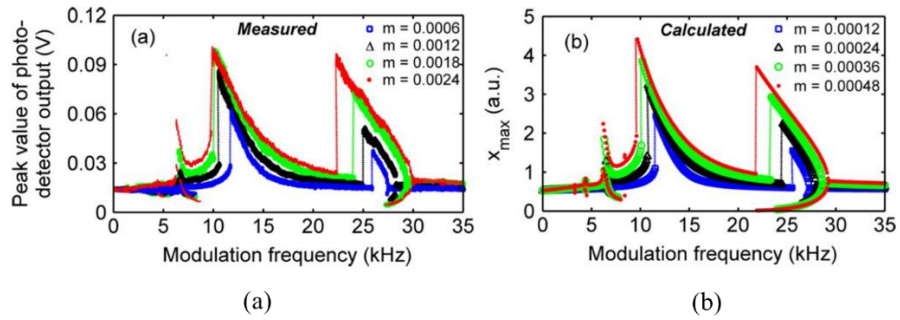


Figure 2.22: (a.) Experimental (b.) Theoretical non-linear responses of the loss-modulated EDFRL for a range of modulation indices when varying the modulation frequency (Kumar and Vijaya, 2015a)

There are some other studies such as Saucedo-Solorio, et al., 2003, Yue, et al., 2009; Feng, et al., 2009; Kumar and Vijaya, 2017b; Kumar and Vijaya, 2015b, and Onubogu, Pua and Faidz, 2021; that also shows that the EDFL exhibits a non-linear dynamical behavior when subjected to loss modulation. Table 2.3 summarizes some studies carried out on the loss-modulated EDFL and the dynamic features observed.

Table 2.3: Summary of literature on EDFL under loss modulation describing their laser configurations and behaviors observed

LOSS MODULATION			
Paper authors	Laser Configuration	Type of Analysis	Dynamic Behaviors observed
Ghosh, Goswami, and Vijaya, 2010	Erbium-doped fiber ring laser having an intracavity lithium niobate (LiNbO ₃) based electro-optic modulator	Experimental	Period-1 bistability Harmonic and period-2 sub-harmonic resonances Chaotic behaviour
Ghosh and Vijaya, 2014		Experimental	Linear and non-linear resonances High harmonics and sub-harmonic resonances Multistability
Kumar and Vijaya, 2015		Experimental and theoretical with good agreement	Linear and non-linear regimes Periodic states leading to chaos
Saucedo-Solorio, et al., 2003	Erbium-doped fiber laser (linear or ring) with modulated losses	Theoretical	A variety of bifurcations and attractors Co-existence of numerous attractors that are seen in the primary saddle-node bifurcation.

Regardless of all these existing studies on pump and loss modulations, the study of the bifurcation of the EDFL is infinite because, for every new EDFL configuration, novel characteristics are detected especially when they are subjected to modulation. The novel characteristics observed also imply new applications of the EDFL. It is important to note that the main research gap in all these pump and loss modulation studies is that none of the researchers tried to understand the main cause of the instabilities observed due to intensity fluctuations during their pump and loss-modulation studies.

In this research, the external loss modulation is performed in a novel way by the use of a loudspeaker to imitate the acoustic waves or vibration

emanating from a water pipeline as this is the main anticipated use of the EDFL in this research. In most of the existing studies described in this thesis, a theoretical model based on the EDFL configuration was used to describe the experimental results. The EDFLL and EDFRL configurations in this research are not exactly the same as those studied by other authors and their laser dynamics cannot be described by the existing theoretical models. The model of Pisarchik, Kir'yanov and Barmenkov (2005) is closely related to the configurations of the EDFLL and EDFRL. Therefore, some modifications for improvement of the model would be made on the current model and presented in Chapter 3, to obtain a model that depicts the behavior of the EDFLL and EDFRL well.

Even though acousto-optic detection is now possible with the utilization of other existing optical fiber-based systems, the advantages of the EDFL sensor in this research still make it unique with excellent potential in pipeline monitoring regardless of the instabilities observed as it revealed high sensitivity at its resonance frequency.

2.4 Summary

In this chapter, the fundamental concept and working principle of the EDFL have been explained. Also, a review of existing literature on the use of EDFL for acoustic wave detection has been presented from which the presence of instability related to intensity fluctuations in the sensor was confirmed. This led to another literature review on the laser dynamics behavior (bifurcation,

chaotic condition, resonance, optical bistability, etc.) of the EDFL triggered by pump modulation. This review aimed to understand the dynamical behaviors present in the pump-modulated EDFL system. In addition, previous studies on the dynamic behavior exhibited by loss-modulated EDFL have also been reviewed. This is because acoustic waves generate a loss in the resonator of the laser and so it is important to understand the dynamical behaviors exhibited by the loss-modulated EDFL system. All studies presented have confirmed that the EDFL switches from linear to non-linear dynamic behaviors when subjected to modulation with a change in the initial conditions.

CHAPTER 3

METHODOLOGY

3.1 Introduction

The methods used in executing this research are summarized in the flow diagram in Figure 3.1.

Literature review (Chapter 2) is first carried out to give an overview of the present knowledge in this research whilst identifying the applicable methods, theories, and most importantly the existing research gap. Step 1 of the methodology consists of the design of the EDFL sensor and field test of the sensor on a water pipeline to detect leakage and the location of the leakage. Step 2 involves a breakdown of the analysis (Step 2.1 and Step 2.2) to be performed to understand the sensor's behavior and the cause of the instability observed due to intensity fluctuations. The experimental configurations of the linear and ring lasers and their working principle when used for sensing are also described in Step 2. Step 2.1 comprises the experimental pump and loss modulations of the linear and ring lasers; while Step 2.2 comprises the derivation of the laser rate equations, a description of the parameters used in the calculations, and the steps carried out for numerical simulation of the pump and loss modulated linear and ring lasers. Step 3 involves a comparison of:

- the results of the theoretical pump-modulated linear laser with the results of the experimental pump-modulated linear laser,
- the results of the theoretical pump-modulated ring laser with the results of the experimental pump-modulated ring laser,
- the results of the theoretical loss-modulated linear laser with the results of the experimental loss-modulated linear laser, and
- the results of the theoretical loss-modulated ring laser with the results of the experimental loss-modulated ring laser.

If the theoretical and experimental results do not match, the theoretical model would be re-modified and the numerical simulations repeated until an acceptable match is seen from which conclusions are made.

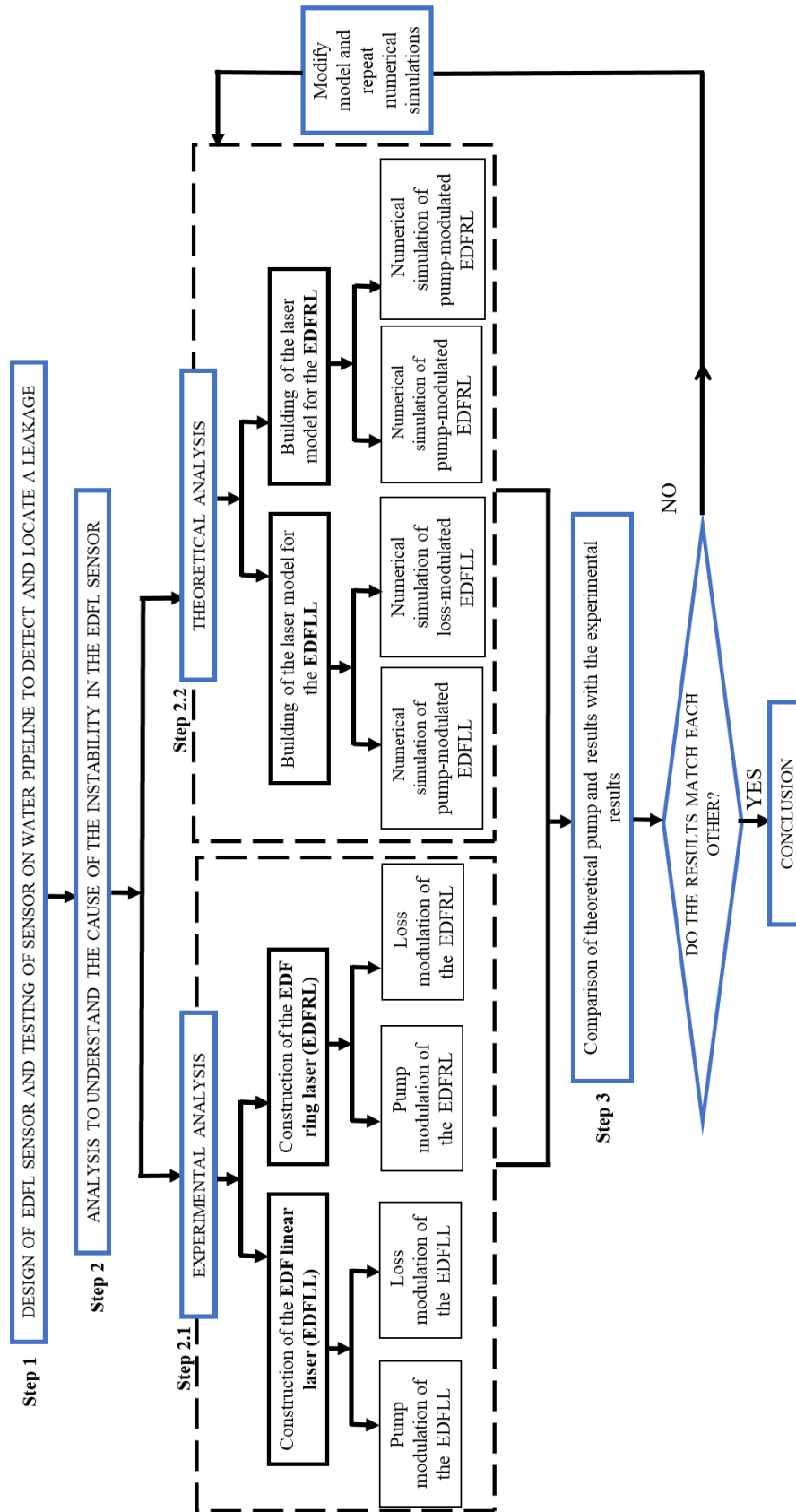


Figure 3.1: Flow diagram of the methodology utilized in executing the research

3.1 Design of the EDFL Sensor for Test on a Water Pipeline

After the literature review has been completed, the next part of the methodology is the design of the EDFL. The EDFL configuration used as a sensor for field tests on the water pipeline to detect and locate a leakage is presented in Figure 3.2. The cavity of the EDFL is linear and hence called erbium-doped fiber linear laser (EDFLL).

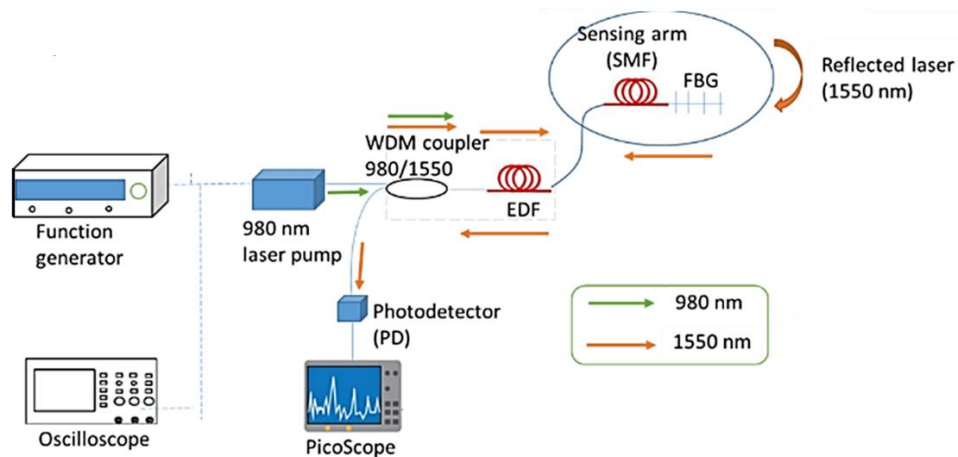


Figure 3.2: Erbium-doped fiber linear laser (EDFLL) set-up for field test on the pipeline

The EDFLL is pumped by a 980 nm semiconductor laser diode pump (Gooch and Housego EM595) with 245 mW maximum pump power. The 10 m length EDFLL cavity in Figure 3.2 consists of a 3 m length wavelength division multiplexer (WDM) of 980/1550 nm wavelength attached to an EDF of 3 m length, having cladding of 125 μm diameter and a core of 8 μm diameter. For the detection of vibration and acoustic waves, a single mode fiber (SMF) of 3 m length is attached to the EDF as a sensing arm. The SMF is then attached to a

one-sided fiber Bragg grating (FBG) having $1550 \text{ nm} \pm 0.3 \text{ nm}$ central wavelength with more than 99 % reflectance. The FBG end is flatly cleaved at a right angle to create Fresnel reflection that sends feedback to the laser system such that it reflects photons of only 1550 nm wavelength to the cavity. The output received is transformed from optical to electrical with the help of a high-speed photodetector (model: THORLABS-DET08CFC/M InGaAs biased detector, 5 GHz maximum bandwidth, operating spectral range 800 - 1700 nm). The electrical output is finally sent to the oscilloscope called PicoScope 6, 3000 series (a USB-powered PC oscilloscope with 200 MHz analog bandwidth and 1 GS/s real-time sampling) for viewing and monitoring of the laser output. This experimental configuration does not include a polarizer. It is vital to note that the EDFLL system operates just over the lasing threshold state, which occurs when the optical cavity begins to emit stimulated emission but remains stable.

The working principle of the EDFLL is as follows: The laser pump is used to launch the laser into the 980/1550 nm WDM coupler which couples the 980 nm wavelength light to the EDF that is connected to the sensing arm. Inside the EDF, the erbium ions absorb the 980 nm photons, and then photons between 1520 nm to 1560 nm are freely released under spontaneous emission. However, only photons of 1550 nm are reflected by the FBG to the cavity of the laser. The reflected 1550 nm photons then stimulate the erbium ions to emit more 1550 nm photons.

The proposed sensor has several advantages compared to a commercial acoustic sensor. One important advantage is the possibility to fully attach the

flexible sensing arm on the surface of the pipeline thereby increasing the contact area of the pipe and the sensor. Also, the sensors' set-up gives room for the addition of other components if need be. Most importantly, the sensitivity of the sensor can be adjusted by the variation of the length of the SMF and the laser input power.

3.2 Testing of the EDFL Sensor on a Real Water Pipeline to Detect the Presence of Leakage and the Location of the Leakage.

Experiments were carried out to confirm that the EDFL sensor can really detect leakage on a pipeline and also find the leakage location. The sensed environment is a water pipeline installed above the ground level. The top, front, and side views of the galvanized iron test pipeline used for the experiments are shown in Figure 3.3 with dimensions. The pipeline is designed as a continuous connection from the pump to the tank. The water pipe of 40,000 mm length, 82 mm inner diameter, and 90 mm outer pipe diameter; was connected to a tank receiving water from a 4-kW power water pump. The pressure at which water flows in the pipe from the tank is adjustable, ranging from 1 bar to 3 bar.

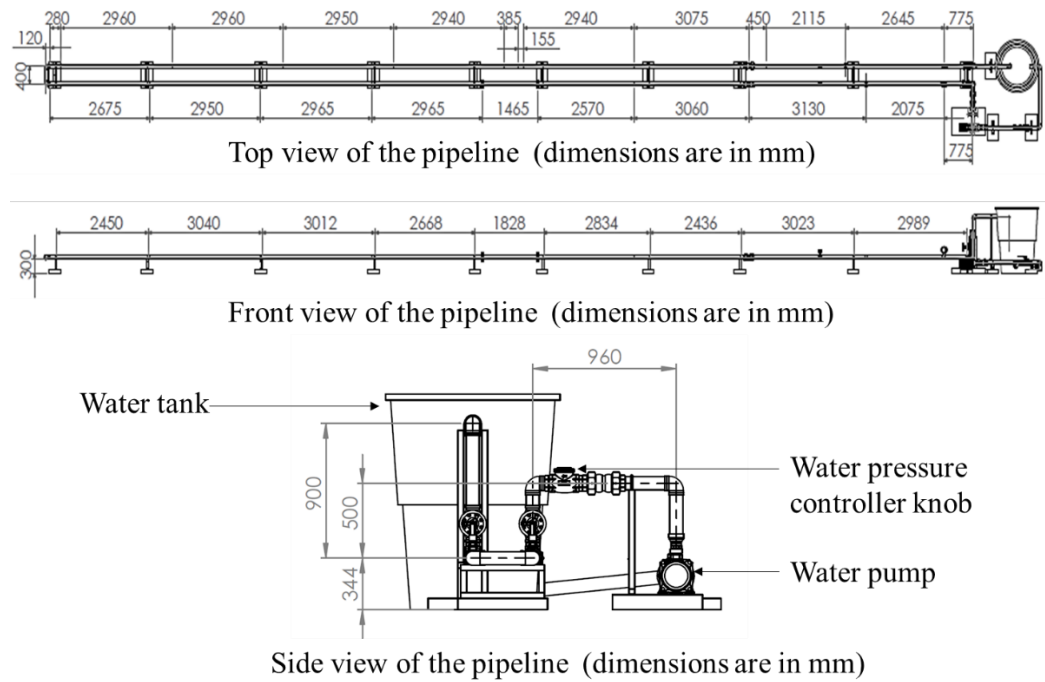
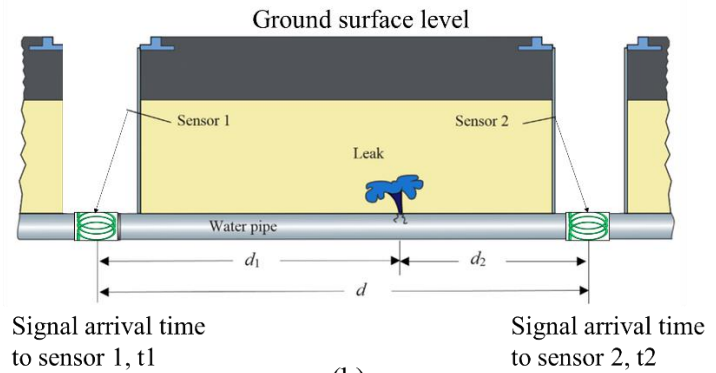


Figure 3.3: Field test pipeline showing dimensions and different views of the pipeline setup

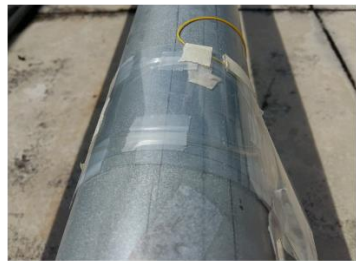
For the field test, two identical EDFLL sensors were separately positioned firmly on the top surface of the galvanized iron water pipeline as illustrated in Figure 3.4 (b), a distance away from a 0.5 cm diameter drilled artificial leakage hole respectively. The diameter of the leak hole was chosen randomly as 0.5 cm standard size for the field tests because the diameter of leakage can be of any size. Two identical sensors are required to pinpoint a leakage location by calculating the time delay in acoustic wave detection captured by the two sensors.



(a)



(b)



(c)



(d)

Figure 3.4: (a) Real photo of the test pipeline used for field experiments; (b) Illustration of the anticipated application of the EDFL for pipe leakage detection and location; (c) real photo of one EDFL sensor placed on the test pipeline; (d) close photo of the sensor showing its flexibility

Both sensors receive the acoustic waves emanating from the leakage to determine whether a leak has occurred. The first experiment performed was to confirm that the EDFL sensor can detect leakage and show the difference between “no leakage” and “leakage” conditions during water flow in the pipe at a certain pressure (Figure 3.5 (a)). The second experiment was carried out to detect the location of the leak (Figure 3.5 (b)) via the cross-correlation

method. During the “no leakage” condition, a few peaks were seen in the signal while during the “leakage” condition, more peaks appeared.

For water pressure of 1 bar and distance of 1.5 m between the two sensors, 200 sets of signal data were collected, each set having 10004 samples at a time step of 0.01 ms equivalent to a sampling rate of 100 kHz. At the same water pressure and a distance of 1.7 m between the two sensors, another 200 sets of signal data were collected, each set having 10004 samples at a time step of 0.01 ms equivalent to a sampling rate of 100 kHz. At water pressure of 2 bar, and distances of 1.5 m, 1.7 m, 3 m, and 4 m between the two sensors; 200 sets of signal data were again collected for each distance, each set having 10004 samples at a time step of 0.01 ms. Lastly, at a water pressure of 3 bar, and distances of 1.5 m, 1.7 m, 2 m, 3 m, and 4 m between the two sensors; 200 sets of signal data were again collected for each distance, each set having 10004 samples at a time step of 0.01 ms. The signals consisted of some background noise embedded in the leakage information and may require de-noising to remove the background noise and improve the signal-to-noise ratio. Wavelet decomposition is the major de-noising method widely used where a signal is de-noised in three steps: decomposition details coefficients thresholding, and reconstruction. However, the signals obtained showed distinct peaks generated by the acoustic wave detected from the leakage and did not necessarily need de-noising to calculate the time lag or delay between the two sensors. Hence, simple exponential smoothing with a damping factor of 0.6 was used to reduce the noise to double confirm that the peak obtained was due to the leakage and not background noise (Figure 3.5 (b)). The red arrows in Figure 3.5 (b) indicate

the time when both sensors detected the acoustic waves emanating from the leakage, from which the time delay and d_1 and d_2 were calculated based on the following cross-correlation equations:

$$t_1 = \frac{d_1}{c}; t_2 = \frac{d_2}{c}; \Delta t = t_2 - t_1 = \frac{d_2 - d_1}{c}; \text{ Since } d_1 + d_2 = d;$$

$$d_1 = \frac{d - c \cdot \Delta t}{2}; d_2 = \frac{d + c \cdot \Delta t}{2}$$

where d = the distance between sensor 1 and sensor 2; d_1 = distance from sensor 1 (channel A) to the leakage; d_2 = distance from sensor 2 (channel 2) to the leakage; c is the speed of sound of water leaking from the pipe (495 m/s according to De Lima, et al., 2018); Δt is obtained by calculating the time difference between two successive peaks from the two sensors where t is the time spent for the acoustic wave to travel from the leakage point to the sensor.

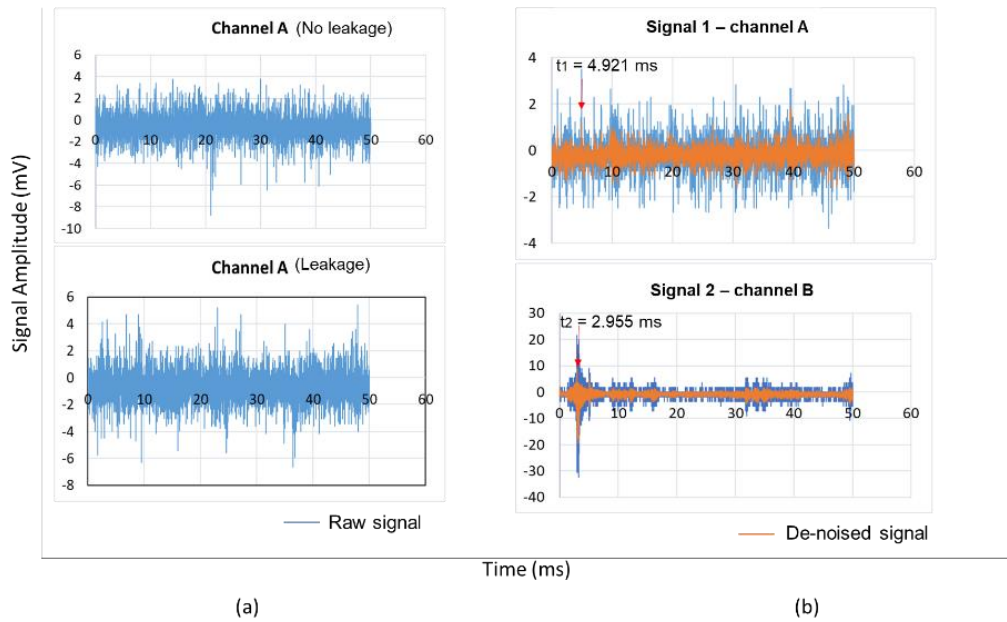


Figure 3.5: Waveform of the signal from (a) sensor 1 placed on the pipeline with water flowing at a pressure of 1 bar (without leakage and with leakage) (b) sensors 1 and 2 placed 3 m apart on the pipeline with water flowing at a pressure of 2 bar

Results obtained from the pipeline field test experiments are shown in Table 3.1.

Table 3.1: Results obtained from the field test experiments

Pressure (bar)	Total distance between 2 sensors (m)	Original/expected distance (m)		Cross-correlated/measured distance (m)		Percentage error (%) of the sensor with respect to:		Accuracy (%) of the sensor with respect to:	
		d_1	d_2	d_1	d_2	d_1	d_2	d_1	d_2
1	1.5	0.5	1.0	0.4	1.1	20.70	10.40	79.3	89.6
	1.7	0.7	1.0	0.6	1.1	13.90	9.75	86.1	90.3
2	1.5	0.5	1.0	0.6	0.9	25.3	12.60	74.8	87.4
	1.7	0.7	1.0	0.8	0.9	16.10	11.30	83.9	88.7
	3.0	2.0	1.0	2.0	1.0	0.70	1.30	99.3	98.7
3	4.0	3.0	1.0	2.9	1.1	4.50	13.40	95.5	86.6
	1.5	0.5	1.0	0.4	1.1	15.30	7.70	84.7	92.3
	1.7	0.7	1.0	0.6	1.1	12.90	9.00	87.1	91.0
	2.0	1.0	1.0	1.0	1.0	4.10	4.10	95.9	95.9
Average	3.0	2.0	1.0	1.8	1.2	7.80	15.60	92.2	84.4
	4.0	3.0	1.0	2.9	1.1	3.70	11.00	96.3	89.0
Average						11.4	9.7	88.6	90.4

From Table 3.1, the average percentage errors of the cross-correlated distance from sensor 1 to the leakage (d_1) and sensor 2 to the leakage (d_2) are 11.4 % and 9.7 % respectively with high accuracies of approximately 89 % and 90 %. The overall accuracy for both sensors is an average of 89 % and 90 %, giving 90 % accuracy which is quite good. However, to obtain more accurate leak locations, the generalized cross-correlation maximum likelihood (GCC-ML) method with a leak location accuracy of 93.2 % or more preferably the empirical mode decomposition – independent component analysis (EMD-ICA) based frequency domain cross-correlation method (97.3 % accuracy) can also be used (Kothandaraman, et al., 2020).

Regardless of the high sensitivity of the EDFL in pipeline leakage detection, it was observed that sometimes, especially when the sensor is further away from the leak point (see signal 1-channel A in Figure 3.5 (b)), there is a lot of instability in the sensor as numerous peaks are seen. This was observed for other field test results obtained at other water pressures mostly for the sensor placed further away from the leak point. To understand the behavior of this EDFL sensor, it was very necessary to carry out experimental and theoretical analysis to see if the bifurcation happening in the EDFL as experienced by other researchers (refer to Chapter 2: Literature review) is the root cause of the instability.

3.3 Experimental Analysis to Understand the Cause of the Instability in the EDFL Sensor

To understand the cause of the instability in the sensor, pump, and external cavity-loss modulations were carried out on the EDFLL configuration. Pump and loss modulations are ways of activating the laser dynamics of the EDFL. The working principle of the EDFL as a sensor is based on loss modulation.

For comparison, the same experiments were carried out on the Erbium-doped fiber ring laser (EDFRL) configuration as well. Figures 3.6 and 3.7 illustrate the experimental configuration of the EDFLL and EDFRL under pump and loss modulations respectively, inclusive of the actual photos of the experimental setup in the lab. These EDFLL and EDFRL resonator or cavity designs occupy less space and are economical as they consist of affordable devices.

3.3.1 Experimental Configuration of the EDFLL

The experimental configuration of the EDFLL is the same as explained in Chapter 3.1. Figure 3.6 illustrates the pump-modulated EDFLL where the green and orange arrows symbolize the optical directions of the photons having 980 nm and 1550 nm wavelengths.

During pump modulation, a manual function generator (GWINSTEK GFG-8020H with 0.2 Hz ~ 2 MHz frequency bandwidth and 50 Hz ~ 5 MHz frequency response), as well as a digital oscilloscope (MEGURO MO-1020, DC 20 MHz frequency bandwidth with maximum input voltage of 300 V peak), are connected to the 980 nm laser diode pump. The laser pump is then modulated with a sinusoidal waveform at different voltages and frequencies.

For the external cavity-loss modulation of the EDFLL, a loudspeaker is used as the modulator. The 8 cm by 8 cm sized loudspeaker (with 20 W nominal rated power and frequency ranging from 100 Hz to 20 kHz) is positioned right on top of the EDF in a way that the perimeter of the EDF is fully covered up. To induce losses in the EDFLL cavity, modulation of the loudspeaker's amplitude and frequency is carried out with the same manual function generator and a digital oscilloscope (Matrix MDS1102E, 100 MHz bandwidth with real-time sample rate of 1 GS/s per channel).

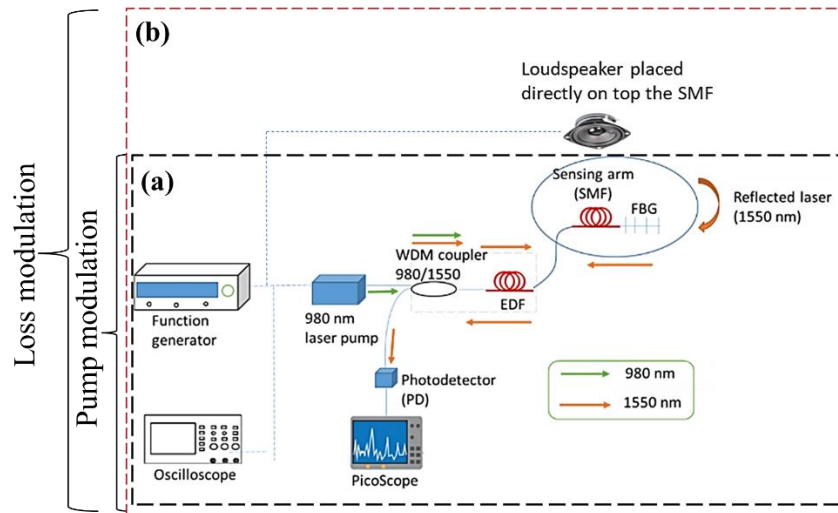


Figure 3.6: Experimental configuration of the (a) EDFLL under pump modulation; (b) EDFLL under loss modulation.

3.3.2 Experimental Configuration of the EDFRL

The EDFRL configuration as shown in Figure 3.7 under **pump modulation** has the same configuration as the EDFLL starting from the laser pump to the SMF. The details of the EDF and the WDM are the same as that stated in Chapter 3.1. The SMF is then connected to an isolator of 1560 nm to convey the photons in a single direction in the laser cavity.

The isolator is connected to a 90/10 coupler that collects 10 % laser power from the cavity, guiding it toward the photodetector for monitoring. 90 % of the laser output is re-directed to the ring cavity. This experimental configuration does not include a polarizer and the resonator of the EDFRL is approximately 13 m in length. During pump modulation, the voltage and frequency of the laser pump (980 nm wavelength) are controlled using a function generator.

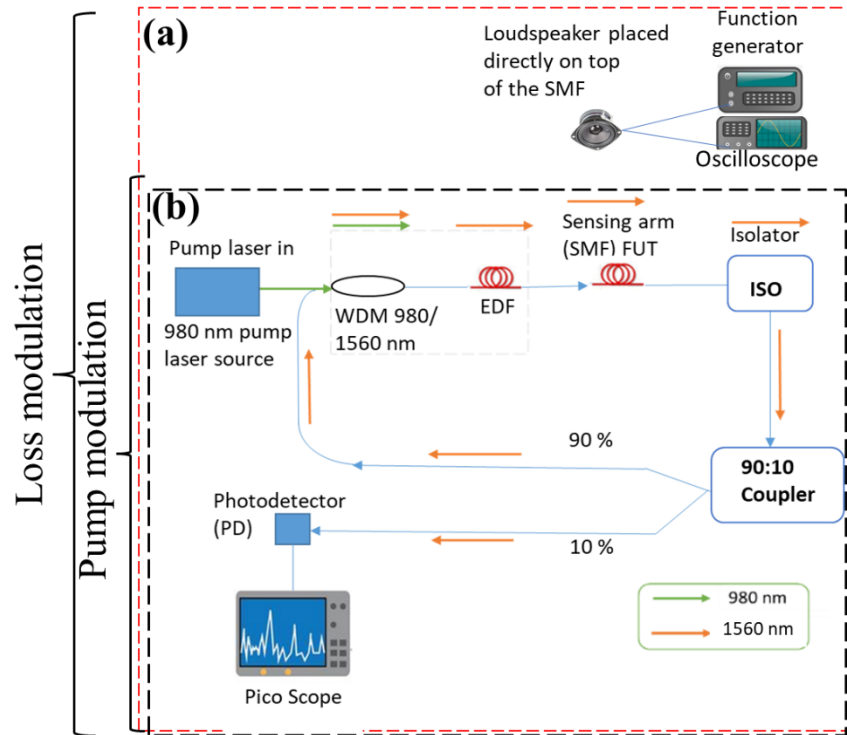


Figure 3.7: Experimental configuration of the (a) EDFRL under pump modulation; (b) EDFRL under loss modulation

3.3.3 Experimental Pump Modulation of the EDFLL

Before any modulations were carried out, the optical spectrum of the EDFLL was checked by slowly increasing the laser pump power from 0 mW until a sharp peak indicating self-lasing was seen at 1549.7 nm via the Optical Spectrum Analyzer ((OSA) model: Anritsu MS9740A with 600 nm to 1750 nm measurement range). Figure 3.8 indicates the lasing wavelength which matches the wavelength of the FBG. An increase in the laser pump power leads to a decrease in the turn-on time and an increase in the spiking power. In this way, the damping effect is eventually reduced (Pua, et al., 2012).

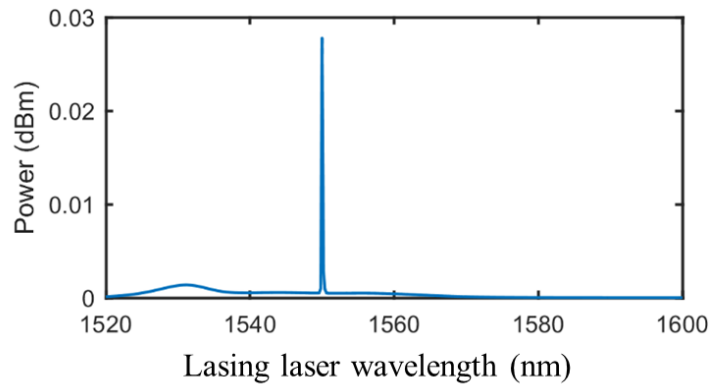


Figure 3.8: Optical spectrum of the EDFLL

As explained earlier, what happens in the EDFLL cavity is that as the laser is pumped into the EDF, the laser pump power is absorbed by the erbium ions at the ground level until population inversion is achieved at the upper level. Stimulated emission causes the population inversion to drop thereby initiating absorption to occur. The absorption and emission process continues altering to produce a laser output that exhibits gradually declining intensity peaks, leading to a near-sinusoidal damped oscillation. With continuous pumping, the laser output finally stabilizes to a fixed value.

After evaluating the optical spectrum of the EDFLL, experiments on the pump-modulated EDFLL were performed to observe the dynamic behaviors exhibited by the EDFLL, especially for its resonance characteristics, and linear and chaotic dynamics. Throughout the experiments, sinusoidal modulation of the current from the laser pump diode with frequency is activated via the harmonic signal ($A \sin(2\pi ft)$) of the modulation. The harmonic signal is applied externally from the function generator to the laser pump (Pisarchik, Barmenkov and Kir'yanov, 2003). A and f in the harmonic signal represent the modulation

amplitude (MA) and modulation frequency (MF) respectively. When laser pump power is adjusted, a resonant peak appears as seen on the Pico Scope. This is the resonance frequency (ω_r) of the EDFLL which is directly proportional to the pump power. Since the EDFLL is a resonator, it can have many resonance frequencies. Hence pump modulation was performed in the lab several times for a range of resonance frequencies.

In this thesis, out of all the experimental results obtained, three major EDFLL pump modulation results are presented for modulation from 1 kHz to 60 kHz. The input parameters used in obtaining the pump modulation results are presented in Table 3.2.

Table 3.2: Input Parameters used when pump-modulating the EDFLL from 1 kHz to 60 kHz

S/No.	Resonance frequency (kHz)	Modulation amplitude (V)	Laser pump power (mW)
1	7	0.2 (corresponding to the optical power of 16.5 mW as obtained from the laser diode pump manual)	95
2	7	0.4	107
3	13	0.1	201
4	19	0.4	52.6

It is important to note that the EDFL setup is extremely sensitive to any external disturbances. This includes movement of the laser set-up since during experiments, its components were not permanently fixed to a position or boxed up as a movable sensor. For this reason, another EDFLL pump modulation was carried out on a different day when the laser set-up was disconnected and re-

connected with input condition no. 4 as shown in Table 3.2. In comparison to the other three input conditions, the result is still similar as expected. To observe the features of the optical output, Pico Scope 6 was used which displays the results in the time domain (higher section) and frequency domain (lower section). The output power of the laser has a linear relationship with the current from the pump laser diode. For each MF, the amplitude of the intensity of the laser with the highest peak was noted during variation from low MF to high MF and the other way around to get the bifurcation diagrams displaying the EDFLL's dynamic behavior. Full details of the experimental results can be found in the results and discussion (Chapters 4 and 5).

3.3.4 Experimental Pump Modulation of the EDFRL

Before pump modulating the EDFRL, the lasing wavelength of the set-up was checked just like that of the EDFLL. The wavelength of the EDFRL during lasing was obtained at 1560 nm (Figure 3.9) as seen in the OSA, while gradually increasing the pump power from 0 to 120 mW where self-lasing occurs.

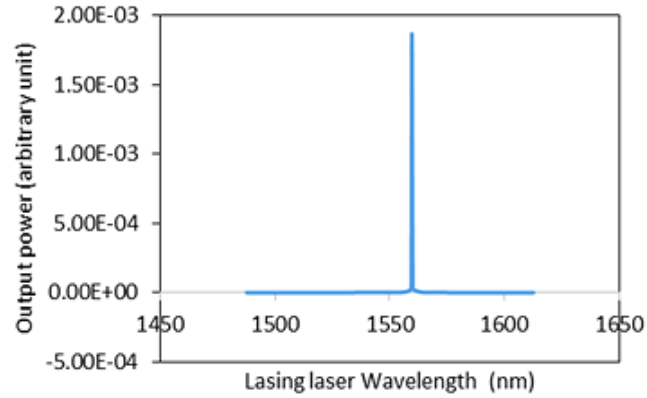


Figure 3.9: Optical spectrum of the EDFRL.

Self-spiking periodic oscillations are seen when increasing the laser pump power from 0 mW to 136.4 mW with zero external modulations because of the saturable loss inside the EDF. Just as in the EDFLL, the amplitude and resonance frequency of the oscillations in the EDFRL is dependent on the laser pump power (Reategui, et al, 2004). It was also observed that no resonance peak appears at the laser pump power of ≤ 110.0 mW. But, an increase in the pump power causes the active laser medium to absorb additional energy leading to a shorter build-up time for population inversion and hence lasing (Figure 3.11) (Pua, et al., 2012a). A tiny resonance peak (which is not so obvious) starts to appear around the pump power of 110.1 mW and increases until 218.2 mW which is almost the highest power of the diode laser pump. At low ω_r as Figure 3.10 shows, a non-linear sinusoidal response is displayed implying instability. However, the ω_r increases when there is an increase in the laser pump power, and a linear sinusoidal response (implying a stable response) having a higher amplitude is displayed from 190.9 mW to 218.2 mW pump powers as shown in Figure 3.10. It can therefore be resolved that for the EDFRL configuration, regulating the laser pump power from 110.4 mW to 180.7 mW

leads to a shift in the ω_r from 2 kHz to 10 kHz. This limited range could be because the EDFRL resonator is too long. Also, the laser diode pump power is limited to 245 mW max only.

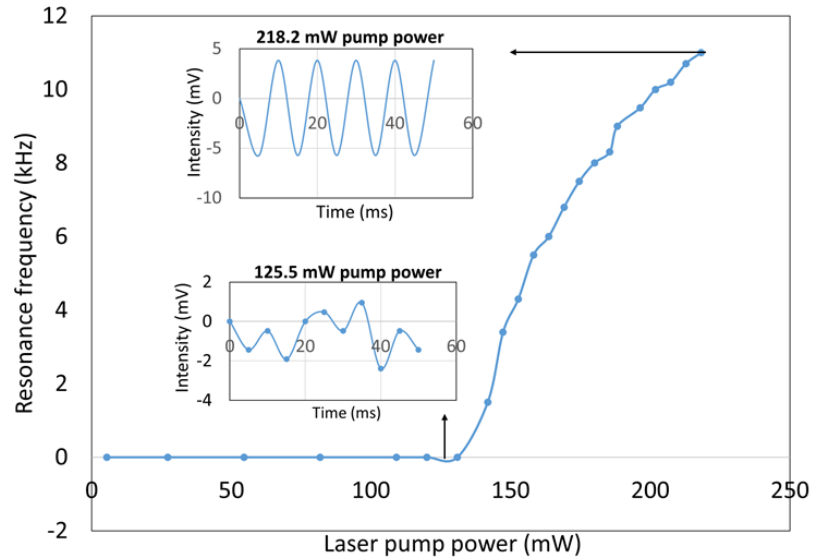


Figure 3.10: Graph of the resonance frequency (ω_r) vs the laser pump power of the EDFRL (Onubogu, et al., 2020). (The two insets show the time domain of the laser output acquired at pump powers of 125.5 mW and 218.2 mW)

The EDFRL was subjected to pump modulation to study the behavior of the laser for its resonance features, and linear and non-linear (chaotic) dynamics. Similar to the EDFLL, the diode laser pump was directly modulated by a sinusoidal signal obtained via the function generator that regulates the driving current of the diode laser pump. Pump modulation on the EDFRL was carried out for five input conditions. These input parameters are shown in Table 3.3. To further prove the accuracy and the similarity between the experimental results, more experiments were carried out on another day, using different values of ω_r and MA. All the results obtained were similar, hence only one extra result is

presented in the results and discussion in Chapter 4 for input conditions of 9 kHz ω_r at 0.4 V MA with a pump power of 188.6 mW and a frequency modulation range of (1 to 60) kHz.

Table 3.3: Input parameters used when pump-modulating the EDFRL from 1 kHz to 30 kHz

S/No.	Resonance frequency (kHz)	Modulation amplitude (V)	Laser pump power (mW)
1	2	0.4	110.4
2	3	0.4	120
3	5	0.4	127.6
4	7	0.4	150.6
5	10	0.4	180.7

With frequency and driving amplitude modulations of the laser pump, the behavior of the EDFRL changed from linear to non-linear (Kumar, and Vijaya, 2015). The EDFRL characteristics were revealed in time and frequency domain diagrams as seen in the oscilloscope (Pico scope 6). As the MF was varied from 1 kHz to 30 kHz and from 30 kHz to 1 kHz, the maximum peak-to-peak amplitude of the laser output was noted for each MF and plotted to obtain the bifurcation diagrams. The results and discussion in Chapter 4 gives full details of the bifurcation diagrams to understand the behavior of the EDFRL.

The bifurcation diagram does not only show the behavior of the laser but also illustrates the abrupt variations that occur during the modulation of a selected parameter. For a better understanding of the laser behavior, some chosen time domain and frequency domain diagrams obtained while pump

modulating the EDFRL from low frequency to high frequency are presented in Chapter 4. Time and frequency domains obtained from high to low-frequency modulations were not presented because the laser behavior is quite similar when modulating in either ascending or descending frequencies. The only difference is that ω_r is higher when modulating in descending order compared to when modulating in ascending order creating a delay between the input and output of the laser because of the switch in route. As a result, hysteresis loops forming the OB regions are seen in the bifurcation diagrams. In the past, other authors have identified similar optical bi-stable behaviors in their ring laser configurations when subjected to pump modulation as well (Pisarchik, Barmenkov and Kir'yanov, 2003; Reategui, et al., 2003, Pisrachik, and Barmenkov, 2005; Luo, Tee and Chu, 1998; Sola, Martin and Alvarez, 2002, etc.). However, the behavior displayed by the EDFRL as seen in the time domain diagrams is quite fascinating as well as very unique compared to those presented by other authors. Luo, Tee and Chu, 1998 and Pua, et al., 2012a observed that at modulation frequency much higher than the resonant frequency, the laser output is a clean sinusoidal waveform rather than pulsed. In this research, the whole optical output obtained is sinusoidal as seen in the results and discussion sections which is most probably as a result of the pump power being only up to a maximum of 245 mW and also possibly the long resonator length.

3.3.5 EDFLL subjected to experimental external loss modulation

To investigate the EDFLL's behavior when subjected to external cavity loss modulation, several parameters for instance: the modulation amplitude, modulation frequency, pump power, total cavity loss, etc. can be modulated. As mentioned earlier, external loss modulation of the EDFLL in this research was carried out with the use of a loudspeaker as the modulator with a variation of its modulation amplitude and modulation frequency in the range of 1 kHz to 20 kHz. The loudspeaker is placed directly on top of the EDF so that the EDF can quickly detect the sound waves emanating from the loudspeaker during modulation. The loudspeaker with acoustic waves between 1 kHz and 20 kHz is the selected modulator to imitate to a high degree the acoustic waves emanating through the leakage point of a pipeline transporting water, since the detection of leakage in a water pipeline is the anticipated use of the EDFL.

At a pump power of 39 mW, continuous laser emission was achieved in the EDFLL as measured experimentally. This is called the threshold pump power. At this pump power, the small-signal gain is equivalent to the cavity losses. To observe the dynamic behavior of the EDFLL under cavity loss modulation, five sets of experiments were carried out with input parameters presented in Table 3.4.

Table 3.4: Input parameters used when loss-modulating the EDFLL from 1 kHz to 20 kHz

S/No.	Resonance frequency (kHz)	Modulation amplitude (V)	Laser pump power (mW)
1	4	0.8	45
2	8	0.8	50
3	10	0.8	63
4	16	0.8	79
5	20	0.8	90

The loudspeakers' MF was then varied from (1 to 20) kHz and (20 to 1) kHz; while the laser output response for each frequency was observed via the Pico Scope. The highest peak-to-peak amplitude of the laser output for all MFs was measured and plotted in the results and discussion section. Results obtained during the experimental and theoretical external loss modulation (refer to Chapter 5) displayed the presence of linear and chaotic or non-linear behaviors in the loss-modulated EDFLL system.

3.3.6 EDFRL Subjected to Experimental External Loss Modulation

At the threshold pump power of 34.8 mW, continuous laser emission was achieved in the EDFRL as measured experimentally. Similar to the EDFLL under loss modulation, loss is also externally induced in the cavity of the EDFRL via the same loudspeaker. For the entire loss modulation experiments carried out on the EDFRL, a pump power of 76.79 mW was used to obtain 14 kHz of ω_r . In this case, the MA and the MF of the loudspeaker were the modulated parameters. During frequency modulation of the

loudspeaker, there was no response observed on the Pico Scope at 200 mV MA and below. Therefore, to understand the dynamic behavior of the EDFRL, different values of MA ranging from 200 mV to 1000 mV were used as shown in Table 3.5 for different cavity-loss modulation experiments. For each MA, the frequency was modulated from 1 kHz – 20 kHz and 20 kHz – 1 kHz.

Table 3.5: Input parameters used when loss-modulating the EDFRL from 1 kHz to 20 kHz

S/No.	Resonance frequency (kHz)	Modulation amplitude (V)	Laser pump power (mW)
1	14	0.2	76.79
2	14	0.5	76.79
3	14	0.9	76.79
4	14	1.0	76.79

During cavity-loss modulation, the maximum peak-to-peak amplitude of the laser output was measured for every MF and plotted as illustrated in the results and discussion section. The results gotten during the experimental and theoretical external loss modulation (refer to Chapter 5 of this thesis) disclosed the appearance of linear and chaotic behaviors in the loss-modulated EDFRL system.

3.4 Amplitude modulation of the EDFRL

Amplitude modulation was carried out experimentally on the EDFRL where ω_r and MF remained the same for each set of experiments. The motive behind this experiment was to find out the possibility of determining the extent

of the leakage on the pipeline based on the amplitude of the signal of the acoustic waves detected by the EDFL sensor. This experiment was carried out for the EDFRL only because the result is expected to be similar for the EDFLL. For the 5 sets of experiments with input parameters shown in Table 3.6, the input amplitude was modulated from 400 mV to 5000 mV (Onubogu, et al., 2020).

Table 3.6: Input parameters used for amplitude modulation of the EDFRL

S/No.	Resonance frequency (kHz)	Modulation frequency (kHz)	Laser pump power (mW)
1	2	2	110.4
2	3	3	120.0
3	5	5	127.6
4	7	7	148.1
5	10	10	180.7

During amplitude modulation, the maximum peak-to-peak amplitude of the laser output was noted from the time domain diagrams as seen in Pico scope 6 and plotted in the results and discussion section.

3.5 Theoretical Analysis of the EDFL under Pump Modulation to Predict the Experimental Results

To describe or predict the experimental results, a theoretical model is essential. Other similar studies as discussed in the Literature review chapter of this thesis presented either a simple or complex theoretical model that is linked to the configuration of their EDFL. In most cases, these models gave a good

description of their experimental results. The configurations of the EDFLL and EDFRL are similar to those of other authors but not exactly the same, hence their present theoretical models cannot give a correct description of the behaviors of the EDFLL and EDFRL. However, it was observed that the theoretical model of Pisarchik, Kir'yanov and Barmenkov (2005) (presented in Chapter 2.2 of this thesis) is closely related to the EDFLL and EDFRL configurations. Hence, some alterations and improvements were made to their present model to obtain the best model which describes the laser configurations in this thesis and yields correct simulation results matching the experimental results well (Onubogu, et al., 2022).

In the first modification, the ω_r of the EDFL at a certain time was considered because the EDFL has the possibility of having several values of ω_r at certain times as it is a resonator. This is very significant to classify the frequency sensitivity range of the EDFL to its detection of acoustic waves and vibration. In the theoretical model of Pisarchik, Kir'yanov and Barmenkov (2005), the ω_r of the EDFL was not considered, only the ω_{r0} . They also produced theoretical results for mainly two cases only. The first case is when the ω_{r0} is lower than the MF and the second case is when the ω_{r0} is higher than the MF. In the second modification, a chirp driving function is employed so that the simulation runs at one time over a fixed range of MFs instead of one frequency for every modulation; where the first and last MFs and the simulation time are specified in the MATLAB code. This aids in obtaining theoretical results that are much more precise. In contrast with Pisarchik, Kir'yanov and Barmenkov's original model which does not display the self-

pulsating behavior, the modified model displays the self-pulsating behavior of the EDFL and EDRFL in the absence of modulation since the saturable absorber phenomenon is included in the model (Onubogu, et al., 2022).

The modified model used for the theoretical analysis is built from two rate equations of a class B laser for the laser power inside the cavity, L_p (s^{-1}), and the population inversion \overline{N}_2 (dimensionless where $0 \leq \overline{N}_2 \leq 1$). L_p is the sum of the power of the waves being transported inside the laser cavity and \overline{N}_2 symbolizes the entire erbium ion concentration at N_2 along the pumped active fiber length (Pisarchik, et al., 2005; Luo, et al., 1998; Reátegui, 2004). The rate equations are shown below (Onubogu, et al., 2022):

$$\frac{dL_p}{dt} = S_e(t) + 4LL_p \frac{1}{2t_R} \{Q_0 Q_w [\overline{N}_2 (\varepsilon_1 - \varepsilon_2) - 1] - \alpha_{th}\} \quad (3.1)$$

$$\frac{d\overline{N}_2}{dt} = P_{pump}(t) - (\Theta_{12} Q_w L_p) \frac{1}{\pi r_0^2} (\overline{N}_2 \varepsilon_1 - 1) - \frac{\overline{N}_2}{\tau_2} \quad (3.2)$$

The description of all the variables in Equations (3.1) and (3.2) and other initial conditions employed in the theoretical analysis are found in Table 3.7. Equations (3.1) and (3.2) define the EDFL's dynamic behavior in the absence of external modulation. To activate the chaotic behavior of the EDFL, it is essential to introduce an extra variable through an external modulating signal. Hence, pumped laser power at the fiber entrance (PP) becomes:

$$PP(t) = PP_1^0 [1 + A_m \sin 2\pi F_m t] \quad (3.3)$$

where PP_1^0 is the average pump power at the fiber entrance in the absence of modulation, meaning ($A_m = 0$). Parameters F_m (modulation frequency denoted as MF in this thesis) and A_m (driving or modulation amplitude denoted as MA in this thesis) can be modulated in the experiment and numerical simulation because they depend on the pump power. In the absence of modulation, $PP = PP_1^0$ where PP_1^0 [] can be modulated to get an estimate of the ω_{r0} (that is almost equal to the ω_r of the laser) at different levels of pump power. Thus, the EDFL's ω_r is always set by increasing or reducing the input pump power before pump modulation is performed.

With the parameters in Tables 3.2 and 3.3 and Equations (3.1), (3.2), and (3.3), the dynamic behavior of the pump-modulated EDFLL and EDFRL can be analyzed theoretically via the time domain and frequency domain and also the bifurcation plots obtained. For a swift theoretical analysis to be performed, Equations (3.1) and (3.2) are simplified by normalization in the following way:

In Equation (3.1),

$$S_e(t) = \frac{Q_o \lambda_g^2 L \overline{N_2}(t) r_0^2 10^{-3}}{\tau_2 t_R \Theta_{12} 4(\pi r_f)^2} \quad (3.4)$$

In Equation (3.2),

$$P_{pump}(t) = \frac{PP[1 - e^{[-LQ_p + LQ_p \overline{N_2}(t)]}]}{\pi r_0^2 L N_0} \quad (3.5)$$

Equation (3.4) can be restated as: $S_e(t) = q_1 \overline{N_2}(t)$; given that:

$$q_1 = \frac{Q_o \lambda_g^2 L r_0^2 10^{-3}}{\tau_2 t_R \Theta_{12} 4(\pi r_f)^2}$$

Equation (3.5) can be restated as: $P_{pump}(t) = PP(t)q_2[1 - e^{-q_3(1-\overline{N}_2(t))}]$;

given that $q_2 = \frac{1}{\pi r_0^2 L N_0}$ and $q_3 = L Q_p$

Assuming that $(\Sigma_1 - \Sigma_2)$ in Equation (3.1) is equal to \mathfrak{u}_1 ; and in Equation (3.2),

$\Sigma_1 = \mathfrak{u}_2$; then Equation (3.1) can be re-written as:

$$\frac{dL_p}{dt} = q_1 \overline{N}_2(t) + 4LL_p \frac{1}{2t_R} \{Q_0 Q_w [\overline{N}_2(\mathfrak{u}_1) - 1] - \alpha_{th}\} \quad (3.6)$$

And Equation (3.2) can be re-written as:

$$\begin{aligned} \frac{d\overline{N}_2}{dt} &= PP(t)q_2[1 - e^{-q_3(1-\overline{N}_2(t))}] - (\Theta_{12} Q_w L_p) \frac{1}{\pi r_0^2} (\overline{N}_2 \mathfrak{u}_2 - 1) \\ &\quad - \frac{\overline{N}_2}{\tau_2} \end{aligned} \quad (3.7)$$

To normalize Equations (3.6) and (3.7);

First referring to Equation (3.6), assuming $N_1 = Q_w [\overline{N}_2(\mathfrak{u}_1) - 1]$, therefore

$$\overline{N}_2 = \frac{Q_w + N_1}{Q_w \mathfrak{u}_1} \text{ and } \frac{d\overline{N}_2}{dt} = \frac{dN_1}{Q_w \mathfrak{u}_1 dt}.$$

Furthermore, dividing the entire Equation (3.6) by q_1 to allow cancellation of q_1 and then replacing I_p with $\frac{L_p}{q_1}$ and

multiplying the whole Equation (3.6) by τ_2 where $\vartheta = \frac{t}{\tau_2}$ gives:

$$\frac{dI_p}{dt} = \frac{\tau_2}{Q_w \mathfrak{u}_1} (Q_w + N_1) + 2LQ_0 I_p N_1 \frac{\tau_2}{t_R} - 2L\alpha_{th} I_p \frac{\tau_2}{t_R} \quad (3.8)$$

Similarly, referring to Equation (3.7) and assuming that

$$N_2 = Q_w [\overline{N}_2(\mathfrak{u}_2) - 1], \text{ therefore } \overline{N}_2 = \frac{Q_w + N_2}{Q_w \mathfrak{u}_2} \text{ and } \frac{d\overline{N}_2}{dt} = \frac{dN_2}{Q_w \mathfrak{u}_2 dt}$$

Also, dividing the entire Equation (3.7) by q_1 where $I_p = \frac{Lp}{q_1}$ and then

multiplying Equation (3.7) by τ_2 where $\vartheta = \frac{t}{\tau_2}$ gives:

$$\frac{dN_2}{dt} = \frac{PP\tau_2 Q_w \dot{u}_2 q_2}{q_1} \left[1 - e^{\left[-q_3 \left(1 - \frac{Q_w + N_2}{Q_w \dot{u}_2} \right) \right]} \right] - \frac{(\Theta_{12} Q_w \tau_2 \dot{u}_2)}{\pi r_0^2} I_p N_2 - \frac{Q_w + N_2}{q_1}$$

To eradicate the denominator q_1 , the equation above is multiplied by q_1 to obtain:

$$\frac{dN_2}{dt} = PP\tau_2 Q_w \dot{u}_2 q_2 \left[1 - e^{\left[-q_3 \left(1 - \frac{Q_w + N_2}{Q_w \dot{u}_2} \right) \right]} \right] - \frac{(\Theta_{12} Q_w \tau_2 \dot{u}_2)}{\pi r_0^2} I_p N_2 q_1 - (Q_w + N_2) \quad (3.9)$$

Since $\frac{Q_w + N_1}{Q_w \dot{u}_1} = \frac{Q_w + N_2}{Q_w \dot{u}_2}$; then $N_1 = \frac{N_2 \dot{u}_1 + (\dot{u}_1 - \dot{u}_2) Q_w}{\dot{u}_2}$

Therefore Equation (3.8) becomes:

$$\begin{aligned} \frac{dI_p}{dt} &= \frac{\tau_2}{Q_w \dot{u}_1} \left(Q_w + \frac{\dot{u}_1 N_2}{\dot{u}_2} \right) + 2LQ_0 \left(\frac{\tau_2}{t_R} \right) \left(\frac{\dot{u}_1}{\dot{u}_2} \right) I_p N_2 - 2L \left(\frac{\tau_2}{t_R} \right) \left(\alpha_{th} - \right. \\ &\left. \frac{(\dot{u}_1 + \dot{u}_2)}{\dot{u}_2} Q_w \right) I_p \end{aligned} \quad (3.10)$$

Introducing constants, Equation (3.10) can be written as:

$$\frac{dI_p}{dt} = K_1 \left(Q_w \frac{\dot{u}_2}{\dot{u}_1} + N_2 \right) + K_2 I_p N_2 - K_3 I_p \quad (3.11)$$

Where K_1 , K_2 and K_3 are:

$$K_1 = \frac{\tau_2}{Q_w \hat{u}_1}$$

$$K_2 = 2LQ_0 \left(\frac{\tau_2}{t_R} \right) \left(\frac{\hat{u}_1}{\hat{u}_2} \right)$$

$$K_3 = 2L \left(\frac{\tau_2}{t_R} \right) \left(\alpha_{th} - \frac{(\hat{u}_1 + \hat{u}_2)}{\hat{u}_2} Q_w \right)$$

Introducing constants like in Equation (3.10), Equation (3.9) can be written as:

$$\frac{dN_2}{dt} = R_1 \left[1 - e^{\left[-LQ_p \left(1 - \frac{Q_w + N_2}{Q_w \hat{u}_2} \right) \right]} \right] - R_2 I_p N_2 - (Q_w + N_2) \quad (3.12)$$

where R_1 and R_2 are:

$$R_1 = PP\tau_2 Q_w \hat{u}_2 q_2 ; \text{ re-calling that } q_2 = \frac{1}{\pi r_0^2 L N_0}, R_1 \text{ becomes:}$$

$$R_1 = PP \frac{\tau_2 Q_w \hat{u}_2}{\pi r_0^2 L N_0} \text{ (PP represents the laser pump power at the fiber entrance)}$$

$$R_2 = \frac{(\Theta_{12} Q_w \tau_2 \hat{u}_2)}{\pi r_0^2} q_1 ; \text{ re-calling that } q_1 = \frac{Q_o \lambda_g^2 L r_0^2 10^{-3}}{\tau_2 t_R \Theta_{12} 4(\pi r_f)^2}, R_2 \text{ becomes}$$

$$R_2 = \frac{(\Theta_{12} Q_w \tau_2 \hat{u}_2)}{\pi r_0^2} \frac{Q_o \lambda_g^2 L r_0^2 10^{-3}}{\tau_2 t_R \Theta_{12} 4(\pi r_f)^2}$$

For the EDFLL and the EDFRL under pump modulation, Equation (3.11) is used to calculate the normalized laser power density, while

Equation (3.12) is used to calculate the normalized population inversion at the meta-stable level of the EDFL.

As stated earlier, the pump power in the numerical simulation is a chirp signal that delivers a continual array of MFs. Hence, the laser pump power at the fiber entrance becomes:

$$PP(t) = PP_1^0 [1 + A_m \sin(2\pi (F_m + cc \cdot t)t)] \quad (3.13)$$

where cc is the co-efficient that represents the chirp measured in Hz/s.

Additional initial parameters including the normalized inlet pump power (s^{-1}) and the MA (V) are set before the numerical simulation is run. As previously stated, ω_r of the laser system is determined by the input laser pump power. The first and last MFs are inputted into the MATLAB code together with the total chirp time during modulation which causes the frequency of the chirp to either increase (up-chirp) or decrease (down-chirp) accordingly. During simulation, a random preliminary point is used for each run as is typical in laser transient calculations. As a result, the laser response for a specific frequency when the MF is increasing may not be similar when it is decreasing since the initial condition is not the same (Sola, Martin and Alvarez, 2002). In the simulation code, the differential equations are solved with ODE45 which is the 4th-order Runge-Kutta method with adaptive step size to generate the laser response. Just as in the experimental analysis, the theoretical bifurcation diagram of the laser response is gotten by plotting the maximum-peak-to-peak amplitude measured at every MF from the time domain during

modulation, both for up-chirp and down-chirp. The frequency domain is also saved as all these diagrams indicate the dynamic behavior of the EDFL.

Table 3.7: Variables and input parameters employed in the theoretical analysis of the pump modulated and loss modulated EDFL and EDFRL (Variables and input conditions/parameters without units are non-dimensional) (Onubogu, et al., 2022)

Variable	Description	
\bar{N}_2	$\bar{N}_2 = \left(\frac{1}{n_0 L}\right) \int_0^L N_2(z) dz$	
L_p (s ⁻¹)	The average population of the meta-stable level along the length of the pumped active fiber	
N_1	Sum of light waves power contra-propagating in the cavity of the laser.	
N_2	Ground level 1 population	
S_e	Meta-stable level 2 population	
PP	$S_e = \frac{Q_0 \lambda_g^2 L \bar{N}_2 r_0^2 10^{-3}}{\tau_2 t_R \theta_{12} 4(\pi r_f)^2}$	
P_{pump}	Spontaneous discharge into the fundamental laser mode.	
R_1	Pump power at the entrance of the fiber: $PP = PP_1^0 [1 + A_m \sin 2\pi F_m t]$	
	Pump power: $P_{pump} = \frac{PP [1 - e^{-L Q_p + L Q_p N_1}]}{\pi r_0^2 L N_0}$	
	$R_1 = PP \frac{\tau_2 Q_w \bar{N}_2}{\pi r_0^2 L N_0}$ where $\frac{\tau_2 Q_w \bar{N}_2}{\pi r_0^2 L N_0} = 4.819 \times 10^{-18}$	
Parameter	Value	Definition
L (cm)	300 1300	Full length of the EDF in the case of a linear laser Full cavity length (1000 cm) plus the length of the EDF (300 cm)
R_{FBG}	0.8	The FBG coupler's total reflection coefficient.
l_{FBG} (cm)	20	Total length of the FBG coupler ends within the cavity.
r_f (cm)	2.94×10^{-4}	$r_f = r_0 \left(0.65 + \frac{1.619}{V^{1.5}} + \frac{2.879}{V^6}\right)$ The EDF's fundamental mode radius.
r_0 (cm)	2.6×10^{-4}	The radius of the EDF's core.
MFD (m)	5.2×10^{-6}	The EDF's Mode Field Diameter
n_0	1.45	The refractive index of a "cold" EDF's core
NA	0.22 - 0.24	Fiber's numerical aperture
t_R (ns)	31 10	$t_R = \frac{2n_0(L+l_{FBG})}{c}$ {for linear cavity laser} $t_R = \frac{L}{c}$ {for ring cavity laser}
τ_2 (ns)	10^7	The time taken for movement of the photon within the cavity in one cycle.
N_o (cm ⁻³)	5.4×10^{19}	The life span of the erbium ions in upper level 2.
c (cm/s)	2.9979×10^{10}	$N_o = N_1 + N_2$ The total concentration of erbium ions that are present in the active fiber
$\theta_{21} = \theta_{12}$ (cm ²)	0.3×10^{-20}	The rate at which the photons move through the cavity.
ξ_1	2.0	θ_{21} = Transverse-section of the return stimulated transition from upper level 2 to ground level 1. θ_{12} = Transverse-section of the absorption transition from ground level 1 to upper level 2.
		$\xi_1 = \frac{\theta_{12} + \theta_{21}}{\theta_{12}}$ The coefficient that illustrates the correlation between stimulated transitions and absorption.

Table 3.7 continued: Variables and input parameters employed in the theoretical analysis of the pump modulated and loss modulated EDFLL and EDFRL (Variables and input conditions/parameters without units are non-dimensional) (Onubogu, et al., 2022)

Parameter	Value	Definition	
Θ_{23} (cm ²)	9×10^{-22}	Transverse-section of the excited-state absorption (ESA) from upper level 2 to upper level 3.	
ξ_2	0.4	$\xi_2 = \frac{\Theta_{23}}{\Theta_{12}}$ The coefficient that depicts the correlation occurring at the laser wavelength between the ground-state absorption (Θ_{12}) and the ESA transverse-sections (Θ_{23})	
\hat{u}_1	1.6	$\xi_1 - \xi_2$	
\hat{u}_2	2.0	ξ_1	
Q_w	82.9×10^{-2}	$Q_w = 1 - e^{-2(r_0/r_f)}$ The factor denoting a match between the core volume of the erbium-doped active fiber and the laser fundamental mode.	
Q_0 (cm ⁻¹)	5.34×10^{-2}	$Q_0 = N_0 \Theta_{12}$ The co-efficient describing the EDF's resonant-absorption or small signal-absorption characteristics at the laser wavelength.	
Q_p (cm ⁻¹)	0.025	The co-efficient that defines the EDF's resonant or small-signal absorption characteristics at the pump wavelength.	
λ_g (cm)	1.550×10^{-4} (EDFLL) 1.560×10^{-4} (EDFRL)	The wavelength of the EDFL (gotten from the optical spectrum analyzer during experiments) (Onubogu, et al., 2020; Onubogu, and Pua, 2022)	
V	2.30	The parameter that links the fiber core radius and the numerical aperture (NA) as: $V = \frac{(NA)2\pi r_0}{\lambda_g}$	
α_{th}	38.37×10^{-3}	$\alpha_{th} = \gamma_0 + \left(\frac{1}{2L}\right) \ln\left(\frac{1}{R_{FBG}}\right)$ { for linear cavity laser } $\alpha_{th} = \gamma_0$ { for ring cavity laser } The laser threshold losses that occur within the cavity.	
γ_0	0.038	The non-resonant fiber loss	
Normalized parameters, values and formula for linear and ring lasers			
Parameter	Linear laser (EDFLL)	Ring laser (EDFRL)	Formula
K_1	0.00603	0.00603	$\frac{\tau_2}{Q_w \hat{u}_1}$
K_2	6.2×10^7	19.19×10^7	$2L Q_0 \left(\frac{\tau_2}{t_R}\right) \left(\frac{\hat{u}_1}{\hat{u}_2}\right)$
K_3	2.03×10^7	6.26×10^7	$2L \left(\frac{\tau_2}{t_R}\right) \left(\alpha_{th} - \frac{(\hat{u}_1 + \hat{u}_2)}{\hat{u}_2} Q_w\right)$
R_1	4.819×10^{-18} PP	4.819×10^{-18} PP	$PP \frac{\tau_2 Q_w \hat{u}_2}{\pi r_0^2 L N_0}$ Note: Because PP is altered to set the ω_r prior to simulation, R_1 is not exactly constant. Here, the constant is $\frac{\tau_2 Q_w \hat{u}_2}{\pi r_0^2 L N_0}$
R_2	1.46×10^4	4.5×10^4	$\frac{(\Theta_{12} Q_w \tau_2 \hat{u}_2)}{\pi r_0^2} \frac{Q_0 \lambda_g^2 L}{\tau_2 t_R \Theta_{12}} \frac{r_0^2 10^{-3}}{4(\pi r_f)^2}$

Note. Adapted directly from Onubogu, N.O., Pua, C.H., Faidz, A-R and Rose, W.C., 2022. Numerical analysis of the behavioral response of pump-modulated linear and ring erbium-doped fiber lasers, Optik, 266 (169519). <https://doi.org/10.1016/j.ijleo.2022.169519>

For external loss modulation of the EDFLL and EDFRL, the loss parameter α_{th} in parameter K_3 is varied sinusoidally as:

$$\alpha_{th}(t) = \alpha_{th_1}^0 [1 + A_m \sin(2\pi (F_m + cc \cdot t)t)] \quad (3.14)$$

where the loudspeaker's amplitude and frequency are A_m and F_m that can be modulated, while the pump power PP is fixed and $\alpha_{th_1}^0$ is the total intra-cavity losses of the EDFLL or EDFRL resonator. Hence, for loss modulation, Equation (3.11) becomes:

$$\frac{dI_p}{dt} = K_1(Q_w \frac{v_2}{v_1} + N_2) + K_2 I_p N_2 - (2.69e9 \cdot \alpha_{th}(t) - 3.8797e9) I_p \quad (3.15)$$

$$\frac{dI_p}{dt} = K_1(Q_w \frac{v_2}{v_1} + N_2) + K_2 I_p N_2 - (1.935e8 \cdot \alpha_{th}(t) - 2.89e8) I_p \quad (3.15i)$$

Equation (3.15) is the normalized laser power density for the EDFRL under loss modulation and Equation (3.15i) is the normalized laser power density for the EDFLL under loss modulation.

For the normalized population inversion during loss modulation, Equation (3.12) becomes:

$$\frac{dN_2}{dt} = PP \left[1 - e^{\left[-LQ_p \left(1 - \frac{Q_w + N_2}{Q_w v_2} \right) \right]} \right] - R_2 I_p N_2 - (Q_w + N_2) \quad (3.16)$$

Equation (3.16) is the normalized population inversion at upper level 2 for the loss-modulated EDFLL and EDFRL. Like that of pump modulation, the laser pump power at the fiber entrance is:

$$PP(t) = PP_1^0 [1 + A_m \sin(2\pi (F_m + cc \cdot t)t)]$$

The parameters used in the experimental and theoretical pump and loss modulations of the EDFLL and the EDFRL are also shown in Chapter 4, Tables 4.1 and 4.2, and in Chapter 5, Table 5.1 of this thesis.

3.6 Summary

In this chapter, the design of the EDFL sensor used for field tests on a water pipeline to detect leakage and its location has been presented. Field test on a water pipeline has been carried out and the results confirmed that the EDFL sensor can detect leakage by showing a clear difference between “no leakage” and “leakage” conditions during water flow in the pipe. Also, the EDFL has shown its leak location detection capability with 90 % accuracy. A breakdown of the analysis to be carried out to understand the sensor’s behavior including an in-depth description of the experimental configurations of the EDFLL and EDFRL and their working principle has been presented. A description of the pump and external cavity-loss modulations to be carried out experimentally on the EDFLL and EDFRL has also been presented. The derivation of the equations used for theoretical pump and loss modulations and all parameters used in the calculations have been presented as well. The results

of the experiments and simulation using theoretical equations are presented in the next two chapters.

CHAPTER 4

PUMP MODULATION OF THE EDFLL AND EDFRL

As explained earlier in Chapter 3, the main purpose of carrying out pump modulation is to trigger the laser dynamics of the EDFL and study its behavior to confirm whether bifurcations occur during pump modulation as this seems to be the cause of the instability in the sensor.

Pump modulations of the EDFLL and the EDFRL were carried out experimentally in the lab at UTAR, Sungai Long campus, and theoretically using MATLAB. The experimental setups and procedure are well described in Chapters 3.3.1 and 3.3.3 for the EDFLL and in Chapters 3.3.2 and 3.3.4 for the EDFRL. The improved theoretical model used to simulate the EDFLL and EDFRL output (bifurcation) with pump modulation is presented in Chapter 3.5 where Equation (3.11) is used to calculate the normalized laser power density, and Equation (3.12) is used to calculate the normalized population inversion at the meta-stable level of the EDFL. The initial conditions/parameters set before the experiments and numerical simulations are carried out are presented in Table 4.1 for the EDFLL and Table 4.6 for the EDFRL.

4.1 Pump modulation of the EDFLL

Four sets (set 1, set 2, set 3, and set 4) of experimental and numerical results are presented for the pump-modulated EDFLL. For each set, different values of pump power, ω_r , and MA are used to understand the impact of a combination of these parameters on the laser output (bifurcation). For easy identification of the results presented; set 1, set 2, set 3, and set 4 are named EDFLL1, EDFLL2, EDFLL3, and EDFLL4. The initial conditions for both experimental and numerical analysis for the 4 sets are shown in Table 4.1. The resonance peaks obtained experimentally and numerically are also indicated in Table 4.1 for quick matching/comparison.

Table 4.1: Initial conditions used for the experimental and numerical pump modulation of the EDFLL and the resonance peaks observed experimentally and numerically

PUMP MODULATION OF THE EDFLL								
Laser Set-up	MA (V)	Normalized MA (symbolized as 'm' in simulation)	ω_r (kHz)	MF range (kHz)	Input PP – Experiment (mW)	Normalized input PP - simulation (s^{-1})	Peaks from experiments (kHz)	Peaks from Simulation (kHz)
EDFLL1 (Fig. 4.1)	0.2	0.25	7	1 – 60	95.0	390	>8,11,19,49 9, 14, 32<	>8,12,21,48 8, 12, 26<
EDFLL2 (Fig. 4.3)	0.4	0.38	7	1 – 60	107.0	390	> 7,10,17,46 8, 13, 29 <	>7,11,19,46 7, 11, 24<
EDFLL3 (Fig. 4.4)	0.1	0.09	13	1 – 60	201.0	590	> 16, 26 16, 21 <	>14, 26 14, 21<
EDFLL4 (Fig. 4.5)	0.4	0.38	19	1 – 45	52.6	980	>5, 9, 12, 17, 29 6, 9, 12, 20 <	>6, 9, 12, 17, 29 10, 17<

*MA = Modulation Amplitude; ω_r = Resonance Frequency; MF = Modulation Frequency; PP = Pump power; > = Low to high frequency modulation; < = High to low frequency modulation

Tables 4.2, 4.3, and 4.4 are used to quantitatively analyze the bifurcation results obtained for all pump modulations of the EDFLL1, 2, 3, and 4. The bifurcation diagrams (experimental and numerical) obtained and presented in Chapter 4.1.1

to Chapter 4.1.4 were analyzed and compared in terms of “the resonance peaks” observed, “the saturation point” observed, and “the distance between the OB regions” all when modulating from low to high frequency and vice versa. The percentage error and percentage accuracy for all the compared parameters were obtained and presented in Tables 4.2, 4.3, and 4.4 and further explained in Chapter 4.1.1 to Chapter 4.1.4.

Table 4.2: Quantitative analysis of the bifurcation results obtained for all four pump modulation experiments of the EDFLL1, 2, 3, and 4 in terms of resonance frequency peak.

Laser configuration	Resonance peaks (kHz)		Percentage error (%)	Percentage accuracy (%)	Resonance Peaks (kHz)		Percentage error (%)	Percentage accuracy (%)
	Exp. L to H	Num. L to H			Exp. H to L	Num. H to L		
EDFLL 1	8	8	0.00	100.00	9	8	11.11	88.89
	11	12	8.33	91.66	14	12	14.29	85.71
	19	21	9.52	90.48	32	26	18.75	81.25
	49	48	2.04	97.96				
Average			4.97	95.03			14.72	85.28
EDFLL2	7	7	0.00	100.00	8	7	12.50	87.50
	10	11	9.09	90.91	13	11	15.38	84.62
	17	19	10.53	89.47	29	24	17.24	82.76
	46	46	0.00	100.00				
Average			4.90	95.10			15.04	84.96
EDFLL3	16	14	12.50	87.50	16	14	12.50	87.50
	26	26	0.00	100.00	21	21	0.00	100.00
	Average		6.25	93.75			6.25	93.75
EDFLL4	5	6	16.67	83.33	6	-	-	-
	9	9	0.00	100	9	-	-	-
	12	12	0.00	100	12	10	16.67	83.33
	17	17	0.00	100	20	17	15.00	85.00
	29	29	0.00	100				
Average			3.33	96.67			15.83	84.17
Total average for EDFLL 1, 2, 3 and 4			4.87	95.13			12.96	87.04
	Total percentage error obtained when matching the experimental and numerical bifurcation diagram is the average of 4.87 % and 12.96 % which is 8.91 %				Total percentage accuracy obtained when matching the experimental to numerical bifurcation diagram is the average of 95.13% and 87.04 % which 91.09 %			

*Where “L to H” means Low to High and “H to L” means high to low; “exp.” means experimental and “num.” means numerical.

Table 4.3: Quantitative analysis of the bifurcation results obtained for all four pump modulation experiments of the EDFLL1, 2, 3, and 4 in terms of the saturation frequency in the bifurcation diagram.

Laser configuration	Resonance peaks (kHz)		Percentage error (%)	Percentage accuracy (%)	Resonance Peaks (kHz)		Percentage error (%)	Percentage accuracy (%)
	Exp. L to H	Num. L to H			Exp. H to L	Num. H to L		
EDFLL1	53	50	5.66	94.33	52	50	3.85	96.15
EDFLL2	50	48	4.00	96.00	51	48	5.88	94.12
EDFLL3	42	34	19.05	80.95	42	34	19.05	80.95
EDFLL4	50	48	4.00	96.00	51	48	5.88	94.12
Total average for EDFLL 1, 2, 3 and 4			8.18	91.82			8.66	91.34
	Total percentage error obtained when matching the experimental and numerical bifurcation diagram is the average of 8.18 % and 8.66 % which is <u>8.42 %</u>				Total percentage accuracy obtained when matching the experimental to numerical bifurcation diagram is the average of 91.82 % and 91.34 % which <u>91.58 %</u>			

*Where “L to H” means Low to High and “H to L” means high to low; “exp.” means experimental and “num.” means numerical.

Table 4.4: Quantitative Analysis of the Bifurcation Results Obtained for All Four Pump Modulation Experiments of the EDFLL1, 2, 3 and 4 in Terms of the Width of OB Regions in the Bifurcation Diagram

Laser configuration	Width of OB region (exp.) (kHz)	Width of OB region (num.) (kHz)	Percentage error (%)	Percentage accuracy (%)
EDFLL1	5	4	20.00	80.00
	6	9	33.33	66.67
	18	24	25.00	75.00
Average			26.11	73.89
EDFLL2	3	4	25.00	75.00
	5	7	28.57	71.43
	19	23	17.39	82.61
Average			23.65	76.35
EDFLL3	6	6	0	100.00
	Average		0	100.00
EDFLL4	3	3	0	100.00
	7	7	0	100.00
	10	13	23.08	76.92
Average			7.69	92.31
Total average			Total percentage error obtained when matching	Total percentage error obtained when matching

			the experimental and numerical bifurcation diagram is <u>14.36</u>	the experimental and numerical bifurcation diagram is <u>85.64</u>
--	--	--	--	--

*Where “L to H” means Low to High and “H to L” means high to low; “exp.” means experimental and “num.” means numerical.

4.1.1 Experimental and Theoretical Results of the Pump-modulated EDFLL1

Starting with the experimental analysis, results are presented for EDFLL1 with the initial parameters as shown in Table 4.1. Before modulation is carried out, the voltage (modulation amplitude, MA) of the laser was set at 0.2 V while the laser pump power was set at 95 mW to obtain 7 kHz of ω_r . After inputting the initial conditions, the manual function generator is tuned from 1 kHz MF to 60 kHz of MF and vice versa to get the experimental bifurcation diagrams. During pump modulation, the highest amplitude of the laser output from peak to peak was measured for every MF and plotted as the bifurcation diagram presented in Figure 4.1(a).

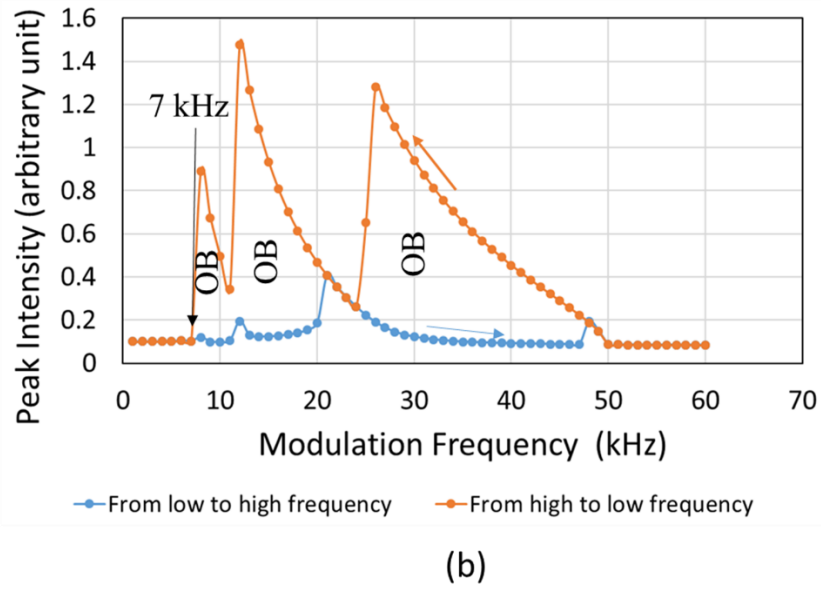
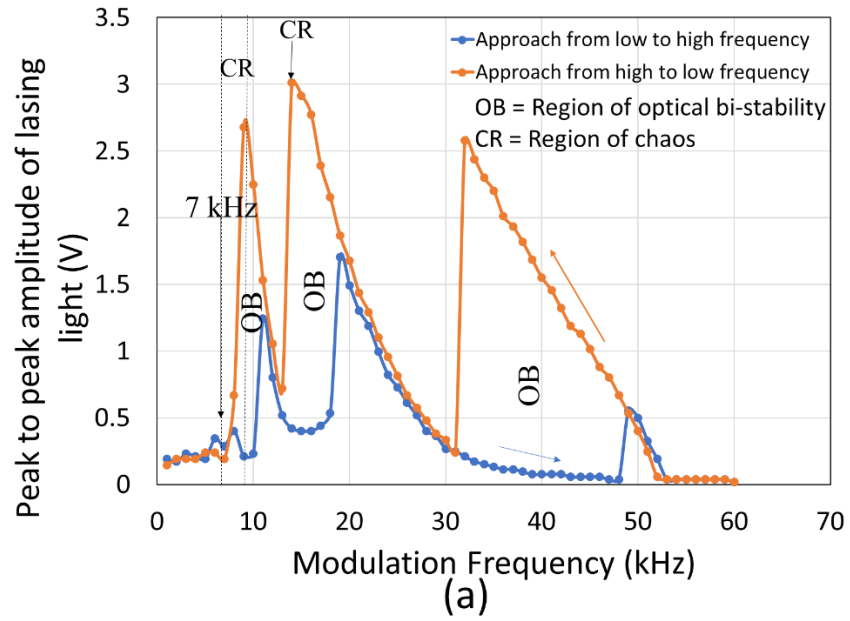


Figure 4.1 (a) Experimental (Onubogu, et al., 2019) and (b) theoretical (Onubogu, et al., 2022) bifurcation diagrams displaying the dynamical behaviors of the EDFLL1 when subjected to pump modulation at MA of 0.2 V and 7 kHz ω_r obtained by frequency variation from 1 kHz to 60 kHz and from 60 kHz to 1 kHz.

From Figure 4.1 (a), the first resonant peak appeared at 8 kHz (which is close to the main fixed ω_r of the system) when tuning the MF from 1 kHz to 60 kHz. Other peaks appeared at 11 kHz MF, 19 kHz MF, and 49 kHz MF as presented in Table 4.1 or 4.2. When tuning the MF from 60 kHz to 1 kHz, another three resonant peaks appeared at 9 kHz MF, 14 kHz MF, and 32 kHz MF. Period-doubling bifurcation and three optical bistability regions were observed as shown in Figure 4.1. The delay in the laser system's input and output because of the alteration in route causes optical bi-stability (OB). OB can be defined as a characteristic displayed by some optical devices in which two resonant transmission states are possible and steady, reliant on the input conditions. Regions of chaos occurred from 6 kHz MF to 9 kHz MF and at 14 kHz MF also, which is around or at the resonance frequency of the laser system indicating the EDFLL1's instantaneous response to external disturbances at its ω_r . This also means that the laser configuration can be employed as a highly responsive sensor in pipeline monitoring to detect when a leakage has occurred (Onubogu, et al., 2019). Figure 4.2 clearly shows the chaotic routes (irregular lasing peaks arising because of population inversion and the laser intensity interacting with each other inside the laser cavity). Period doubling bifurcation was observed at MF of 5 kHz and from 6 kHz until 9 kHz MF, a region of chaos was observed. At 10 kHz MF, resonantly enhanced pulses appeared. The cycle continued until chaos occurred again showing the natural tendency for chaos to occur in EDFLL1 when subjected to pump modulation.

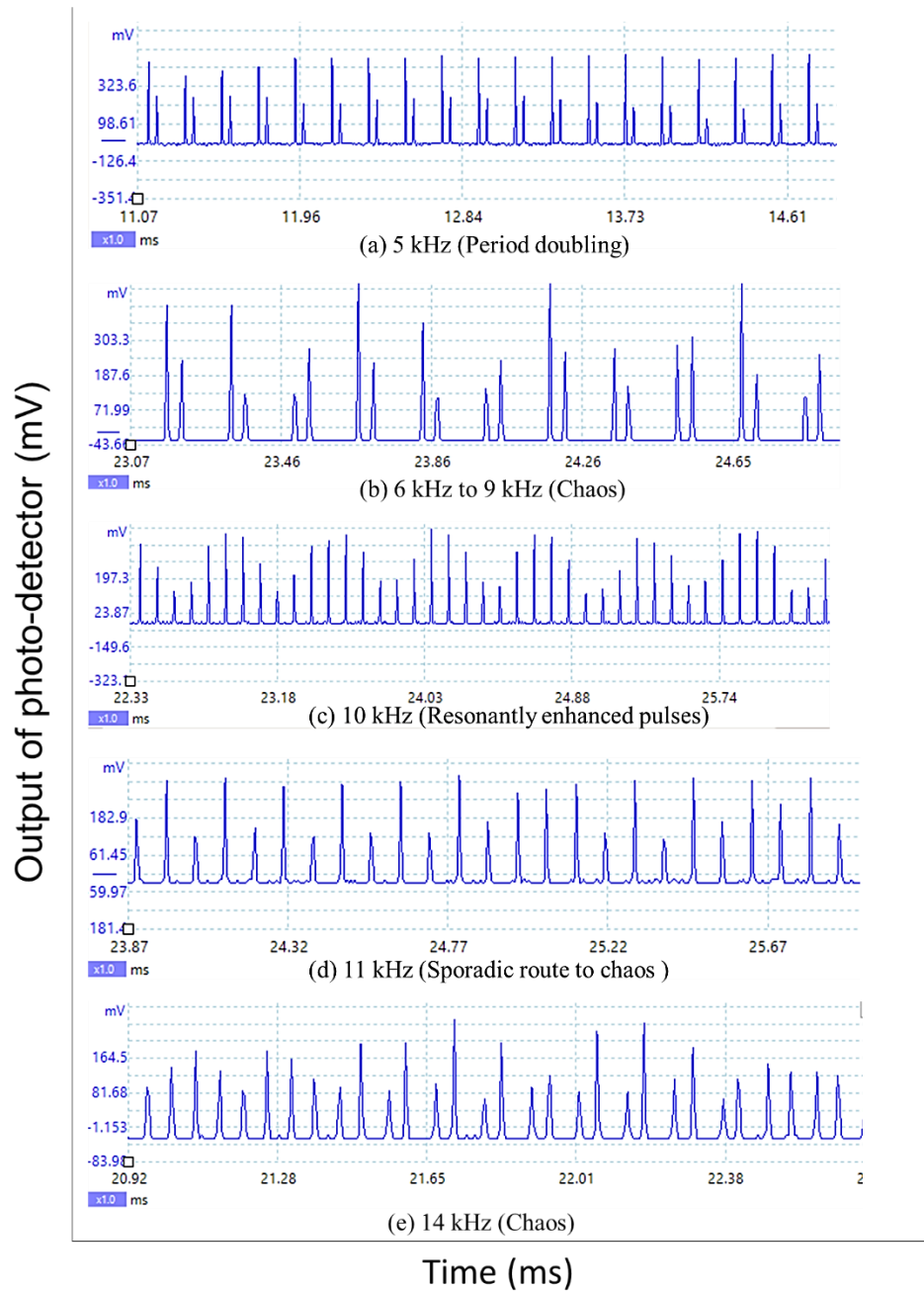


Figure 4.2: Time domain of the EDFLL1 sensor displaying its routes to chaos (Onubogu, et al., 2019).

For the theoretical simulation, values relating to the values used in the experiment were used in the calculations to achieve the normalized parameter values presented in Table 4.1. Before theoretical pump modulation was carried out, the following were the initial conditions of the EDFLL1: MA symbolized

as $m = 0.25$ (corresponding to 0.2 V); 427 s^{-1} normalized input pump power (corresponding to 95 mW) to give 7 kHz ω_r ; 1 kHz initial MF and 60 kHz final MF with a 3 seconds chirp duration. With these initial conditions, an ascending chirp was obtained, while the initial and final MF are transposed to obtain a descending chirp. The maximum peak-to-peak intensity obtained at every MF during ascending and descending chirps was recorded and plotted as the theoretical bifurcation diagram in Figure 4.1 (b).

A comparison of the experimental and theoretical bifurcation diagrams in Figure 4.1 revealed that all the resonance peaks and branches obtained experimentally are also seen in the theoretical bifurcation diagram as well. However, sometimes there is a minor shift in the frequency at which the resonance peak appears, either to the next one, two or three frequencies ahead or behind (Onubogu et al., 2020) giving a percentage accuracy of 95.03 % (from low to high frequency modulation) and 85.28 % (from high to low frequency modulation) as calculated in Table 4.2. A comparison of the frequency at which saturation occurred experimentally and theoretically in Figure 4.1 indicated a percentage accuracy of 94.33 % (from low to high frequency modulation) and 96.15 % (from high to low frequency modulation) as calculated in Table 4.3.

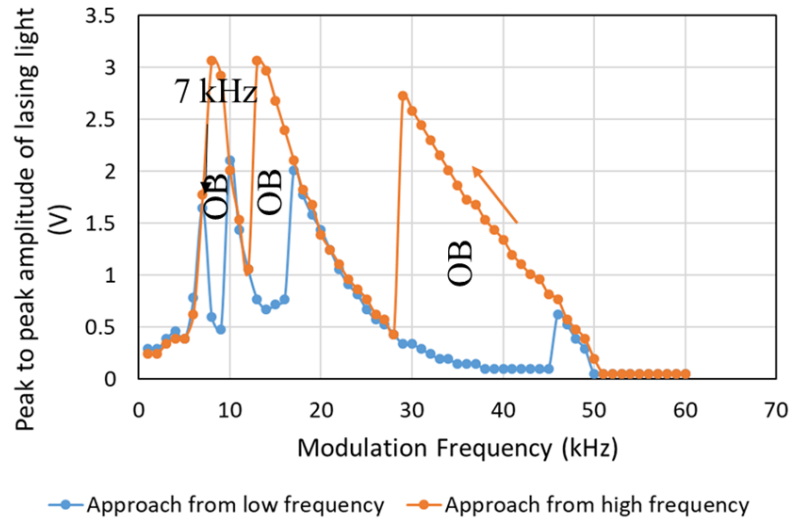
Also, the peak heights may not match experimentally and theoretically which is still satisfactory regardless (Sola, Martin and Alvarez, 2002). This is expected because the mathematical calculations for the values employed in the numerical simulation involved some estimations and approximations. For example, the total laser power inside the cavity across the length of the EDF was

averaged during the calculations; whereas in the practical sense, it is better to consider the differences in power from one end to the other end of the EDF. However, this cannot be easily achieved theoretically. Furthermore, every single loss resulting from fiber splicing and connection of other devices may not be theoretically accounted for. A very important fact to also remember is the EDFL's extreme response to vibrations and other external disturbances that even a touch or a minor change in the set-up during the experiments can lead to an alteration in the anticipated results. This issue was unavoidable because the experimental setup was not set in a fixed position to allow for easy conversion from EDFLL to EDFRL configurations due to limited equipment. It was also observed that the profile shape, regions of chaos, and width of the various regions of OB obtained experimentally were appropriately predicted theoretically to an acceptable extent with 73.89 % accuracy. Hence, it can be concluded that the EDFLL1 system response can be modeled or theoretically predicted. Other authors (Sola, Martin and Alvarez, 2002; Pisarchik, Kir'yanov and Barmenkov, 2005; Luo, et al., 1998; Kumar, and Vijaya, 2015; Reategui, et al, 2003) have also obtained similar results. A comparison of the time domain and frequency domain of the experimental and theoretical bifurcation results (not presented in this thesis) indicated a good agreement too.

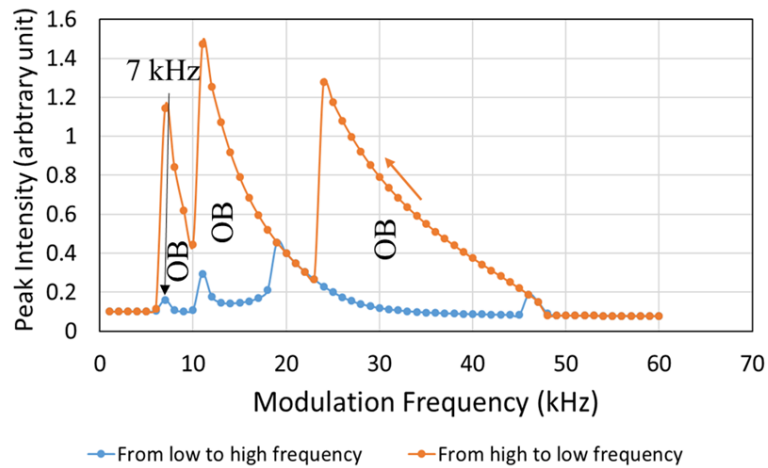
4.1.2 Experimental and Theoretical Results of the Pump-modulated EDFLL2

To circumvent any inconsistency and firmly demonstrate that the theoretical model truly describes the pump-modulated EDFLL well, a second

theoretical bifurcation result in comparison with the experimental result is presented in Figure 4.3. The initial conditions for the EDFLL2 before experimental pump modulation was carried out are MA of 0.4 V and laser pump power of 107 mW (corresponding to 7 kHz ω_r) from the laser diode pump to the EDF. The manual function generator was then tuned from 1 kHz MF to 60 kHz MF and back again. The laser's maximum peak-to-peak amplitude was measured for each frequency change during modulation. For the theoretical simulation, initial conditions for the EDFLL2 before pump modulation are: MA symbolized as $m = 0.38$ (corresponding to 0.4 V); 390 s^{-1} normalized input pump power (corresponding to 107 mW) to obtain 7 kHz ω_r ; 1 kHz initial MF and 60 kHz final MF with a 3 seconds chirp duration to get an ascending chirp during pump modulation. The initial MF and final MF are transposed to obtain the descending chirp. The maximum peak-to-peak intensity at every MF during ascending and descending chirps was recorded and plotted as the theoretical bifurcation diagram in Figure 4.3 (b).



(a)



(b)

Figure 4.3 (a) Experimental and (b) theoretical bifurcation diagrams describing the dynamic behaviors of the EDFLL2 subjected to pump modulation at MA of 0.4 V and 7 kHz ω_r gotten by frequency variation from 1 kHz to 60 kHz and from 60 kHz to 1 kHz (Onubogu, et al., 2022).

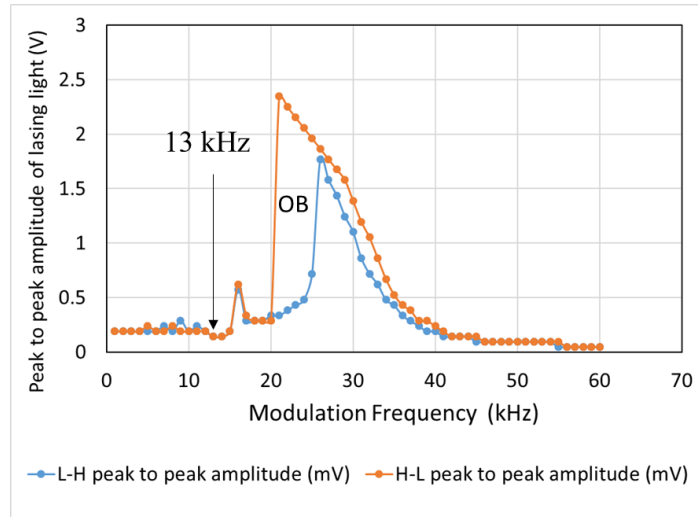
Similar physiognomies as seen in Figure 4.1 were observed when the experimental and the theoretical bifurcation diagrams in Figure 4.3 were compared with each other. Resonance peaks at (7, 10, 17, and 46) kHz for the ascending chirp and (8, 13, and 22) kHz for the descending chirp are depicted in

the experimental bifurcation diagram in Figure 4.3 (a). In Figure 4.3 (b), the theoretical bifurcation diagram exhibited resonance peaks at (7, 11, 19, and 46) kHz for the ascending chirp and at (7, 11, and 24) kHz and vice versa. For the ascending chirp, the 1st peak appeared at 7 kHz both experimentally and theoretically, where 7 kHz is the fixed ω_r of the EDFLL2 (Onubogu, et al., 2022). The resonance peaks appearing experimentally and theoretically are a close or exact match to each other with an accuracy of 95.10 % for the ascending chirp and 84.96 % for the descending chirp (Table 4.2). A comparison of the frequency at which saturation occurred experimentally and theoretically in Figure 4.3 showed an accuracy of 96 % and 94.12 % for the ascending and descending chirps respectively as shown in Table 4.3. Also, it was observed that the various regions of OB obtained experimentally were predicted theoretically with 76.35 % accuracy. Hence, it can be concluded that the experimental bifurcation result can be predicted theoretically.

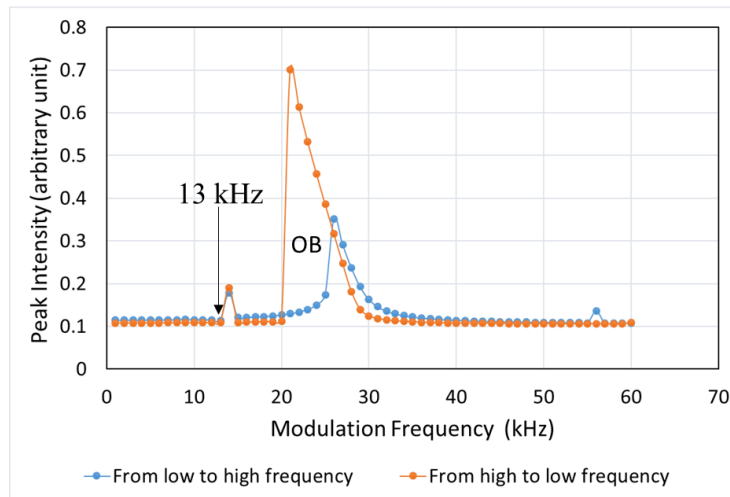
4.1.3 Experimental and Theoretical Results of the Pump-modulated EDFLL3

To further prove the correctness of the theoretical model for the pump-modulated EDFLL, another theoretical bifurcation result in comparison with the experimental bifurcation result is presented in Figure 4.4. To obtain the experimental bifurcation diagram illustrated in Figure 4.4 (a), the MA was decreased to 0.1 V while 201 mW laser power was pumped (corresponding to 13 kHz ω_r) from the laser diode pump to the EDF. The manual function

generator was then tuned from 1 kHz MF to 60 kHz MF and the other way around. To get the theoretical bifurcation diagram in Figure 4.4 (b), initial conditions for the EDFLL3 before pump modulation as shown in Table 4.1 are: MA symbolized as $m = 0.09$ (corresponding to 0.1 V); 590 s^{-1} normalized input pump power (corresponding to 201 mW) to obtain 13 kHz ω_r ; 1 kHz initial MF and 60 kHz final MF with a 3 seconds chirp duration to obtain an ascending chirp during pump modulation. The first and last MF are transposed to obtain the descending chirp. The maximum peak-to-peak intensity at every MF during ascending and descending chirps was recorded and plotted as the theoretical bifurcation diagram in Figure 4.4 (b).



(a)



(b)

Figure 4.4: (a) Experimental and (b) theoretical bifurcation diagrams describing the EDFLL3's dynamic behaviors when subjected to pump modulation at MA of 0.1 V and 13 kHz ω_r gotten by frequency variation from 1 kHz to 60 kHz and from 60 kHz to 1 kHz (Onubogu, et al., 2022).

In Figure 4.4 (a), the ascending chirp of the experimental bifurcation diagram exhibited resonance peaks at 16 kHz and 26 kHz while the descending chirp exhibited resonance peaks at 16 kHz and 21 kHz. In Figure 4.4 (b), the

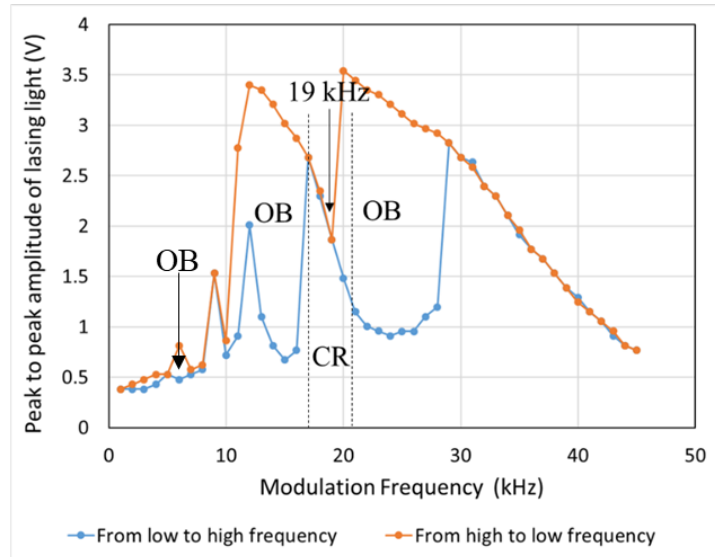
ascending chirp of the theoretical bifurcation diagram exhibited resonance peaks at 14 kHz and 26 kHz, and 14 kHz and 21 kHz for the descending chirp (Onubogu, et al., 2022). The fixed ω_r of the EDFLL3 system is 13 kHz and there is a resonance peak very close to the ω_r (at 14 kHz) for ascending and descending chirps. Figure 4.4 and Table 4.2 showed that the resonance peaks of the ascending and descending chirp obtained both experimentally and theoretically match well with an accuracy of 93.75 %. A comparison of the frequency at which saturation occurred experimentally and theoretically in Figure 4.4 indicated an accuracy of 80.95 % for both the ascending chirp and the descending chirp as calculated in Table 4.3. It was also observed that the profile shape and width of the various regions of OB obtained experimentally were appropriately predicted theoretically with 100 % accuracy.

4.1.4 Experimental and Theoretical Results of the Pump-modulated EDFLL4

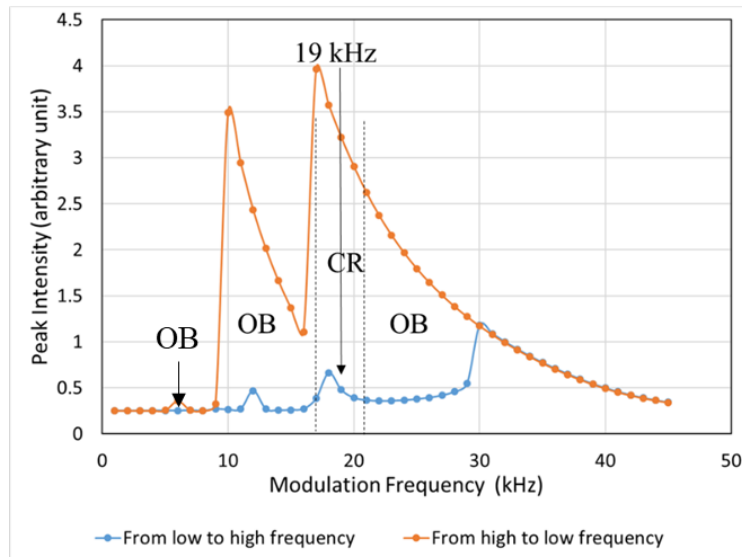
EDFLL4 is the fourth linear laser configuration but in this case, the set-up was completely dismantled, packed up, and then constructed again the next day before the experiment was performed. This is in contrast with the EDFLL1, EDFLL2, and EDFLL3 where the set-up was left in a fixed position for all three experiments. The EDFLL4 experiment was carried out to check if there are any differences in the results obtained from dismantling and re-constructing the laser set-up. However, the result obtained is still as expected and similar to the result obtained from the other EDFLL experiments. This is a confirmation that dismantling and re-constructing the set-up does not really

have an effect on the sensitivity of the sensor and hence similar results are obtained.

The parameters used in obtaining the bifurcation diagrams for the EDFLL4 are shown in Table 4.1. To get the experimental bifurcation diagram illustrated in Figure 4.5 (a), the MA was set to 0.4 V while the laser was pumped at a power of 52.6 mW (equivalent to 19 kHz ω_r) from the laser pump to the EDF. After that, the frequency was varied from 1 kHz MF to 45 kHz MF. To get the theoretical bifurcation diagram in Figure 4.5 (b) for the EDFLL4, the initial conditions inputted before pump modulation is performed are: MA symbolized as $m = 0.38$ (corresponding to 0.4 V); 980 s^{-1} normalized input pump power which corresponds to 52.6 mW; 1 kHz initial MF and 45 kHz final MF with a 3 seconds chirp duration to obtain an ascending chirp during pump modulation. Transposing the initial and final MF results in the descending chirp.



(a)



(b)

Figure 4.5: (a) Experimental and (b) theoretical bifurcation diagrams describing the EDFLL4's dynamic behaviors when subjected to pump modulation at MA of 0.4 V and 19 kHz ω_r gotten by frequency variation from 1 kHz to 45 kHz and from 45 kHz to 1 kHz (Onubogu, and Pua, 2022).

In Figure 4.5 (a), the experimental bifurcation diagram exhibited resonance peaks at (5, 9, 12, 17, and 29) kHz for the ascending chirp and at (6, 9, 12, and 20) kHz for the descending chirp (Onubogu, and Pua, 2022). It is important to note that the second OB region appears to be wider than the first OB region as expected. There are three OB regions here even though the first OB region existing between 5 kHz and 7 kHz is quite small but obvious. In the theoretical bifurcation diagram in Figure 4.5 (b), resonance peaks appear at 6 kHz, 9 kHz, 12 kHz, 17 kHz, and 29 kHz for the ascending chirp and at 10 kHz and 17 kHz vice versa. The EDFLL4 system has a fixed ω_r of 19 kHz, and the resonance peaks for both ascending and descending chirps can be seen nearby the ω_r (at 17 kHz) which is within the chaotic region.

Figure 4.5 and Table 4.2 showed that the resonance peaks obtained both experimentally and theoretically match well with an accuracy of 95.13 % for the ascending chirp and 87.04 for the descending chirp. A comparison of the frequency at which saturation occurred experimentally and theoretically in Figure 4.5 indicated an accuracy of 96 % for the ascending chirp and 94.12 % for the descending chirp as calculated in Table 4.3. More so, it was observed that the width of the various regions of OB obtained experimentally was predicted theoretically with an accuracy of 92.31 %.

The time domains for different MFs of the EDFLL4 under pump modulation were captured and plotted in Figure 4.6 to further understand the laser dynamics behavior of the EDFLL4.

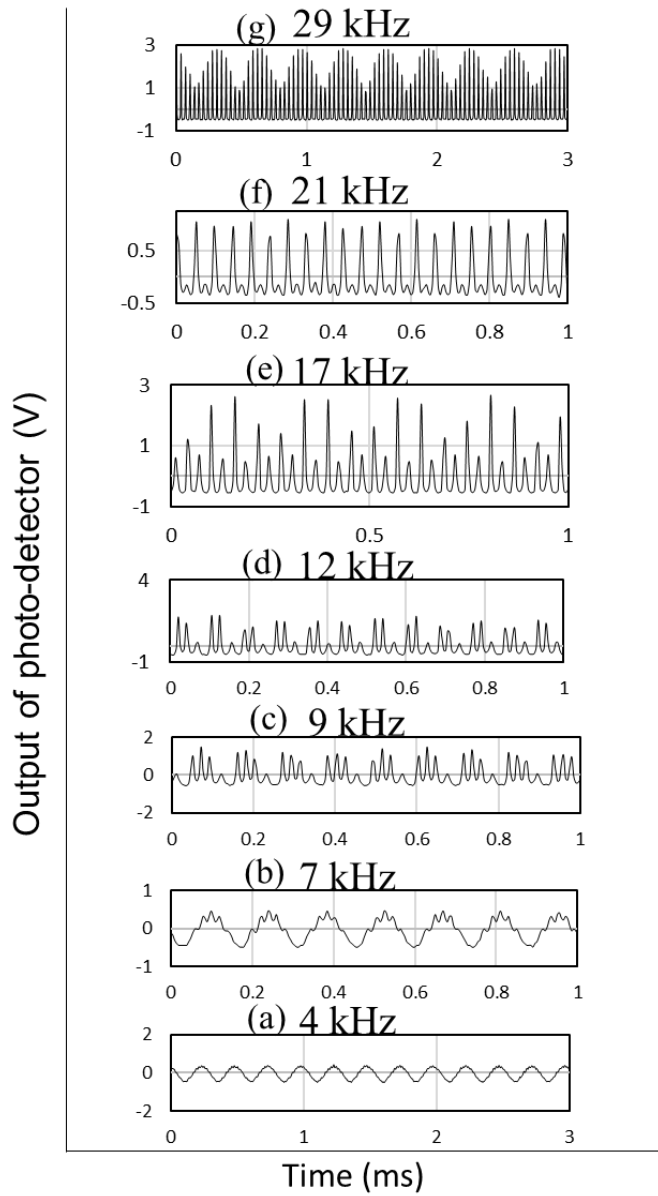


Figure 4.6: Time domain plots for some selected MFs of the pump-modulated EDFLL4 at MA of 0.4 V and 19 kHz ω_r (Onubogu, and Pua, 2022).

Table 4.5 gives a detailed description of the linear to non-linear behaviors observed.

Table 4.5: Detailed description of the linear to non-linear behaviors observed when the EDFLL4 was subjected to pump modulation at MA of 0.4 V and 19 kHz ω_r

Modulation Frequency Range (kHz)	Behavior Exhibited
1 – 6	A lasing waveform similar to that of amplitude modulation was seen as displayed in Figure 4.6 (a) for 4 kHz.
7	Four tiny peaks appeared on the apex of each sinusoidal wave as shown in (Figure 4.6 (b)).
8	The four tiny peaks decreased to two peaks in each sinusoidal wave.
9 – 10	Period-doubling bifurcation was observed where three long pulses and one tiny pulse were seen reiterating as in Figure 4.6 (c).
11	Three peaks appeared at the top of a sinusoidal waveform
12 – 13	Two long peaks followed by a small peak were generated repetitively (Figure 4.6 (d)).
14 – 16	A single sinusoidal wave appeared repeatedly with 2 tiny peaks on the crest.
17 – 20	Repetitive resonantly enhanced pulses with some peaks having a much higher amplitude than the rest were seen ((Figure 4.5 (e)). This indicated a period-doubling route to chaos.
21	Chaos occurred (Figure 4.6 (f)).
22 – 34	Period-doubling bifurcation was seen again but with a higher order of pulses appearing repeatedly as illustrated in Figure 4.6 (g).
35 – 37	Chaos was observed after which resonantly improved pulses of higher order appearing repeatedly were seen followed by stable pulsation from MF of 38 kHz to 45 kHz.
38 – 45	Stable pulsation

It is important to note that 17 kHz to 21 kHz marked the first region of chaos as shown in Figure 4.5, where 19 kHz is the ω_r of the laser system. At this chaotic region and the exact ω_r , the EDFLL4 has maximum sensitivity to external perturbations and can be employed for ultrasonic wave detection and

even detection of acoustic waves with even low frequencies. In this way, the EDFL sensor can be employed for water, oil, or gas pipeline monitoring for the detection of a vandalization or leak in the pipe. This is the anticipated use of this sensor. Bio-mimicking and multi-stable switching are other probable applications of the sensor. The chaotic paths observed and the existence of chaos after a series of period-doubling indicate the propensity for chaos to occur in the EDFLL4 as anticipated in an EDFL subjected to pump modulation for some variations of the MF with constant pump power.

The dynamical behaviors described for the EDFLL (1, 2, 3, and 4) under pump modulation confirm the occurrence of bifurcation. There is also an effect observed on the bifurcation of the EDFLL from the variation of the ω_r and the MA during various pump modulation experiments. In the EDFLL1 pump modulation experiment where the MA was 0.2 V and 7 kHz ω_r , three OB regions were observed. However, the second OB region appeared to be wider than the first and had the highest amplitude while the third OB region was the widest. In the EDFLL2 pump modulation experiment where the MA was increased to 0.4 V and the ω_r remained the same, three OB regions were also observed having a similar pattern with that of 0.2 V MA. When the MA was decreased to 0.1 V (EDFLL3 pump modulation experiment), only one OB region was observed even though the ω_r was increased to almost twice the ω_r in EDFLL1 and EDFLL2. Lastly, in the EDFLL4 pump modulation experiment, the MA was increased to 0.4 V and the ω_r was almost thrice the ω_r of EDFLL1 and EDFLL2. Three OB regions with similar patterns to that observed for the EDFLL1 were

gotten regardless of the high ω_r . In conclusion, the bifurcation observed in all the EDFLL pump modulation experiments indicated that as the MA is increased, more OB regions appear (Sola, Martin and Alvare, 2002), regardless of the ω_r and pump power value until a saturation point is reached.

It can be concluded that the response of the pump-modulated EDFLL can be modeled and predicted theoretically with an overall average accuracy of 91.09 % for the resonance frequency peaks (Table 4.2); 91.58 % for the frequency after which saturation is observed (Table 4.3) and 85.64 % for the width of the OB regions (Table 4.4). Other authors such as Sola, Martin and Alvarez, 2002; Pisarchik, Kir'yanov and Barmenkov, 2005; Luo, et al., 1998; Kumar, and Vijaya, 2015; Reategui et al., 2003) have succeeded in producing theoretical results that described all the characteristics experimentally observed.

4.2 Pump Modulation of the EDFRL

Six sets of experimental and numerical results are presented for the pump-modulated EDFRL. For all sets, the MA is a fixed value while the pump power and ω_r are different for each set to understand the impact of varying this input condition on the laser output (bifurcation). For easy identification of the results presented; set 1, set 2, set 3, set 4, set 5, and set 6 are named EDFRL1, EDFRL2, EDFRL3, EDFRL4, EDFRL5, and EDFRL6. The initial conditions for both experimental and numerical analysis for the six sets are shown in Table 4.6. The resonance peaks obtained experimentally and numerically are also indicated in Table 4.6 for quick matching/comparison.

Table 4.6: Initial conditions used for the experimental and numerical pump modulation of the EDFRL

PUMP MODULATION OF THE EDFRL								
Laser Set-up	MA (V)	Normalized MA (Symbolized as 'm' in Simulation)	ω_r (kHz)	MF Range (kHz)	Input PP – Experiment (mW)	Normalized Input PP - Simulation (s^{-1})	Peaks from Experiments (kHz)	Peaks from Simulation (kHz)
EDFRL1 (Fig. 4.7)	0.4	0.38	2	1 – 30	110.4	70	>2,4,8,20 5, 8, 21<	>2,4,7,17
EDFRL2 (Fig. 4.8)		0.38	3	1 – 30	120.0	94	>3,5,9,20 3, 5, 8, 20<	>3,5,8,20
EDFRL3 (Fig. 4.9)		0.38	5	1 – 30	127.6	104	>4,7,20 5, 8, 22<	>5,9,21
EDFRL4 (Fig. 4.10)		0.38	7	1 – 30	150.6	220	>5,10 5, 10<	>7,12
EDFRL5 (Fig. 4.11)		0.38	10	1 – 30	180.7	400	>3,5,7,13 7, 11<	>10,16
EDFRL 6 (Fig. 4.12)	0.4	0.38	9	1 – 60	188.6	390	>9,13,21,54 10, 16, 34<	>9,13,23,55 8, 13, 29<

*MA = Modulation Amplitude; ω_r = Resonance Frequency; MF = Modulation Frequency; PP = Pump power; > = Low to high frequency modulation; < = High to low frequency modulation

Tables 4.7 and 4.8 are used to quantitatively analyze the bifurcation results obtained for all pump modulations of the EDFRL1, 2, 3, 4, 5, and 6. The plotted bifurcation diagrams presented in Chapter 4.2.1 to Chapter 4.2.6 were analyzed and compared in terms of “the resonance peaks” and “the saturation point” observed when experimentally and numerically pump-modulating the EDFRL from low to high frequency only. From the analysis, the percentage error and percentage accuracy of the compared parameters were obtained and presented in Tables 4.7 and 4.8 and further explained in Chapter 4.2.1 to Chapter 4.2.6.

Table 4.7: Quantitative Analysis of the Bifurcation Results Obtained for All Six Pump Modulation Experiments of the EDFRL1 to 6 in Terms of Resonance Frequency Peak.

Laser Configuration	Resonance Peaks (kHz)	Resonance Peaks (kHz)	Percentage Error (%)	Percentage Accuracy (%)
	Exp. L to H	Exp. L to H		
EDFRL 1	2	2	0.00	100.00
	4	4	0.00	100.00
	8	7	12.50	87.50
	20	17	15.00	85.00
Average			6.89	93.13
EDFRL2	3	3	0.00	100.00
	5	5	0.00	100.00
	9	8	11.11	88.89
	20	20	0.00	100.00
Average			2.78	97.22
EDFRL3	4	5	20.00	80.00
	7	9	22.22	77.78
	20	21	4.76	95.24
Average			21.11	78.89
EDFRL4	5	7	28.57	71.43
	10	12	16.67	83.33
Average			22.62	77.38
EDFRL5	7	10	30.00	70.00
	13	16	18.75	81.25
Average			24.38	75.63
EDFRL6	9	9	0.00	100.00
	13	13	0.00	100.00
	21	23	8.70	91.30
	54	55	1.82	98.18
Average			2.63	97.37
Total average for EDFRL 1 to EDFRL 6			13.40	86.60

*Where “L to H” means Low to High and “H to L” means high to low; “exp.” means experimental and “num.” means numerical.

Table 4.8: Quantitative analysis of the bifurcation results obtained for all six pump modulation experiments of the EDFRL1 to 6 in terms of the saturation frequency in the bifurcation diagram.

Laser Configuration	Resonance peaks (kHz)		Percentage Error (%)	Percentage Accuracy (%)
	Exp. L to H	Num. L to H		
EDFRL1	23	18	21.74	78.26
EDFRL2	22	21	4.55	95.45
EDFRL3	19	19	0.00	100.00
EDFRL4	19	20	5.00	95.00
EDFRL5	19	25	24.00	76.00
EDFRL6	57	57	0.00	100.00
Total average for EDFRL 1 to 6			9.21	90.79

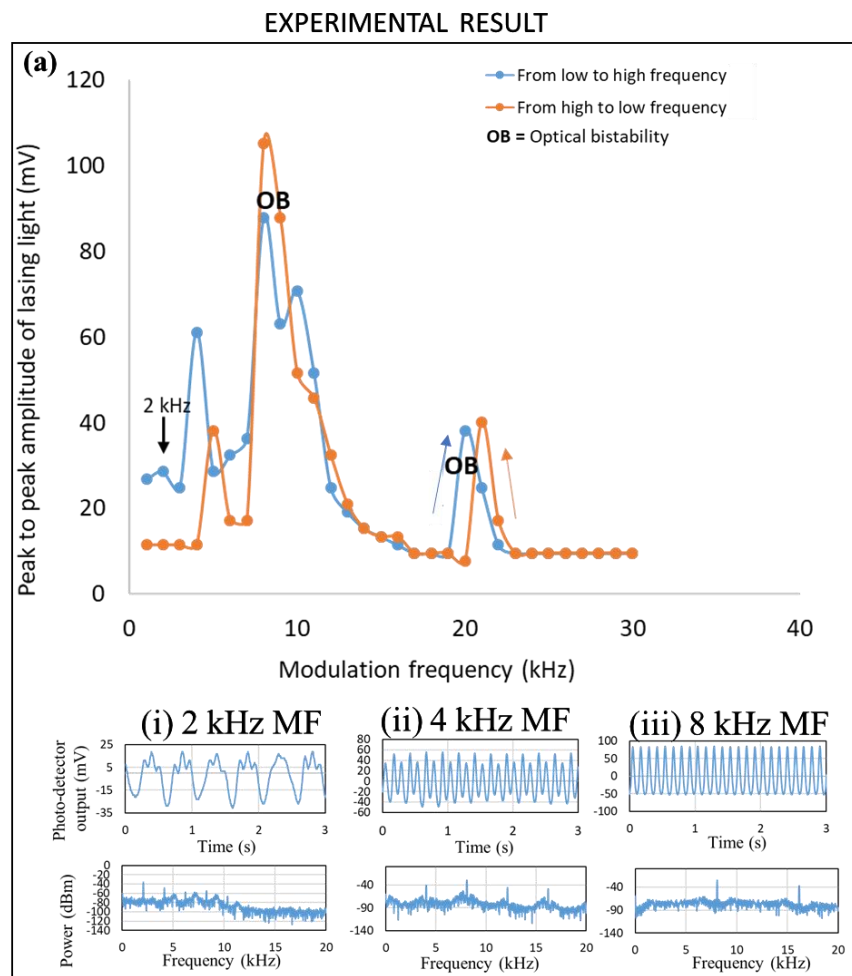
*Where “L to H” means Low to High and “H to L” means high to low; “exp.” means experimental and “num.” means numerical.

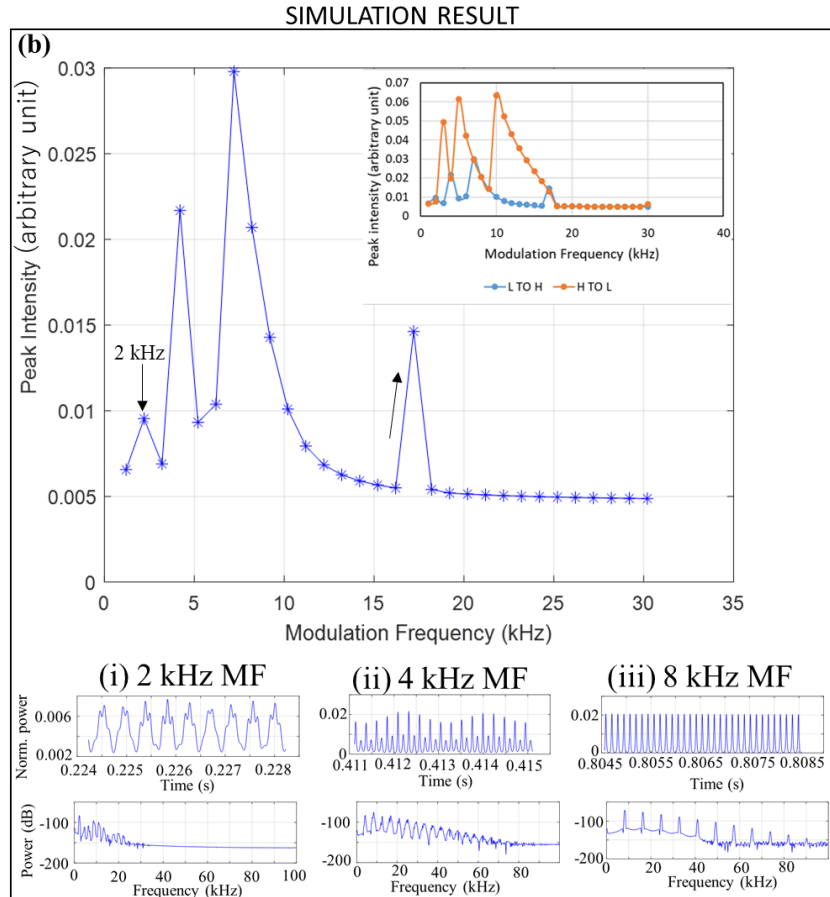
4.2.1 Experimental and Theoretical Results of the Pump-modulated EDFRL1

Experimental and theoretical results are presented for pump-modulated EDFRL with the initial parameters as shown in Table 4.6. Pump modulation experiments on the EDFRL were carried out five times using different ω_r values: 2 kHz (EDFRL1), 3 kHz (EDFRL2), 5 kHz (EDFRL3), 7 kHz (EDFRL4) and 10 kHz (EDFRL5). With a fixed MA of 0.4 V, pump modulation was performed from 1 kHz MF to 30 kHz MF and from 30 kHz MF to 1 kHz MF (Onubogu, et al., 2020). One more experiment was carried out with a longer modulation frequency range (1 kHz MF to 60 kHz MF and vice versa) to confirm the results of the first five experiments. In this case, an initial condition of 9 kHz ω_r (EDFRL6) with a fixed MA of 0.4 V was employed. In all experiments, the laser output's maximum peak-to-peak

amplitude was meticulously measured for each MF and plotted as the bifurcation diagram.

The experimental and theoretical result of the EDFRL1 subjected to pump modulation with an initial condition of 2 kHz ω_r (corresponding to 110.4 mW pump power) is illustrated in Figure 4.7.





Note: L means **low frequency** and H means **high frequency**

Figure 4.7: (a) Experimental and (b) theoretical bifurcation diagrams displaying the EDFRL1's dynamic behaviors obtained by modulating the frequency from 1kHz MF to 30 kHz MF and from 30 kHz to 1 kHz at MA of 0.4 V and 2 kHz ω_r (Onubogu, et al., 2020; Onubogu, et al., 2022).

For the experimental bifurcation diagram in Figure 4.7 (a), five resonant peaks were seen at (2, 4, 8, 10, and 20) kHz while modulating from 1 kHz frequency to 30 kHz frequency (ascending chirp). Some selected time and frequency domain figures are shown underneath the bifurcation diagram to display the dynamical regimes. The frequency domain figures presented beneath the time domain figures show the fundamental resonance peak and higher

harmonic resonance peaks (Onubogu et al, 2020). In the bifurcation diagram, the presence of a resonance peak near the ω_r or exactly at the ω_r of the EDFRL specifies its fundamental resonance and its sensitivity. This means that when the EDFRL is driven at a frequency close to or exactly at its natural frequency, it turns out to be a damped linear oscillator (Onubogu, et al., 2020, Pisarchik, et al., 2005). In the experimental bifurcation diagram, it was observed that an increase in the MF causes a shift in the resonance peaks as observed in the frequency domain. This continued until the EDFRL1 reached a saturation point at MF of 23 kHz where no resonance peak was seen afterward. The saturation point can be called the ω_{ro} of the laser system. At the saturation point or frequency, the laser system relaxes almost at its stable state. A lag in the EDFRL1's input and output caused the resonance peaks of the descending chirp to shift to (5, 8, 11, 16, and 21) kHz, forming two OB regions in the bifurcation diagram.

In explaining the time domain diagrams, a non-linear sinusoidal output denotes a chaotic response while a steady sinusoidal waveform denotes a linear response. Table 4.9 describes the behaviors observed as seen in the time domain diagrams.

Table 4.9: Detailed description of the linear to non-linear behaviors observed when the EDFRL1 was subjected to experimental pump modulation at MA of 0.4 V and 2 kHz ω_r

Modulation frequency range (kHz)	Behavior exhibited
1 – 3	Chaos was observed as three tiny peaks were seen at the apex of most of the non-linear sinusoidal waveforms (Figure 4.7 (a)(i)).
4	A period-doubling path reiterating after every two sinusoidal waveforms was seen as shown in Figure 4.7 (a)(ii).
5	Chaos was observed again.
6	Period-doubling route was observed.
7	Chaos was exhibited again
8 – 12	Linear response was seen (Figure 4.7 (a)(iii))
13	Chaotic response was observed
14 – 15	Linear response was observed
16 – 19	Chaos occurred
20	Stable sinusoidal waveform was seen
21 – 30	Chaos was observed

The dynamic behavior of the EDFRL1 from linear to non-linear showed that at low or high MFs and at frequencies close to or at the ω_{ro} and the ω_r , chaos can be generated. Because of this, the EDFRL is likely to be used for pipeline monitoring for leakage detection and also for bio-systems modeling as well; including the respiratory systems and the heart (Kumar and Vijaya, 2015a) because the chaotic region is a region of very high sensitivity.

For the theoretical result of the EDFRL1, the bifurcation diagram shown in Figure 4.7 (b) is only for modulation from low to high frequency, i.e., ascending chirp. This is because it is much easier for a comparison to be done between the experimental and theoretical bifurcation diagrams this way

due to a strange dynamic behavior that was noticed during modulation. This strange behavior was observed for pump-modulated EDFRL1, EDFRL2, EDFRL3, EDFRL4, and EDFRL5 (please refer to Table 4.6 for their input conditions and Figures 4.8 to 4.11 for their bifurcation diagrams) which were all carried out on the same day. The cause of this is still unidentified and hence entails additional research. In Figure 4.7 (b), a small inset plot shows the actual theoretical bifurcation diagram attained by plotting the maximum amplitude of the laser output measured from peak to peak at each MF during modulation from low to high frequency and the other way around. It clearly demonstrates that there is a match between the behaviors attained experimentally and theoretically during ascending chirp. However, the behaviors obtained both experimentally and theoretically during descending chirp do not match each other. This is quite a novel strange behavior because the same normalized rate equations used to simulate the ascending chirp were also used for the descending chirp. Therefore, it is correct to conclude that the EDFRL1, 2, 3, 4, and 5 bifurcation diagrams of the theoretical descending chirp are appropriately predicted because they all have similar results. Also, the results obtained for other input conditions (inclusive of those not illustrated in this thesis) presented comparable theoretical trends that had a good match with their experimental results. This means that the unusual behavior is not from the theoretical bifurcation but from the experimental bifurcation. This result is presented in this thesis irrespective of the unusual behavior as it may have possible future applications based on further studies wherein the theoretical model can be altered to obtain other results that could be used for other applications. However, it is essential to note that throughout the EDFRL1 to 5

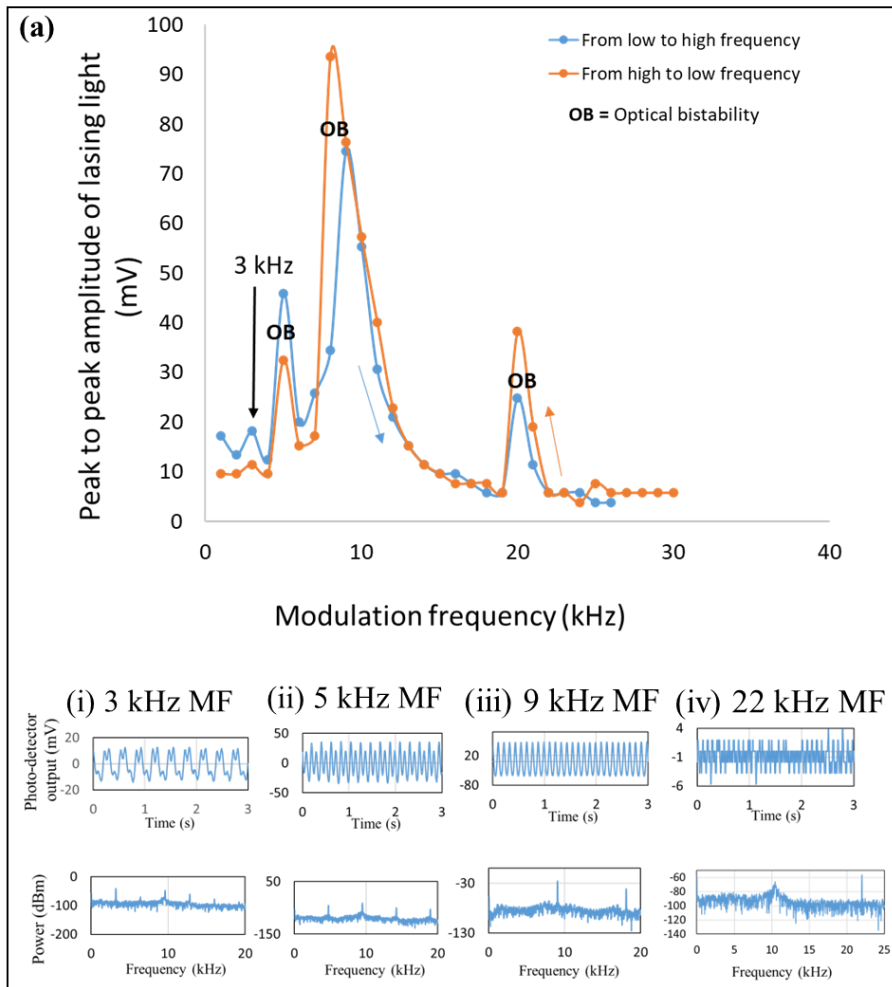
experiments, there were lots of unrestrained background noise (from other students in the lab carrying out their experiments). Still, it cannot be confirmed that the observed unusual behavior is due to the background noise because it is widely known that during frequency modulation, background noise does not affect the results unlike in amplitude modulation (Crosby, 1937). To confirm this; during the simulation, white noise with high amplitude was incorporated during pump modulation to see if similar experimental results would be gotten. It was observed that with and without white noise, there were insignificant variations in the bifurcation diagrams.

When compared to the EDFLL bifurcation results, the experimental and the theoretical bifurcation results of the EDFRL1 exhibited comparable features. In the theoretical bifurcation diagram (Figure 4.7 (b)) for the ascending chirp only, resonance peaks appear at (2, 4, 7, and 17) kHz. The first three peaks are an exact or close match to the first three resonance peaks obtained experimentally with an accuracy of 93.13 %. The ω_r of the EDFRL1 was set at 2 kHz before modulation and during modulation, a peak appeared at 2 kHz experimentally and theoretically. More so, the frequency at which saturation is observed experimentally (Figure 4.7 (a)) matches the frequency at which saturation is observed theoretically (Figure 4.7 (b)) with an accuracy of 78.26 % (Table 4.8). The theoretical time domain and frequency domain diagrams presented for some selected MFs (Figure 4.7 (b)(i), Figure 4.7 (b)(ii), and Figure 4.7 (b)(iii)) show similarities with the time and frequency domain diagrams obtained experimentally.

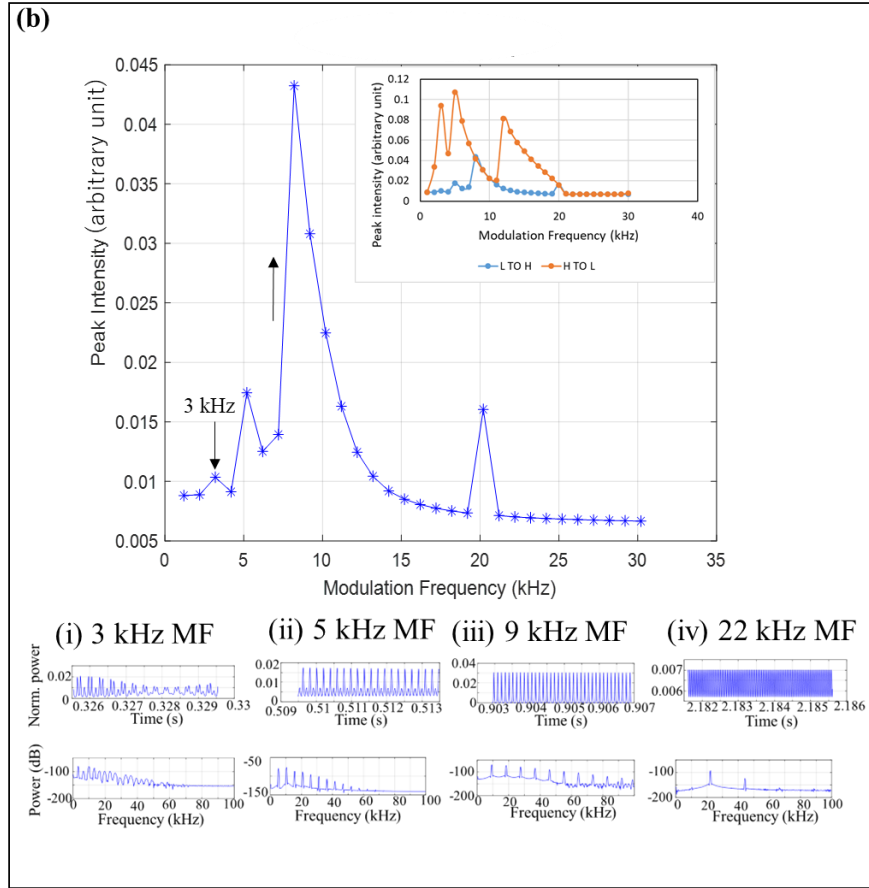
4.2.2 Experimental and Theoretical Results of the Pump-modulated EDFRL2

Similar to the EDFRL1, experimental bifurcation results of the EDFRL2 are presented in Figure 4.8 (a). The MA was set to 0.4 V while the laser was pumped from the laser diode pump at a power of 120 mW (corresponding to 3 kHz ω_r) to the EDF. The MF was modulated from 1 kHz to 30 kHz. To get the theoretical bifurcation diagram in Figure 4.8 (b) for the EDFRL2, the initial simulation conditions before pump modulation as shown in Table 4.6 are: MA symbolized as $m = 0.38$ (corresponding to 0.4 V); 94 s^{-1} normalized input pump power (corresponding to 120 mW pump power) to obtain 3 kHz ω_r ; 1 kHz initial MF and 30 kHz final MF with a 3 seconds chirp duration to obtain an ascending chirp during pump modulation. The initial and final MF are transposed to get the descending chirp.

EXPERIMENTAL RESULT



SIMULATION RESULT



Note: L means **low frequency** and H means **high frequency**

Figure 4.8: (a) Experimental (Onubogu, et al., 2020) and (b) theoretical (Onubogu, et al., 2022) bifurcation figures displaying the EDFRL2 dynamic behaviors obtained by modulating the frequency from 1kHz to 30 kHz MF and from 30 kHz to 1 kHz at MA of 0.4 V and 3 kHz ω_r .

In the ascending chirp of the experimental bifurcation diagram in Figure 4.8 (a), resonance peaks were depicted at (3, 5, 9, and 20) kHz. For the descending chirp, resonance peaks were depicted at (3, 5, 8, and 20) kHz. In Figure 4.8 (b), the theoretical bifurcation diagram obtained from the ascending chirp exhibited resonance peaks at (3, 5, 8, and 20) kHz. The ω_r of the EDFRL2 was set at 3 kHz before modulation and during modulation, a peak appeared at

3 kHz both experimentally and theoretically. It can be concluded that the response of the pump-modulated EDFRL2 can be modeled and predicted theoretically with an average accuracy of 93.13 % for the resonance frequency peaks (Table 4.7) and 95.45 % for the frequency at which saturation is observed (Table 4.8).

The time domain and frequency domains are presented as well for some selected MFs labeled as (i), (ii), (iii), and (iv) in Figure 4.8 (a) and Figure 4.8 (b) which shows that the patterns obtained experimentally are similar to those obtained theoretically. The time domain diagrams indicate the bifurcation from linear to non-linear (chaotic) dynamical regimes of the EDFRL2 just like in the EDFRL1. The fundamental resonance peak and higher harmonic resonance peaks appear in the frequency domain plots. (Onubogu et al, 2020).

4.2.3 Experimental and Theoretical Results of the Pump-modulated EDFRL3

The experimental bifurcation result of the EDFRL3 is presented in Figure 4.9 (a) wherein, the MA was set to 0.4 V and the laser was pumped at a power of 127.6 mW (equivalent to 5 kHz ω_r) from the laser pump to the EDF. The MF was modulated from 1 kHz to 30 kHz. To get the theoretical bifurcation diagram in Figure 4.9 (b) for the EDFRL3, the initial simulation conditions before pump modulation as shown in Table 4.6 are: MA symbolized as $m = 0.38$ (corresponding to 0.4 V); 104 s^{-1} normalized input pump power (corresponding to 127.6 mW) to obtain 5 kHz ω_r ; 1 kHz initial MF and 30 kHz

final MF with a 3 seconds chirp duration to obtain an ascending chirp during pump modulation. The initial and final MF were transposed to get the descending chirp.

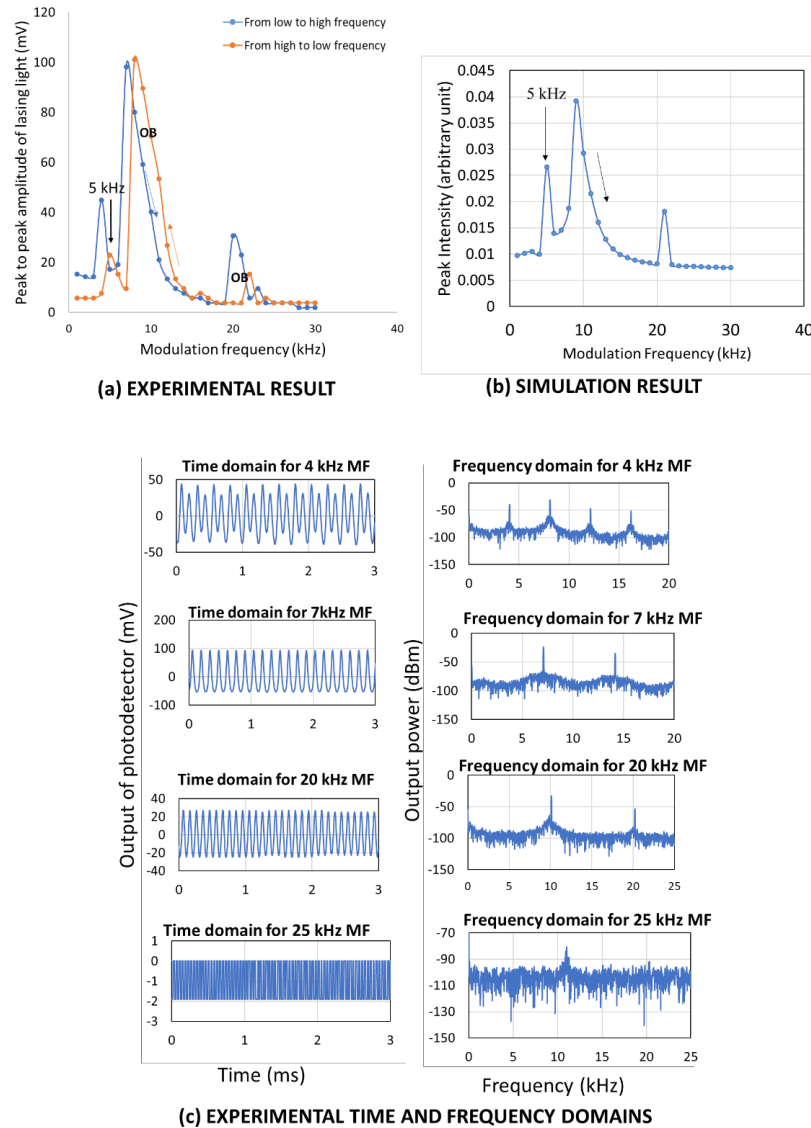


Figure 4.9: (a) Experimental (Onubogu, et al., 2020) and (b) theoretical (Onubogu, et al., 2022) bifurcation diagrams displaying the EDFRL3 dynamic behaviors gotten via frequency variation from 1kHz to 30 kHz MF and from 30 kHz to 1 kHz at 0.4 V MA and 5 kHz ω_r (c) Time domain (left) and frequency domain (right) gotten during experimental pump modulation.

In Figure 4.9 (a), the experimental bifurcation diagram exhibited resonance peaks at 4 kHz, 7 kHz, and 20 kHz for the ascending chirp and 5 kHz, 8 kHz, and 22 kHz for the descending chirp. In the theoretical bifurcation diagram in Figure 4.9 (b) obtained for only the ascending chirp, resonance peaks appeared at 5 kHz, 9 kHz, and 21 kHz. The ω_r of the EDFRL3 was set at 5 kHz before modulation and during modulation, a resonance peak appeared exactly at the ω_r both experimentally and theoretically. It can be concluded that the response of the pump-modulated EDFRL3 can be modeled and predicted theoretically with an average accuracy of 78.89 % for the resonance frequency peaks (Table 4.7) and 100 % for the frequency at which saturation is observed (Table 4.8).

Selected time domain and frequency domain figures are also illustrated in Figure 4.9 (c), which shows the dynamic behaviors of the experimentally pump-modulated EDFRL3 at some MFs. The theoretical time domain and frequency domain figures obtained (not presented in this thesis) were quite similar to those obtained experimentally (Onubogu et al, 2020).

4.2.4 Experimental and Theoretical Results of the Pump-modulated EDFRL4

The experimental bifurcation result of the EDFRL4 is presented in Figure 4.10 (a). The MA was set to 0.4 V while the laser was pumped at a power of 150.6 mW (equivalent to 7 kHz ω_r) and modulated from 1 kHz to 30 kHz and vice versa. To get the theoretical bifurcation diagram in Figure

4.10 (b) for the EDFRL4, the initial simulation conditions before pump modulation as shown in Table 4.6 are: MA symbolized as $m = 0.38$ (corresponding to 0.4 V); 220 s^{-1} normalized input pump power (corresponding to 150.6 mW) to obtain 7 kHz ω_r ; 1 kHz initial MF and 30 kHz final MF with a 3 seconds chirp duration to obtain an ascending chirp during pump modulation. The initial and final MF were transposed to get the descending chirp.

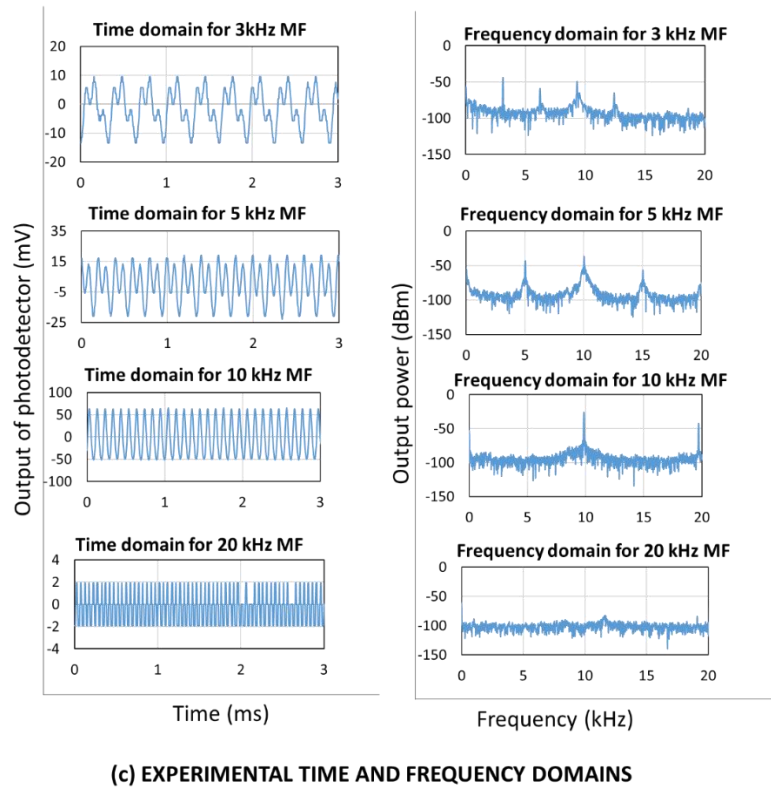
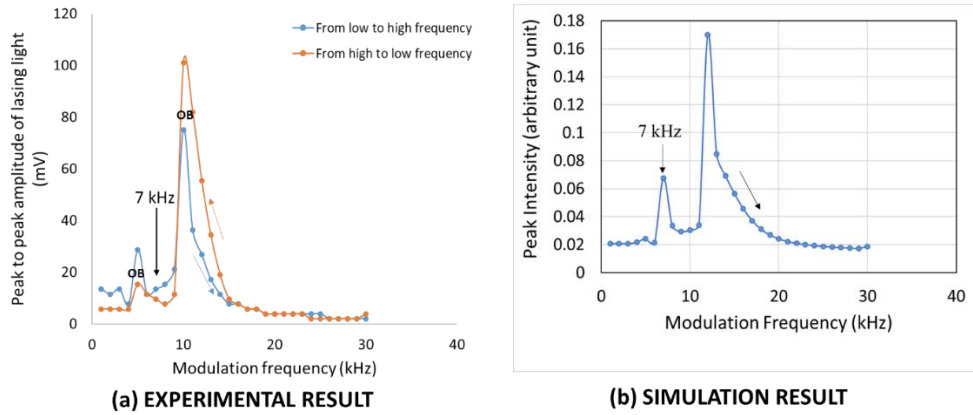


Figure 4.10: (a) Experimental (Onubogu, et al., 2020) and (b) theoretical (Onubogu, et al., 2022) bifurcation figures displaying the dynamic behaviors of the EDFRL4 gotten by frequency variation from 1kHz MF to 30 kHz MF and vice versa at MA of 0.4 V and 7 kHz ω_r (c) Time domain (left) and frequency domain (right) obtained during experimental pump modulation.

In Figure 4.10 (a), the ascending chirp of the experimental bifurcation diagram exhibited resonance peaks at 5 kHz and 10 kHz. Similarly, at 5 kHz and

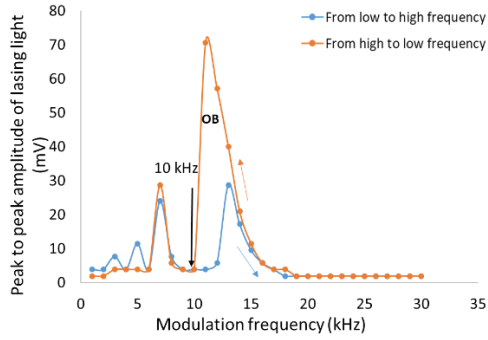
10 kHz, resonance peaks appeared for the descending chirp. In Figure 4.10 (b), the theoretical bifurcation diagram gotten for only the ascending chirp exhibited resonance peaks at 7 kHz and 12 kHz. Prior to modulation, the EDFRL4's ω_r was set at 5 kHz. During modulation, a resonance peak appeared theoretically at 5 kHz. However, a resonance peak appeared at 7 kHz experimentally for reasons explained earlier in Chapter 4.1. This implies that the theoretical simulation can produce even more correct results. It can be concluded that the response of the pump-modulated EDFRL4 can be modeled and predicted theoretically with an average accuracy of 77.4 % for the resonance frequency peaks (Table 4.7) and 95 % for the frequency at which saturation is observed (Table 4.8).

Time domain figures are shown in Figure 4.10 (c), which shows the dynamic behaviors of the experimentally pump-modulated EDFRL4 at some selected MFs. The theoretical time and frequency domain diagrams gotten (not shown in this thesis) were quite similar to those obtained experimentally. The frequency domain figures show the fundamental resonance peak and higher harmonic resonance peaks of the EDFRL4 system (Onubogu et al, 2020).

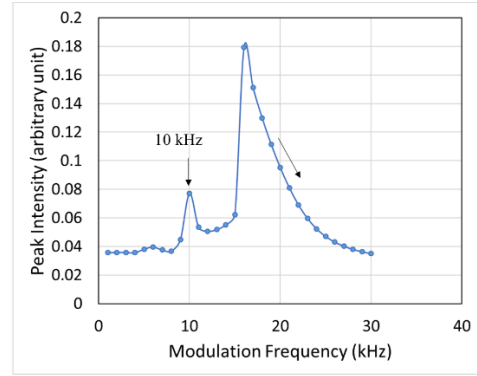
4.2.5 Experimental and Theoretical Results of the Pump-modulated EDFRL5

The experimental bifurcation result of the EDFRL5 is presented in Figure 4.11 (a). Before pump modulation, the MA was set to 0.4 V while the laser was pumped at a power of 180.7 mW (corresponding to 10 kHz ω_r) and modulated from 1 kHz to 30 kHz and vice versa. To get the theoretical

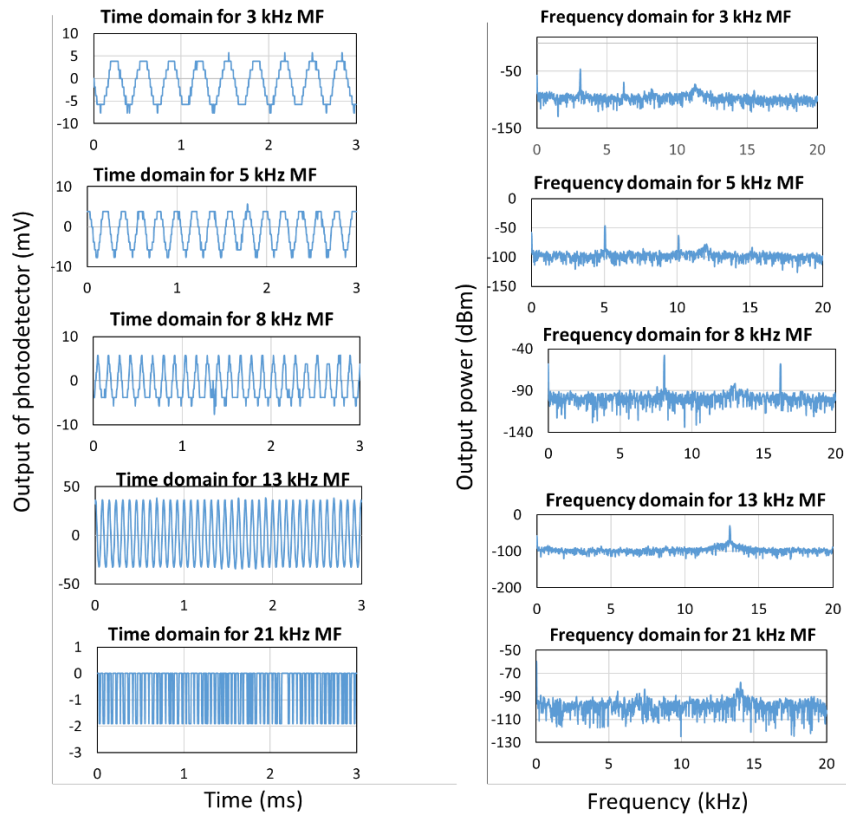
bifurcation diagram in Figure 4.11 (b) for the EDFRL5, the initial simulation conditions before pump modulation as shown in Table 4.6 are: MA symbolized as $m = 0.38$ (corresponding to 0.4 V); 400 s^{-1} normalized input pump power (corresponding to 180.7 mW) to obtain 10 kHz ω_r ; 1 kHz initial MF and 30 kHz final MF with a 3 seconds chirp duration to obtain an ascending chirp during pump modulation. The initial and final MF were transposed to get the descending chirp.



(a) EXPERIMENTAL RESULT



(b) SIMULATION RESULT



(c) EXPERIMENTAL TIME AND FREQUENCY DOMAINS

Figure 4.11: (a) Experimental (Onubogu, et al., 2020) and (b) theoretical (Onubogu, et al., 2022) bifurcation figures displaying the dynamic behaviors of the EDFRL5 gotten by modulating the frequency from 1kHz to 30 kHz MF and vice versa at MA of 0.4 V and 10 kHz ω_r (c) Time domain (left) and frequency domain (right) obtained during experimental pump modulation.

In Figure 4.11 (a), the experimental bifurcation figure exhibited resonance peaks at (3, 5, 7, and 13) kHz for the ascending chirp and at 7 kHz and 11 kHz for the descending chirp. In Figure 4.11 (b), the ascending chirp of the theoretical bifurcation figure exhibited resonance peaks at 10 kHz and 16 kHz. The ω_r of the EDFRL5 was set at 10 kHz before modulation and during modulation, a peak appeared theoretically at 10 kHz, but experimentally a peak appeared at 13 kHz for reasons explained earlier in Chapter 4.1. It can be concluded that the response of the pump-modulated EDFRL5 can be modeled and predicted theoretically with an average accuracy of 75.6 % for the resonance frequency peaks (Table 4.7) and 76 % for the frequency at which saturation is observed (Table 4.8).

The theoretical time and frequency domain diagrams gotten (not shown in this thesis) were quite similar to those obtained experimentally. The time domain diagrams in Figure 4.11 (c), indicate the linear to non-linear (chaotic) dynamical regimes of the EDFRL5. The frequency domain figures show the fundamental resonance peak and higher harmonic resonance peaks of the EDFRL5 (Onubogu et al, 2020).

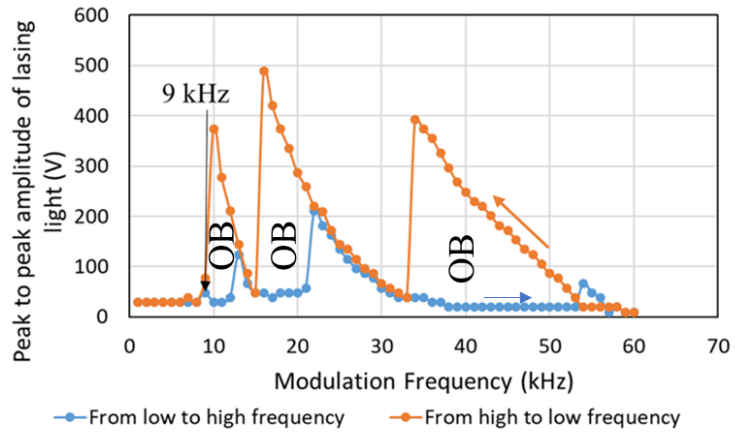
Notwithstanding the strange behavior of the descending chirp, it can still be resolved that the dynamic behavior of the EDFRL can be predicted by the theoretical model with some percentage accuracy. The result also demonstrates that the existence and non-existence of high background noise do not exactly affect the behavior of the EDFRL. This means that the EDFRL can be employed as a reliable detector in areas and locations having high background

noise for instance gas, water, or oil pipelines, as its sensitivity is not interrupted even at low frequencies irrespective of the noise. In this way, it can be utilized for the detection of leaks and their location in such pipelines. This feature is very significant in this research as it has been noticed that most authors only illustrate the dynamic behavior of their laser configuration from a high MF of about 8 kHz and above (Luo, et al., 1998a). The behavior of the laser at low frequencies is not studied or predicted. In this research, chaos is seen even at lower frequencies below 8 kHz depicting its sensitivity at low frequencies.

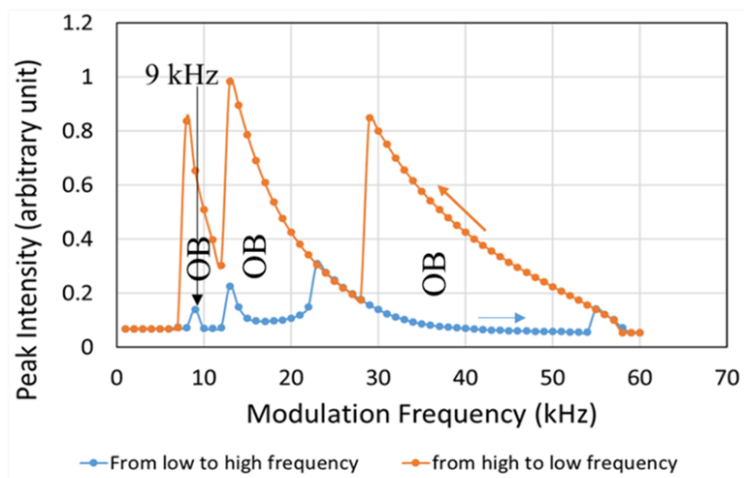
4.2.6 Experimental and Theoretical Results of the Pump-modulated EDFRL6

To evade any discrepancy based on the results obtained for the EDFRL1, EDFRL2, EDFRL3, EDFRL4, and EDFRL5 and to strongly demonstrate that the theoretical model describes the dynamic behavior of the EDFRL to a great extent, another pump-modulated EDFRL6 result is presented. The result in Figure 4.12 (a) was obtained by subjecting the EDFRL to experimental pump modulation on a different day and in a quiet environment to observe and compare the results. The input conditions as stated in Table 4.6 include 188.6 mW pumped laser power (corresponding to 9 kHz ω_r), MA of 0.4 V, and a frequency range of (1 to 60) kHz. Aside from this experiment, more pump-modulation experiments and theoretical analysis were performed on the EDFRL using various ω_r and MA values (not presented in this thesis) of which the results gotten are comparable to that of Figure 4.12. This implies that the numerical models' precision can truly be guaranteed. To get the theoretical

bifurcation diagram in Figure 4.12 (b) for the EDFRL6, the initial simulation conditions before pump modulation as shown in Table 4.6 are: MA symbolized as $m = 0.38$ (corresponding to 0.4 V); 390 s^{-1} normalized input pump power (corresponding to 188.6 mW) to obtain 9 kHz ω_r ; 1 kHz initial MF and 60 kHz final MF with a 3 seconds chirp duration to obtain an ascending chirp during pump modulation. The initial and final MF were transposed to get the descending chirp.



(a)



(b)

Figure 4.12: (a) Experimental and (b) theoretical bifurcation figures displaying the dynamic behaviors of the EDFRL6 obtained by modulating the frequency from 1kHz to 60 kHz MF and from 60 kHz to 1 kHz at MA of 0.4 V and 10 kHz ω_r

In Figure 4.12 (a), the experimental bifurcation diagram exhibited resonance peaks at (9, 13, 21, and 54) kHz for the ascending chirp and at (10, 16, and 24) kHz for the descending chirp. In Figure 4.12 (b), the theoretical bifurcation diagram exhibited resonance peaks at (9, 13, 23, and 55) kHz for the ascending chirp and at 8 kHz, 13 kHz, and 22 kHz vice versa. The ω_r of the

EDFLL6 was set at 9 kHz before modulation and during modulation, resonance peaks for both ascending and descending chirps were seen at the ω_r which is an excellent match. Other resonance peaks nearly or perfectly match each other with an average accuracy of 97.37 % (for the ascending chirp). A comparison of the frequency at which saturation occurred in Figure 4.12 indicated an accuracy of 100 % for the ascending chirp as calculated in Table 4.8.

In conclusion, the observed dynamical behaviors of the EDFRL (1, 2, 3, 4, 5, and 6) under pump modulation certainly confirm the occurrence of bifurcation in the EDFRL. There is also an effect observed on the bifurcation of the EDFRL from the variation of the ω_r with constant MA during the pump modulation experiments. In the EDFRL1 pump modulation experiment where the ω_r was 2 kHz, two OB regions of about the same width were observed with a saturation point at 23 kHz. Increasing the ω_r to 3 kHz (EDFRL2) and 5 kHz (EDFRL3), two OB regions were still depicted of similar width to that of the EDFRL1 having saturation points at 22 kHz and 19 kHz respectively. On increasing the ω_r to 7 kHz (EDFRL4) and 10 kHz (EDFRL5), the second OB region disappeared but the saturation point remained at 19 kHz respectively. This is the opposite of the effect observed in the EDFLL where there has to be an increase or decrease in MA for the OB regions to either increase or decrease likewise. For the EDFRL6 with 9 kHz ω_r , a different effect (similar to that of the EDFLL) was observed. Three OB regions were exhibited where the second OB region is wider than the first and the third is wider than the second.

In all pump modulation experiments on the EDFRLs, the bifurcation structures were more or less similar to each other with a slight difference in that of the EDFRL6. Hence, it is advisable to box up the EDFRL as a movable sensor to avoid high variation in the results.

It has been concluded that the response of the pump-modulated EDFRL can be modeled and predicted theoretically with an overall average accuracy of 86.60 % for the resonance frequency peaks (Table 4.7) and 90.79 % for the frequency after which saturation is observed (Table 4.8).

4.3 Pump Modulation of the EDFRL with Variation of the Amplitude

Amplitude modulation is a vital method employed in electronic communication for the transmission of messages via radio waves. As the aim of the laser system in this research is for pipeline monitoring, amplitude modulation helps in determining the magnitude of the leakage on a pipeline based on the amplitude of the acoustic wave signal emanating from the leakage that is detected by the EDFL sensor.

In amplitude modulation, the MA is modulated or varied unlike in pump modulation where it is kept constant. Five sets of experimental amplitude modulation were performed on the EDFRL configuration with input conditions of 2 kHz ω_r and 2 kHz MF (set 1); 3 kHz ω_r and 3 kHz MF (set 2); 5 kHz ω_r and 5 kHz MF (set 3); 7 kHz ω_r and 7 kHz MF (set 4) and 10 kHz ω_r and 10 kHz MF (set 5) respectively. For each fixed value of ω_r and MF, the input amplitude

is modulated from 400 mV (corresponding to 33.9 mW optical power) to 5000 mV (corresponding to 409 mW optical power). The maximum laser output measured from peak-to-peak is plotted for every frequency modulation to obtain the bifurcation diagram in Figure 4.13.

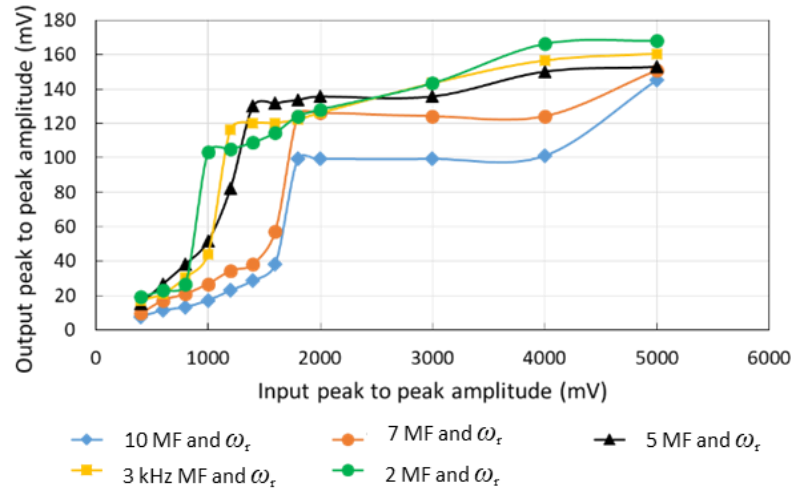


Figure 4.13: Dynamic behavior of the EDFRL subjected to amplitude modulation ranging from 400 mV to 5000 mV MA at 2 kHz MF and 2 kHz ω_r ; 3 kHz MF and 3 kHz ω_r ; 5 kHz MF and 5 kHz ω_r ; 7 kHz MF and 7 kHz ω_r , and 10 kHz MF and 10 kHz ω_r respectively (Onubogu, et al., 2019)

It was observed from Figure 4.13 that an increase in the input amplitude also leads to an increase in the output amplitude until a saturation region is reached where the saturation point progressively moves to higher amplitude. At 2 kHz MF and 2 kHz ω_r (refer to the green line in Figure 4.13), there is a gradual increase in the output amplitude from the input amplitude of 400 mV to 800 mV (Onubogu, et al., 2019). 800 mV input amplitude can be termed the saturation point for this experiment because, after this point, there is an immediate increase

in the output amplitude from 800 mV to 1000 mV. For easy understanding, the behavior can be broken down into three phases: phase 1 - progressively rising to the saturation point, phase 2 - rapid rising stage, and phase 3 - steadily rising phase (Onubogu, et al., 2019). As a result, it is possible to draw the conclusion that the output amplitude increases in tandem with the input amplitude. This behavior is similar for all MFs and ω_r s with higher saturation points at higher MFs and ω_r s. The point of saturation at 3 kHz MF and ω_r is 1000 mV. This saturation point is also the same at 5 kHz MF and ω_r . However, at 7 kHz MF and ω_r , the saturation point shifted again to 1400 mV. Finally, at 10 kHz MF and ω_r , the saturation point is at 1600 mV (Onubogu, et al., 2019). In conclusion, the saturation point moves to a higher amplitude as the MF and ω_r increase during amplitude modulation.

4.4 Summary

In this chapter, the behaviors observed during experimental and theoretical pump modulation of the EDFLL and the EDFRL under several initial conditions have been presented. In summary, the results of the pump modulation of the EDFRL revealed some significant observations:

- The experimental and theoretical bifurcation diagrams presented showed that the EDFLL and EDFRL systems switched from linear to chaotic behaviors during pump modulation. This was a confirmation that bifurcation occurs in the pump-modulated EDFLL and EDFRL.

Some selected time and frequency domain figures have also been presented to display the dynamical regimes of the EDFLL and the EDFRL.

- For both the EDFLL and the EDFRL, the experimental and numerical bifurcation diagrams were analyzed and compared in terms of “the resonance peaks”, “the saturation point” and “the distance between the OB regions”. It has thus been concluded that the response of the pump-modulated EDFLL can be modeled and predicted theoretically with an overall average accuracy of 91.09 % for the resonance frequency peaks (Table 4.2); 91.08 % for the frequency after which saturation is observed (Table 4.3) and 85.64 % for the width of the OB regions (Table 4.4).
- During the pump modulation of the EDFRL, a strange behavior was observed for the first five sets of experiments. The cause of this is still unidentified and hence requires additional research. However, it has been concluded that the response of the pump-modulated EDFRL can be modeled and predicted theoretically with an overall average accuracy of 86.60 % for the resonance frequency peaks (Table 4.7) and 90.79 % for the frequency after which saturation is observed (Table 4.8). Other authors such as Sola, Martin and Alvarez, 2002; Pisarchik, Kir’yanov and Barmenkov, 2005; Luo, et al., 1998; Kumar, and Vijaya, 2015; Reategui, et al, 2003) have succeeded in producing theoretical results that described all the characteristics experimentally observed.

- The dynamic behavior of the EDFLL and the EDFRL from linear to non-linear showed that at selected MFs and frequencies near to or exactly at the ω_r , chaos can be generated.
- At the chaotic region, the EDFLL and EDFRL have maximum sensitivity to external perturbations. Therefore, they can be used for leakage detection in pipeline monitoring and also for bio-systems modeling as well.
- Five sets of experimental amplitude modulation have also been performed on the EDFRL configuration with different input conditions. The main aim of the amplitude modulation was to determine the magnitude of the leakage on a pipeline based on the amplitude of the acoustic wave signal emanating from the leakage that is detected by the EDFL sensor. It was observed that an increase in the input amplitude led to an increase in the output amplitude until a saturation region was reached where the saturation points progressively moved to higher amplitude.

CHAPTER 5

LOSS MODULATION OF THE EDFLL AND EDFRL

The main purpose of carrying out loss modulation on the EDFLL and EDFRL is to trigger their laser dynamics and study their behavior to confirm whether bifurcations occur during loss modulation as bifurcation seems to be the cause of the instability in the sensor.

External cavity loss modulation of the EDFLL and the EDFRL was carried out experimentally in the lab at UTAR, Sungai Long campus, and theoretically using MATLAB. The experimental setups and procedure are well described in Chapter 3.3.1 and Chapter 3.3.5 for the EDFLL and in Chapter 3.3.2 and Chapter 3.3.6 for the EDFRL. The improved theoretical model used to simulate the EDFLL and EDFRL output (bifurcation) with external cavity loss modulation is presented in Chapter 3.5 where Equation (3.15) and Equation (3.15i) are used to calculate the normalized laser power density for the EDFLL and EDFRL respectively. Equation (3.16) is used to calculate the normalized population inversion at the meta-stable level of the EDFLL and EDFRL respectively.

Four sets of loss modulation experiments were carried out on the EDFLL where the MA was the same for all experiments while the ω_r was varied. Four sets of loss modulation experiments were also carried out on the EDFRL but in this case, the ω_r was fixed while the MA was varied for all

experiments. This was done in this way to understand the impact of the variation of the input parameters on the laser output (bifurcation). The initial conditions/parameters for both experimental and numerical analysis are shown in Table 5.1. The resonance peaks obtained experimentally and numerically are also indicated in Table 5.1 for quick matching/comparison.

Table 5.1: Initial conditions/parameters used for the experimental and theoretical loss modulations of the EDFLL and EDFRL

Laser	MA (V)	Normalized MA (symbolized as 'm' in simulation)	ω_r (kHz)	MF Range (kHz)	Input PP - Experiment (mW)	Normalized Input PP - Simulation (s^{-1})	Peaks from Experiments (kHz)	Peaks from Simulation (kHz)
LOSS MODULATION								
EDFLL (Fig. 5.1)	0.8	1.0	4	1– 20	45.00	140	>4, 7, 12, 18 < 7, 12	>4, 7, 12, 18 < 3, 7, 12
	0.8	1.0	8	1– 20	60.20	350	>2, 4, 7 < 7, 9	>2, 4, 8 < 5, 8
	0.8	1.0	10	1– 20	66.00	500	>4, 7, 12 < 4, 7, 12	>2, 7, 10 < 2, 5, 10
	0.8	1.0	16	1– 20	79.10	1500	>3, 16 < 3, 8, 16	>3, 16 < 3, 9, 14
EDFRL (Fig.5.2, Fig. 5.3, Fig. 5.4, Fig. 5.5, Fig. 5.6)	0.2	0.25	14	1– 20	76.79	56	-	-
	0.5	0.53	14	1– 20	76.79	56	>7, 14 <7, 14	>6, 14
	0.9	0.89	14	1– 20	76.79	56	>7, 14 <14	>6, 14
	1.0	1.20	14	1– 20	76.79	56	>8, 14 <8, 14	> 6, 14

*MA = Modulation Amplitude; ω_r = Resonance Frequency; MF = Modulation Frequency; PP = Pump power; > = Low to high frequency modulation; < = High to low frequency modulation.

Tables 5.2 and 5.3 are used to quantitatively analyze the bifurcation results obtained for all four cavity-loss modulations of the EDFLL. The bifurcation diagrams (experimental and numerical) obtained and presented in Chapter 5.1 were analyzed and compared in terms of “the resonance peaks” observed, and “the saturation point” observed when loss-modulating from low to high frequency and vice versa. The percentage error and percentage accuracy

for all the compared parameters were obtained and presented in Tables 5.2 and 5.3.

Table 5.2: Quantitative analysis of the bifurcation results obtained for all four cavity-loss modulation experiments of the EDFLL in terms of resonance frequency peak.

Laser configuration	Resonance peaks (kHz)		Percentage error (%)	Percentage accuracy (%)	Resonance Peaks (kHz)		Percentage error (%)	Percentage accuracy (%)
	Exp. L to H	Num. L to H			Exp. H to L	Num. H to L		
(1) EDFLL	4	4	0.00	100.00	7	7	0.00	100.00
	7	7	0.00	100.00	12	12	0.00	100.00
	12	12	0.00	100.00				
	18	18	0.00	100.00				
Average			0.00	100.00			0.00	100.00
(2) EDFLL	2	2	0.00	100	7	5	28.57	71.43
	4	4	0.00	100	9	8	11.11	88.89
	7	8	12.5	87.5				
Average			4.17	95.83			19.84	80.16
(3) EDFLL	4	2	50.00	5.000	4	2	50.00	5.000
	7	7	0.00	100.00	7	5	28.57	71.43
	12	10	16.67	83.33	12	10	16.67	83.33
Average			22.22	77.78			31.75	68.25
(4) EDFLL	3	3	0.00	100.00	3	3	0.00	100.00
	16	16	0.00	100.00	8	9	11.11	88.89
					16	14	12.50	87.50
Average			0.00	100.00			7.87	92.13
Total average for all EDFLL's			6.60	93.40			14.86	85.14
	Total percentage error obtained when matching the experimental and numerical bifurcation diagram is the average of 6.60 % and 14.86 % which is 10.73 %				Total percentage accuracy obtained when matching the experimental to numerical bifurcation diagram is the average of 93.40% and 85.14 % which 91.09 %			

*Where “L to H” means Low to High and “H to L” means high to low; “exp.” means experimental and “num.” means numerical.

Table 5.3: Quantitative Analysis of the Bifurcation Results Obtained for All Four Cavity-Loss Modulation Experiments of the EDFLL in Terms of the Saturation Frequency in the Bifurcation Diagram.

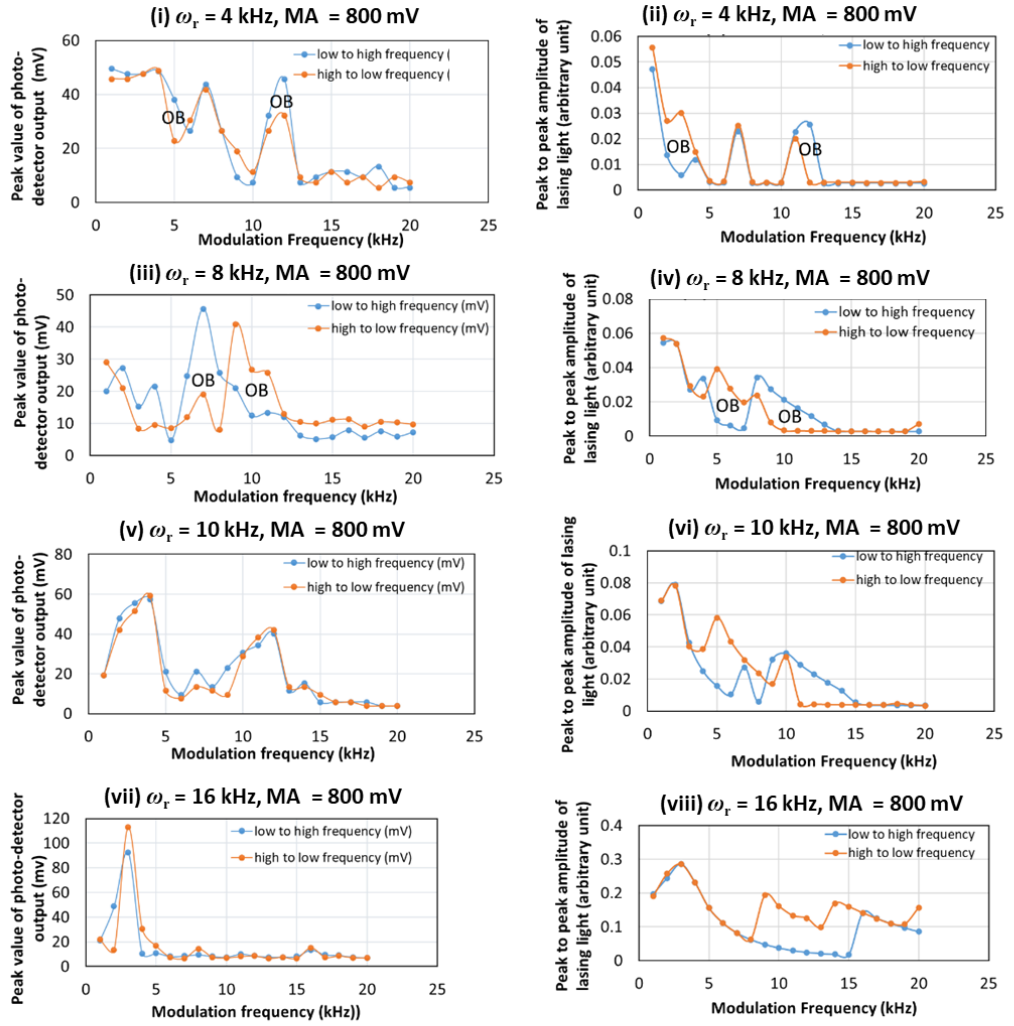
Laser configuration	Resonance peaks (kHz)		Percentage error (%)	Percentage accuracy (%)	Resonance Peaks (kHz)		Percentage error (%)	Percentage accuracy (%)
	Exp. L to H	Num. L to H			Exp. H to L	Num. H to L		
(1) EDFLL	13	13	0.00	100.00	13	12	7.69	92.31
(2) EDFLL	12	14	14.29	85.71	12	14	14.29	85.71
(3) EDFLL	16	15	6.25	93.75	16	15	6.25	93.75
(4) EDFLL	17	17	0.00	100.00	17	14	17.65	82.35
Total average for all EDFLL's			5.13	94.87			11.47	88.53
	Total percentage error obtained when matching the experimental and numerical bifurcation diagram is the average of 8.18 % and 8.66 % which is 8.30 %				Total percentage accuracy obtained when matching the experimental to numerical bifurcation diagram is the average of 91.82 % and 91.34 % which 91.70 %			

*Where “L to H” means Low to High and “H to L” means high to low; “exp.” means experimental and “num.” means numerical.

5.1 Experimental and Theoretical Results of the Loss-modulated EDFLL

For the initial conditions in Table 5.1, the presented results were obtained experimentally and theoretically by externally varying the cavity loss of the EDFLL sinusoidally with time. For all the loss modulation experiments carried out on the EDFLL, the MA was set at 800 mV. The laser was then pumped at various powers to set different resonance frequencies as shown in Table 5.1. It was observed that the pattern of the obtained theoretical bifurcation diagrams may not always be similar to that of the experimental bifurcation diagrams. However, the dynamic behaviors are similar indicating that the behavior of the loss-modulated EDFLL can change from linear to chaotic characteristics reliant on the variation of the input laser pump power

and the MF. It was also observed that the sensitivity of the EDFLL is high at low MFs and also at the ω_r . This is because the bifurcation diagrams show a high amplitude peak between 1 kHz to 5 kHz MF for all fixed ω_r values and another high amplitude peak at the main ω_r (please refer to Figure 5.1).



(a) EXPERIMENTAL LOSS MODULATION

(b) THEORETICAL LOSS MODULATION

Figure 5.1: (a) Experimental and (b) Theoretical bifurcation diagrams obtained at a fixed MA of 800 mV displaying the dynamic behavior of the EDFLL subjected to external cavity-loss modulation gotten by sweeping the loudspeakers' frequency ranging from 1 kHz to 20 kHz and back again for ω_r values of (4, 8, 10 and 16) kHz.

The first experimental bifurcation result of the EDFLL under loss modulation is presented in Figure 5.1 (a)(i), wherein the laser was pumped at a power of 45 mW (which is equivalent to 4 kHz ω_r) and the loudspeaker was

modulated from (1 to 20 kHz). To get the theoretical bifurcation diagram (Figure 5.1 (b) (ii)), the initial simulation conditions as shown in Table 5.1 before loss modulation was performed include: MA symbolized as $m = 1$ which is equivalent to 0.8 V; 140 s^{-1} normalized input pump power which is equivalent to 45 mW to obtain 4 kHz ω_r ; 1 kHz initial MF and 20 kHz final MF with a 3 seconds chirp duration to obtain an ascending chirp during loss modulation. The initial and final MF were transposed to get the descending chirp. The experimental bifurcation diagram exhibited resonance peaks at (4, 7, 12, and 18) kHz for the ascending chirp and at 7 kHz and 12 kHz for the descending chirp. The ω_r of the EDFL was fixed at 4 kHz before modulation and during experimental loss modulation, a peak was exhibited at 4 kHz having a high output amplitude of 48.84 mV. This is the fundamental or main resonance peak. A second peak which is almost twice the ω_r was seen at 7 kHz (very close to 8 kHz ω_r) and is termed the sub-harmonic resonance (Kumar, and Vijaya, 2017). The appearance of resonance peaks at the main and either the first super-harmonic ω_r or the first sub-harmonic ω_r demonstrates the rise in the level of loss in the laser cavity during cavity-loss modulation. This is also an indication of its dynamic chaotic behavior. In the theoretical bifurcation diagram in Figure 5.1 (b)(ii), resonance peaks were exhibited at (4, 7, 12, and 18) kHz for the ascending chirp and at (3, 7, and 12) kHz for the descending chirp. Comparing the ascending and descending chirp of the experimental and theoretical bifurcation diagrams, it is seen that the resonance peaks in both diagrams match perfectly well with 100 % accuracy. The frequency after which saturation is observed experimentally and theoretically

matches each other with an accuracy of 100 % (ascending chirp) and 92.31 % (descending chirp). This confirms that the loss-modulated EDFLL system response can be modeled and predicted accurately. Moreover, two regions of OB were seen in both the experimental and theoretical bifurcation diagrams. The spectrums of the theoretical and experimental time and frequency domain diagrams for each MF (not presented in this thesis) were quite similar to each other, further justifying the accuracy of the model.

In the second experimental bifurcation result of the EDFLL under cavity-loss modulation as presented in Figure 5.1 (a)(iii), the laser was pumped at a power of 60.2 mW (which is equivalent to 8 kHz ω_r), and the loudspeaker was modulated from 1 kHz to 20 kHz. Before loss modulation, the initial simulation conditions as shown in Table 5.1, were inputted to produce the theoretical bifurcation diagram (Figure 5.1 (b)(iv)). These conditions include: MA symbolized as $m = 1$ which is equivalent to 0.8 V; 350 s⁻¹ normalized input pump power which is equivalent to 60.2 mW to obtain 8 kHz ω_r ; 1 kHz initial MF and 20 kHz final MF with a 3 seconds chirp duration to obtain an ascending chirp during loss modulation. The initial and final MF were transposed to get the descending chirp. In the experimental bifurcation diagram, resonance peaks were exhibited at 2 kHz, 4 kHz, 7 kHz, and 18 kHz for the ascending chirp and at 7 kHz and 9 kHz for the descending chirp. The ω_r of the EDFLL was fixed at 8 kHz before modulation and during modulation, a peak appeared at 7 kHz (which is close to the ω_r) with a high amplitude of 45.84 mV. This is the fundamental or main resonance peak. A second peak which is almost half the ω_r was seen at 4 kHz and is termed super-

harmonic resonance (Kumar and Vijaya, 2017). This is an indication of the dynamic chaotic or non-linear behavior of the EDFLL under cavity loss modulation. In the theoretical bifurcation diagram in Figure 5.1 (b)(iv), resonance peaks appeared at 2 kHz, 4 kHz, and 8 kHz for the ascending chirp and 5 kHz and 8 kHz for the descending chirp. Comparison of the experimental and theoretical bifurcation diagrams indicated a good match of the resonance peaks in both diagrams with an accuracy of 95.83 % (ascending chirp) and 80.16 % (descending chirp) as quantitatively analyzed in Table 5.2. Two regions of OB were seen in both the experimental and theoretical bifurcation diagrams. More so, the frequency after which saturation is observed experimentally and theoretically matches each other with an accuracy of 85.71% as calculated in Table 5.3 (for both ascending and descending chirps). The spectrums of the theoretical and experimental time and frequency domain diagrams for each MF (not presented in this thesis) were quite similar to each other, further justifying the accuracy of the model.

In the third and fourth experimental bifurcation results of the EDFLL under loss modulation, as presented in Figures 5.1 (a)(v) and 5.1 (a)(vii), the laser was pumped at a power of 66 mW (which is equivalent to 10 kHz ω_r) and 79.10 mW (which is equivalent to 16 kHz ω_r) respectively while the loudspeaker was modulated from (1 to 20) kHz MF. To get the theoretical bifurcation diagrams in Figure 5.1 (b)(vi) and Figure 5.1 (b)(viii), the initial simulation conditions for 10 kHz and 16 kHz ω_r as shown in Table 5.1 were inputted before loss modulation was performed.

In the third experimental bifurcation diagram (Figure 5.1 (a)(v)), resonance peaks appeared at 4 kHz, 7 kHz, and 12 kHz for the ascending chirp and 4 kHz, 7 kHz, and 12 kHz for the descending chirp. Even though the resonance peaks are the same for both ascending and descending chirps, the amplitudes are different forming small regions of OB. The ω_r of the EDFLL was fixed at 10 kHz before modulation. The nearest peak to 10 kHz ω_r appeared at 12 kHz MF (fundamental or main resonance peak) and the nearest peak to the superharmonic resonance appeared at 4 kHz instead of 5 kHz due to the reasons already explained in Chapter 4.1. This is again a sign of the dynamic linear to the non-linear behavior of the EDFLL under loss modulation. In the theoretical bifurcation diagram in Figure 5.1 (b)(vi), resonance peaks appeared at (2, 7, and 10) kHz for the ascending chirp and at (2, 5, and 10) kHz for the descending chirp. A peak appeared at 10 kHz ω_r symbolizing the resonance frequency of the laser system. Comparison of the third experimental (Figure 5.1 (a)(v)) and theoretical (Figure 5.1 (b)(vi)) bifurcation diagrams indicated an acceptable match of the resonance peaks with an accuracy of 77.78 % (ascending chirp) and 68.25 % (descending chirp) as quantitatively analyzed in Table 5.2. More so, the frequency after which saturation is observed experimentally and theoretically matches each other with an accuracy of 93.75 % (for both ascending and descending chirps). OB regions were seen in the experimental bifurcation diagram but were narrow and not so obvious compared to that of the theoretical bifurcation diagram. The spectrums of the theoretical and experimental time and frequency domain diagrams for each MF (not presented in this thesis) were quite similar to each other, further justifying the accuracy of the model.

In the fourth experimental bifurcation diagram (Figure 5.1 (a)(vii)), resonance peaks appeared at 3 kHz and 16 kHz for the ascending chirp and at (3, 8, and 16) kHz for the descending chirp. The ω_r of the EDFLL was fixed at 16 kHz before modulation; and during modulation, a peak appeared at 16 kHz (fundamental resonance peak). Another peak was seen at 8 kHz (super-harmonic resonance) for the descending chirp which is half of the ω_r (Kumar and Vijaya, 2017). Again, this is an indication of the dynamic behavior of the EDFLL under loss modulation. In the theoretical bifurcation diagram in Figure 5.1 (b)(viii), resonance peaks appeared at 3 kHz and 16 kHz for the ascending chirp and 3 kHz, 9 kHz, and 14 kHz for the descending chirp. One peak appeared at 16 kHz symbolizing the ω_r of the laser system. Comparison of the fourth experimental (Figure 5.1 (a)(vii)) and theoretical (Figure 5.1 (b)(viii)) bifurcation diagrams indicated a good match in the resonance peaks with an accuracy of 100 % (ascending chirp) and 92.13 % (descending chirp) as quantitatively analyzed in Table 5.2. More so, the frequency after which saturation is observed experimentally and theoretically matches each other with an accuracy of 100 % (for the ascending chirp) and 82.35 % (for the descending chirp). OB regions were seen in the experimental bifurcation diagram but were narrower and not so obvious compared to that of the theoretical bifurcation diagram. The spectrums of the theoretical and experimental time and frequency domain diagrams for each MF (not presented in this thesis) were quite similar to each other, further justifying the accuracy of the model.

The observed dynamical behaviors of the EDFLL under external cavity loss modulation confirm the occurrence of bifurcation. There is also an effect

observed on the bifurcation of the EDFLL from the variation of the ω_r . It was observed from all the experimental and theoretical loss-modulated EDFLL bifurcation results that the higher the laser pump power or the ω_r with constant MA, the higher the amplitude or intensity of the first peak seen in the bifurcation diagram. This implies that at a high peak ω_r , the EDFLL would be more sensitive with a high laser response than at a lower peak ω_r . It is also important to note that at constant MA, the number and width of the OB regions decrease with increasing ω_r .

It can be concluded that the response of the loss-modulated EDFLL can be modeled and predicted theoretically with an overall average accuracy of 91.04 % for the resonance frequency peaks (Table 5.2) and 91.70 % for the frequency after which saturation is observed (Table 5.3). Since the MA was set constant while the pump power/ ω_r was changed for each experiment during loss modulation of the EDFLL, loss modulation whereby the amplitude is varied with constant pump power/ ω_r was carried out in the next section to observe the dynamic behavior of the laser in that condition.

5.2 Experimental and Theoretical Results of the Loss-Modulated EDFRL

For the parameters in Table 5.1, the presented results were obtained experimentally and theoretically by externally varying the cavity loss of the EDFRL sinusoidally with time. The laser pump power was set at 76.79 mW to

obtain 14 kHz ω_r for all of the EDFRL cavity-loss modulation experiments. Before starting the experiments, it was observed that from 1 mV to 200 mV MA, no response was seen on the Pico Scope when tuning the frequency of the loudspeaker. But from above 200 mV MA, a signal response was detected. Therefore, four MA's (200 mV, 500 mV, 900 mV, and 1000 mV) were selected to perform four sets of cavity-loss modulation experiments to fully understand the dynamic behavior of the EDFRL (Onubogu, Pua and Faiz, 2021).

Tables 5.4 and 5.5 are used to quantitatively analyze the bifurcation results obtained for all cavity-loss modulations of the EDFRL. The bifurcation diagrams (experimental and numerical) obtained and presented in Figure 5.2 were analyzed and compared in terms of “the resonance peaks” and “the saturation point” observed when loss-modulating from low to high frequency. The percentage error and percentage accuracy for all the compared parameters were obtained and presented in Tables 5.4 and 5.5.

Table 5.4: Quantitative analysis of the bifurcation results obtained for all four cavity-loss modulation experiments of the EDFRL in terms of resonance frequency peak.

Laser configuration	Resonance peaks (kHz)		Percentage error (%)	Percentage accuracy (%)
	Exp. L to H	Num. L to H		
(2) EDFRL (500mV MA)	7	6	14.29	85.71
	14	14	0.00	100.00
Average			7.14	92.86
(3) EDFRL (900 mV MA)	7	6	14.29	85.71
	14	14	0.00	100.00
Average			7.14	92.86
(4) EDFRL (1000 mV MA)	8	6	25.00	75.00
	14	14	0.00	100.00
Average			12.50	87.50
Total average for all EDFRL's			8.93	91.07

*Where “L to H” means Low to High and “H to L” means high to low; “exp.” means experimental and “num.” means numerical.

Table 5.5: Quantitative analysis of the bifurcation results obtained for all four cavity-loss modulation experiments of the EDFRL in terms of the saturation frequency in the bifurcation diagram.

Laser configuration	Resonance peaks (kHz)		Percentage error (%)	Percentage accuracy (%)
	Exp. L to H	Num. L to H		
(1) EDFRL (200 mV MA)	-	-	-	-
(2) EDFRL (500 mV MA)	17	17	0.00	100.00
(3) EDFRL (900 mV MA)	16	17	5.88	94.12
(4) EDFRL (1000 mV MA)	15	16	6.25	93.75
Total average for all EDFRL's			4.04	95.96
	Total percentage accuracy obtained when matching the experimental and numerical bifurcation diagram is <u>95.96 %</u>			

*Where “L to H” means Low to High and “H to L” means high to low; “exp.” means experimental and “num.” means numerical.

For the first experiment carried out, the MA was fixed at 200 mV just to illustrate that no response was detected during modulation of the loudspeaker from 1 kHz MF - 20 kHz MF and vice versa. The output amplitude showed an irregular pattern with sudden increase and decrease at all MFs during the

modulation as illustrated in the bifurcation diagram (Figure 5.2(a)). No distinct peak was detected in the ω_r domain. Therefore, it can be concluded that the dynamics of the EDFRL were not activated at this MA. The reason for this is that at 200 mV MA, the sound or acoustic wave originating from the loudspeaker is insufficient for interaction with the EDFRL to occur such that its dynamic behavior is triggered; irrespective of the increase in MF. This observation is the opposite of that reported by Ghosh and Vijaya (2014). Their EDF was experimentally loss-modulated using a Mach-Zender modulator made of lithium niobate. At MA values as low as 10 mV, their EDF behaved like a harmonic or linear oscillator with damping.

To obtain the theoretical bifurcation diagram, parameters in Table 5.1 are employed when the MA is 200 mV. Similar to the experimental results, the laser spectrum displayed an irregular wave pattern at all MFs (Figure 5.2 (e)). Therefore, a satisfactory agreement is established between the dynamic behaviors exhibited both experimentally and theoretically at 200 mV MA.

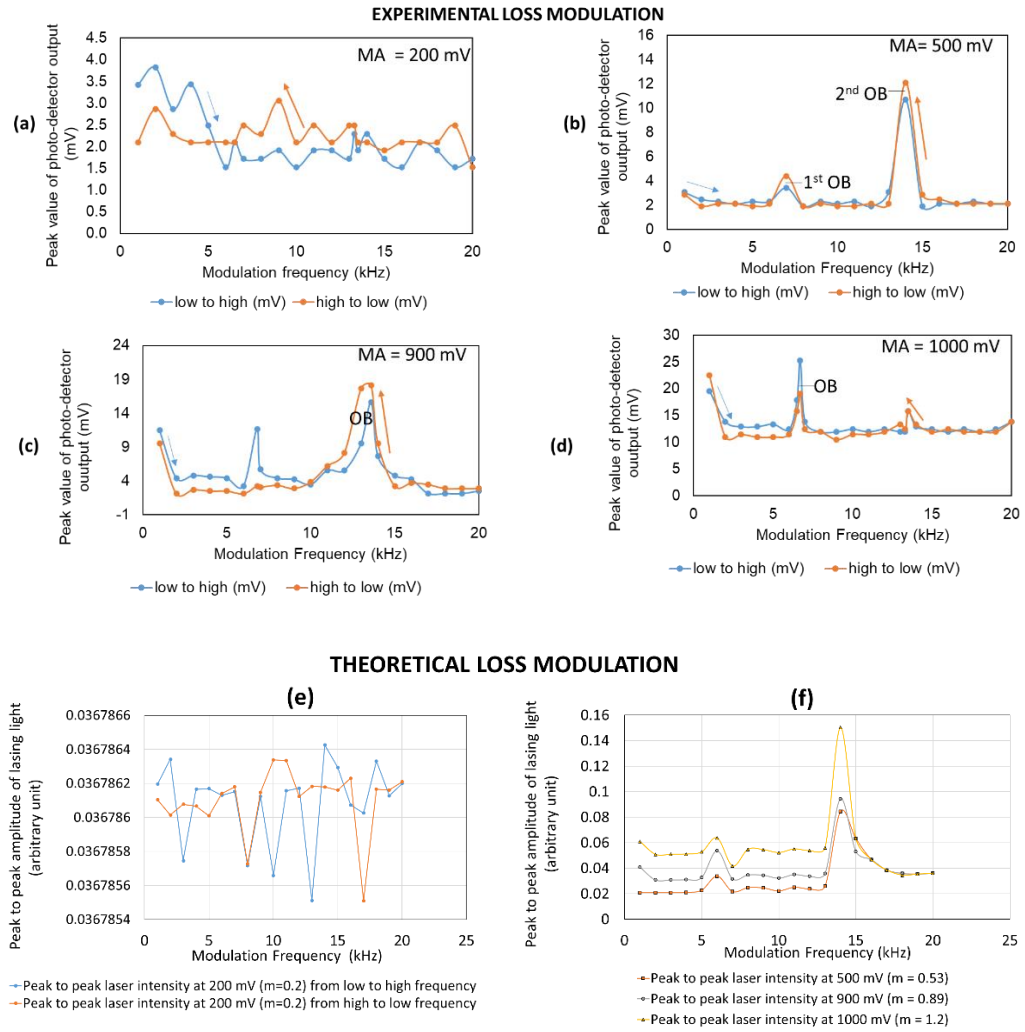


Figure 5.2: Bifurcation diagram obtained at a fixed ω_r of 14 kHz displaying the EDFRL's reaction to external loss modulation gotten by variation of the loudspeaker's frequency from 1 kHz to 20 kHz for MA of (a) 200 mV (experimental result); (b) 500 mV (experimental result); (c) 900 mV (experimental result); (d) 1000 mV (experimental result); (e) 200 mV (theoretical result) and (f) 500 mV, 900 mV, and 1000 mV (theoretical results). (Onubogu, Pua and Faiz, 2021)

On increasing the MA to 500 mV and loss modulating the EDFRL experimentally from 1 kHz – 20 kHz and from 20 kHz – 1 kHz, two distinct peaks were exhibited at 7 kHz and 14 kHz as illustrated in Figure 5.2 (b). The

peak at 7 kHz (having a 3.438 mV output amplitude) is precisely one-half of the fixed ω_r and is referred to as the 1st super-harmonic resonance (Onubogu, Pua and Faidz, 2021; Kumar, and Vijaya, 2017). The fundamental or main resonance peak having an output amplitude of 10.7 mV can be seen at 14 kHz. The appearance of a fundamental resonance peak and superharmonic resonance peak is a sign of the dynamic non-linear behavior and also an indication of a rise in the degree of loss in the cavity of the EDFRL during modulation. This implies that at 500 mV MA, the ω_{ro} is near the EDFRL's ω_r and the EDFRL can then be called a damped non-linear oscillator. ω_{ro} has already been defined previously in this thesis but can also be defined as the frequency wherein optical power is attained at a maximum. The natural frequency of the EDFRL (ω_r) is reliant on: the length of the laser cavity, the input pump power, the total losses incurred by the laser cavity (losses caused by numerous splices and from the addition of several elements along the laser resonator) and the type of gain material used.

To obtain the theoretical bifurcation diagram, parameters in Table 5.1 were employed for 500 mV MA. The bifurcation diagram presented here is from only low to high-frequency modulation so that other bifurcation diagrams for other MA values can be compiled in the same figure without confusion. Similar to the experimental results, two peaks were seen as illustrated in Figure 5.1 (f). The first peak with a lower amplitude was seen at 6 kHz which is quite close to the 1st super-harmonic resonance peak seen experimentally. The second peak appeared at exactly the main resonance of the laser system just like in the experiments too. Therefore, it can be concluded that the response of the loss-

modulated EDFRL at 500 mV MA can be modeled and predicted theoretically with an average accuracy of 92.86 % for the resonance frequency peaks (Table 5.4) and 100 % for the frequency after which saturation is observed (Table 5.5).

Further increasing the MA to 900 mV and loss modulating the EDFRL experimentally from 1 kHz to 20 kHz, a first peak as illustrated in Figure 5.2 (c) was seen at 6.8 kHz (the 1st super-harmonic resonance peak) having 11.65 mV output amplitude. A fundamental resonance peak was seen at 14 kHz having a 15.59 mV higher output amplitude. When loss modulating the EDFRL from 20 kHz to 1 kHz, a single peak having 18.15 mV output amplitude was seen at 14 kHz (fundamental resonance peak). To obtain the theoretical bifurcation diagram, parameters in Table 5.1 were employed for 900 mV MA. Similar to the experimental results, two peaks were seen as illustrated in Figure 5.2 (f). The description of the peaks is exactly as those obtained when MA was 500 mV. Therefore, it can be concluded that the response of the loss-modulated EDFRL at 900 mV MA can be modeled and predicted theoretically with an average accuracy of 92.86 % for the resonance frequency peaks (Table 5.4) and 94.12 % for the frequency after which saturation is observed (Table 5.5).

On increasing the MA to 1000 mV and loss modulating the EDFRL experimentally from 1 kHz to 20 kHz, an unusual behavior was observed. However, the EDFRL still emulated a non-linear oscillator that is damped. Two distinct peaks were seen at approximately 8 kHz (1st super-harmonic

resonance) having a 25.31 mV output amplitude and at 14 kHz (main resonance) having a 15.76 mV output amplitude. When the MA is 500 mV (Figure 5.2 (b)) and 900 mV (Figure 5.2 (c)), the amplitude of the ω_r peak is higher when the loudspeaker's frequency is modulated from 20 kHz MF to 1 kHz MF compared to when it is modulated from 1 kHz MF to 20 kHz MF. The reverse is the case for 1000 mV MA where the amplitude of the 1st super-harmonic resonance peak at 7 kHz is higher (25.31 mV output amplitude) than that of the main resonance peak when sweeping the MF of the loudspeaker from low to high. The behavior that was described by Kumar and Vijaya is once more the reverse here. In their case, a peak at the ω_r having a higher amplitude always appeared during modulation from high frequency to low frequency in comparison to modulating from low frequency to high frequency, thus creating the hysteresis areas seen (Kumar, and Vijaya, 2015). To obtain the theoretical bifurcation diagram, parameters in Table 5.1 were employed for 900 mV MA. Similar to the experimental results, two peaks were seen as illustrated in Figure 5.2 (f). The description of the peaks is exactly as those obtained when MA was 500 mV. Thus, it can be concluded that the response of the loss-modulated EDFRL at 1000 mV MA can be modeled and predicted theoretically with an average accuracy of 87.50 % for the resonance frequency peaks (Table 5.4) and 93.75 % for the frequency after which saturation is observed (Table 5.5).

To further explain other features of the bifurcation diagrams; it is essential to mention that during modulation from low to high and high to low frequency, OB regions were also seen as shown in Figure 5.2 (b), Figure 5.2 (c)

and Figure 5.2 (d) close to or exactly at the main ω_r and 1st super harmonic ω_r . In Figure 5.2 (b), the 1st OB region indicated as “1st OB” appeared from MF of 6 kHz to 8 kHz which is the range of super-harmonic resonance frequency (Onubogu, Pua and Faidz, 2021). The "2nd OB" region in the same figure appeared between MF of 13 kHz and 15 kHz, which is precisely the main resonance frequency range. Although the output amplitudes of the two OB regions differ as the "1st OB" has a lower amplitude of 4.393 mV and the "2nd OB" has a higher amplitude of 12.1 mV, the hysteresis extents of the two OB regions are identical. In Figure 5.2 (c), only one OB region covering a broader extent of 10 kHz MF to 14 kHz MF is seen, in which the main ω_r is 14 kHz with 18.15 mV maximum output amplitude. In Figure 5.1 (d), one quite narrow OB region of 6 kHz MF to 7 kHz MF exists at the 1st super harmonic ω_r (7 kHz) in contrast to the OB regions in Figures 5.2 (b) and 5.2 (c).

To better understand the linear and chaotic behaviors of the EDFRL under cavity-loss modulation, some experimental time domains and frequency domains of the EDFRL obtained during modulation have also been studied and presented for some MFs in Figures 5.2 (a) to 5.2 (d) and displayed in Figures 5.3, 5.4, 5.5 and 5.6. Figure 5.3 illustrates the time domains and frequency domains for 7 kHz, 14 kHz, and 20 kHz MF when MA is 200 mV. The spectrum of the time and frequency domains all show a wave pattern that is uneven for all the MFs, including at the ω_r of 14 kHz too. In Figure 5.3 (b), the frequency domain displays a resonance peak at only 14 kHz ω_r . No peak is seen at other MFs.

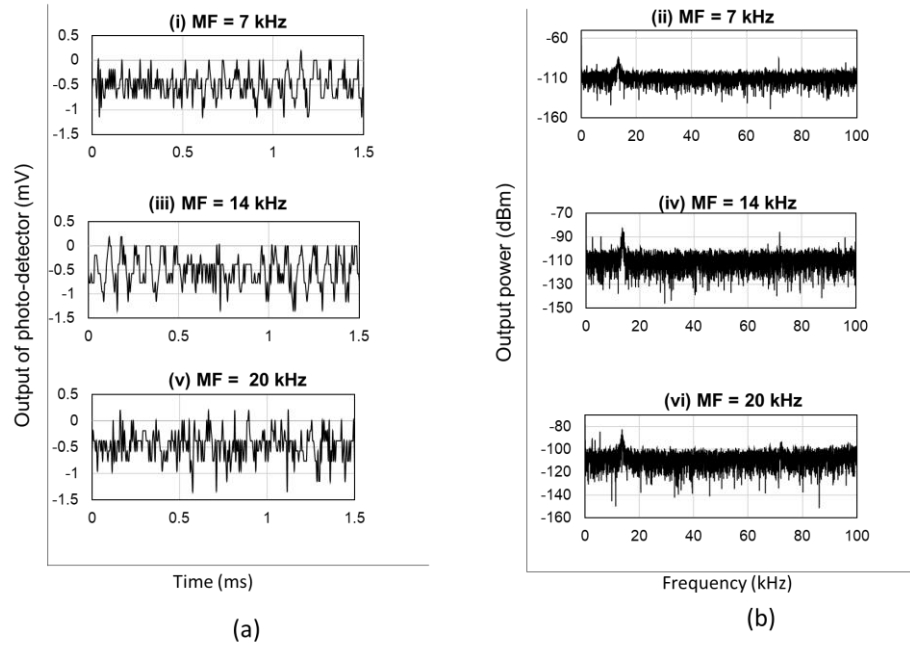


Figure 5.3: (a) Time domain response obtained from experimental loss modulated EDFRL with 14 kHz ω_r and 200 mV MA at (7, 14, and 20) kHz MF; (b) Corresponding frequency domain responses (Onubogu, Pua and Faidz, 2021)

At 500 mV MA, the experimental and theoretical time domains and frequency domains are illustrated in Figure 5.4 for (3, 7, 14, and 18) kHz MF. The time domain spectrum for 3 kHz in Figure 5.4 (a) (i) revealed a chaotic-like irregular wave pattern from 1 kHz MF to 6 kHz MF. Chaos in the EDFRL's cavity was evident from the frequency domain spectral response in Figure 5.4 (b) (ii), which showed a distinct peak at 14 kHz ω_r , a second peak at MF of 3 kHz, and several peaks at higher harmonics. The appearance of a resonant peak at the main ω_r indicated the sensitivity of the EDFRL when it is cavity-loss modulated. At the 1st super-harmonic ω_r (7 kHz), the time domain spectrum in Figure 5.4 (a) (iii) displayed an attempting sinusoidal waveform

meaning an inclination to linearity. In Figure 5.4 (b) (iv), the frequency domain displayed peaks at 7 kHz MF, 14 kHz MF, and also at other higher harmonics. In Figure 5.4 (a) (i) and Figure 5.4 (b) (ii), non-linear behavior was displayed between 8 kHz MF to 13 kHz MF as seen in the time domain response signifying chaos. At 14 kHz MF (also the ω_r of the EDFRL), the time domain figure (Figure 5.4 (a) (v)) displayed a sinusoidal waveform indicating a linear response. In the frequency domain (Figure 5.4 (b) (vi)), a distinct peak is exhibited at 14 kHz ω_r after which another peak called the secondary resonance peak is seen at 28 kHz. Another area of chaos can be seen between 15 and 20 kHz MF (Figure 5.4 (a) (vii) and Figure 5.4 (b) (viii)). The theoretical time and frequency domains illustrated in Figure 5.4 (c.) and (d.) showed a good match with the experimental time and frequency domains. Hence, it can be concluded that at 500 mV MA, chaos does not only occur at the ω_r and superharmonic ω_r of the EDFRL but at other high and low frequencies as well. This means that the cavity-loss modulated EDFRL is more sensitive at 500 mV MA, implying that it can be used for sensing in pipeline monitoring and bio-systems modeling at this MA (Kumar, and Vijaya, 2015).

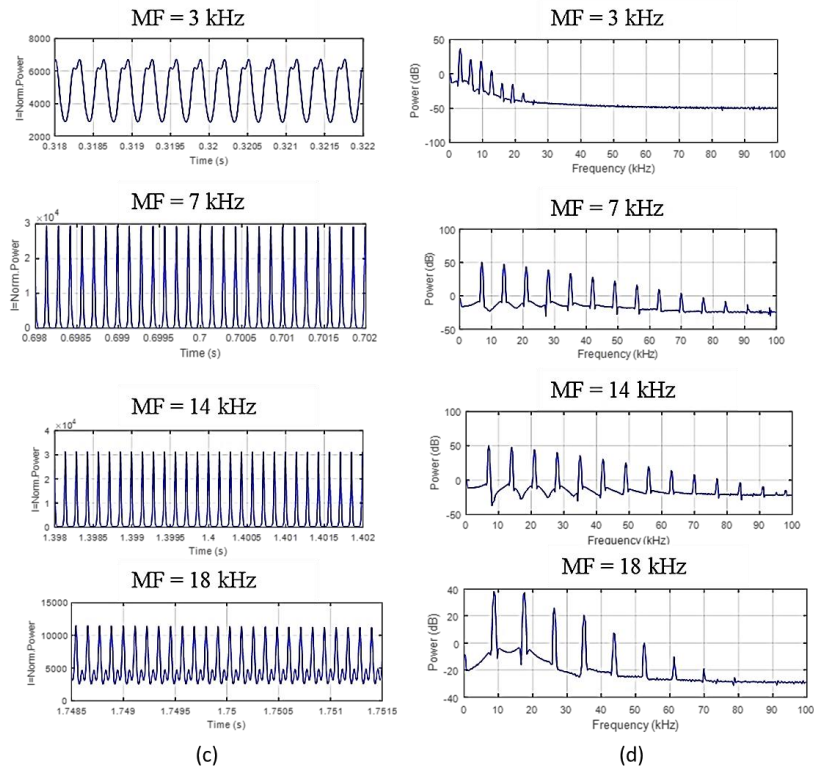
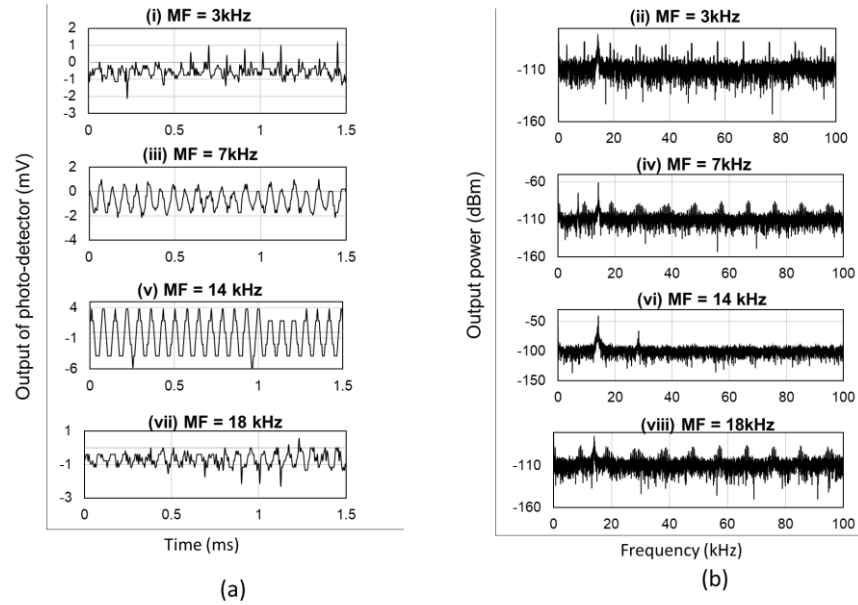


Figure 5.4: (a) Time domain response obtained from experimental loss modulated EDFRL with 14 kHz ω_r and 500 mV MA at (3, 7, 14, and 18) kHz MF; (b) Corresponding frequency domain response (Onubogu, Pua and Faidz, 2021) (c) Theoretical time domain response (d) Theoretical frequency domain response.

For 900 mV MA, the time and frequency domains (Figure 5.5 (a) and Figure 5.5 (b)) of the bifurcation result are presented for (3, 6.8, 10, and 13.6) kHz MF. At 1 kHz MF to 6 kHz MF, chaos was seen in the time domain spectrum as displayed for 3 kHz in Figure 5.5 (a) (i). In Figure 5.5 (b) (ii), the frequency domain spectral response showed an obvious peak at 14 kHz ω_r . Two other peaks also appeared at MF of 3 kHz and 6 kHz MF (harmonic resonance). Linear behavior depicted as a sinusoidal waveform was observed at MF of 6.8 kHz to 7 kHz as illustrated in Figure 5.5 (a) (iii), where 7 kHz is the 1st super-harmonic resonance.

One peak can be seen in the frequency domain diagram (Figure 5.5 (b) (iv)) at 6.8 kHz MF; another peak occurred at 14 kHz ω_r , and the final peak occurred at 27 kHz MF, which is almost the secondary ω_r . The time domain response at MF of 10 kHz (Figure 5.5 (a) (v)) and the frequency domain response (Figure 5.5 (b) (vi)), which shows three peaks at 10 kHz, 14kHz, and 20 kHz MF (secondary harmonic resonance), both demonstrate that chaos exists from MF of 8 kHz to MF of 12 kHz. Meanwhile, at MF of 13 kHz, a tendency toward linearity is seen as indicated in the time and frequency domains. The time domain spectrum for 13.6 kHz MF to 14 kHz MF in Figure 5.5 (a) (vii) illustrates linearity. In Figure 5.5 (b) (viii), the frequency domain displayed a peak at 14 kHz (ω_r) and a 2nd peak at 27.35 kHz MF to 28 kHz (secondary ω_r). Chaos was seen again from 15 kHz MF to 20 kHz MF.

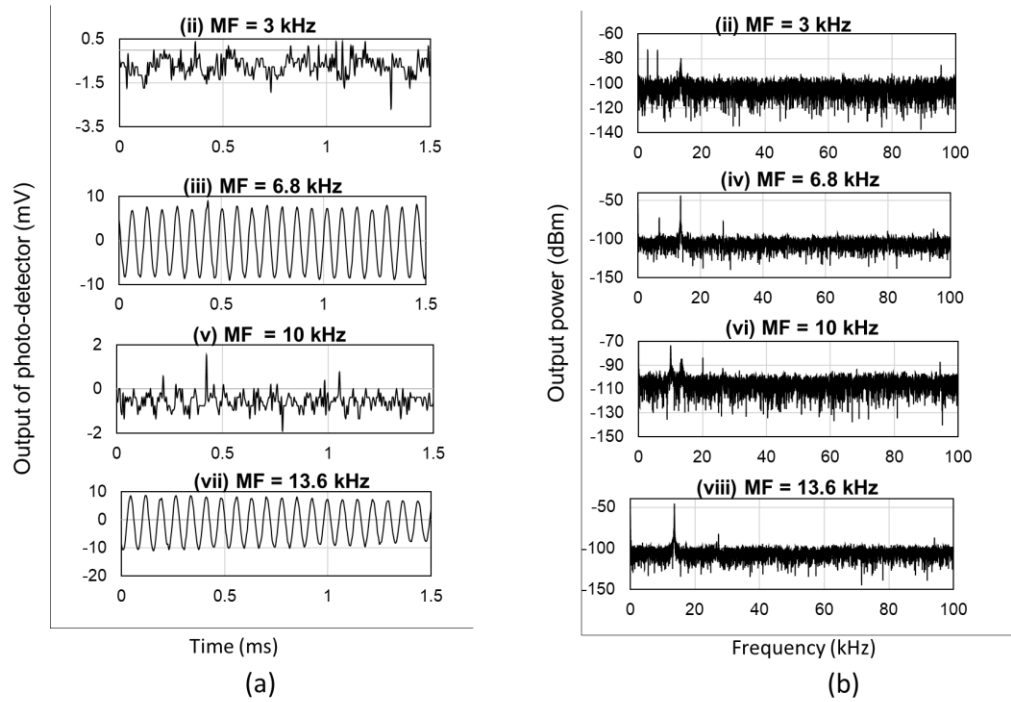


Figure 5.5: (a) Time domain response obtained from experimental loss modulated EDFRL with 14 kHz ω_r and 900 mV MA at MF of 3 kHz; 6.8 kHz; 10 kHz and 13.6 kHz; (b) Corresponding frequency domain (Onubogu, Pua and Faiz, 2021)

For 1000 mV MA, the time and frequency domains (Figure 5.6 (a) and Figure 5.6 (b)) of the bifurcation result are presented for 1 kHz MF, 2 kHz MF, 6.7 kHz MF, and 13.5 kHz MF. In Figure 5.6 (a) (i), the time domain response at 1 kHz MF showed a bit of chaos but tended towards linearity. In Figure 5.5 (b) (ii), the frequency domain spectrum depicted a peak at 1 kHz MF, some harmonic peaks, and another peak at 14 kHz signifying “stable pulsation to chaos”. Chaos was seen from 2 kHz to 6 kHz MF as shown in the time domain response for 2 kHz MF (Figure 5.6 (a) (iii)). A peak can be seen in the frequency domain at 2 kHz MF and 14 kHz ω_r , as shown in Figure 5.6 (b) (iv). A linear

response is seen again at MF of 6.7 kHz to MF of 7 kHz as illustrated by the time domain spectrum in Figure 5.6 (a) (v). The frequency domain spectrum showed a peak at 6.7 kHz MF, a second peak at 14 kHz ω_r , and a third peak at 27.5 kHz (secondary ω_r), as shown in Figure 5.6 (b)(vi). A strange behavior unlike what was seen at other MAs was observed from 8 kHz MF to 20 kHz MF. In the time domain (Figure 5.6 (a) (vii)) and frequency domain (Figure 5.6 (b) (viii)) for MF of 13.5 kHz, chaos was evident throughout, even at 14 kHz ω_r . This is possible because, at 1000 mV MA, the EDFRL gets to a saturation point after 7 kHz; therefore, there is no linearity seen as anticipated. This behavior indicates that the EDFRL subjected to cavity-loss modulation has a higher sensitivity to the acoustic wave emanating from the loudspeaker when the MA is greater than 200 mV but less than or equal to 1000 mV.

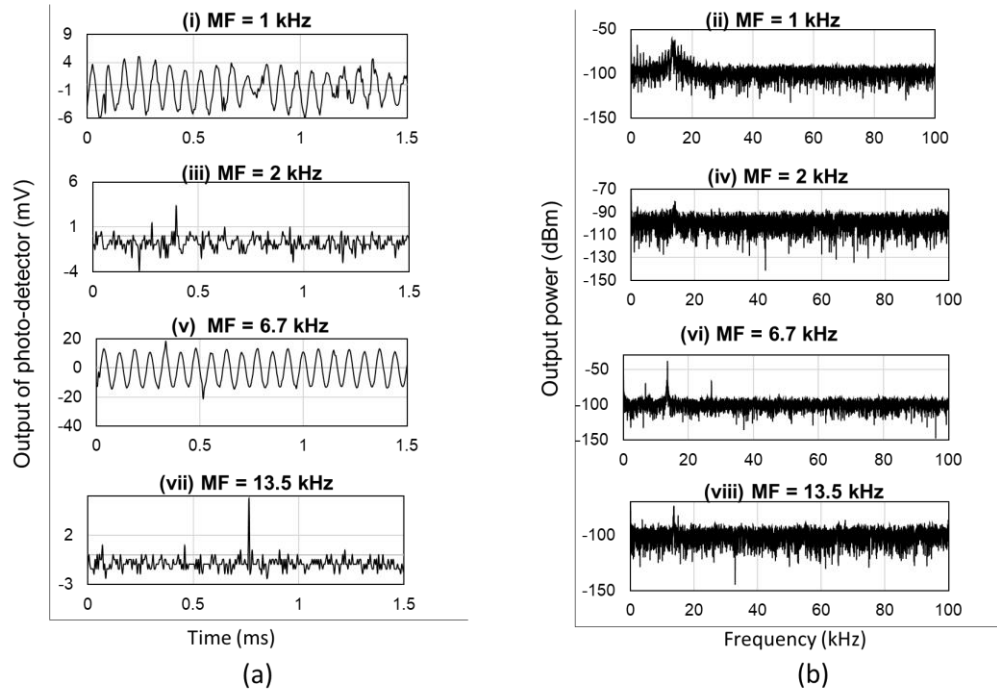


Figure 5.6: (a) Time domain response obtained from experimental loss modulated EDFRL with 14 kHz ω_r and 1000 mV MA at (1, 2, 6.7 and 13.5) kHz MF; (b) Corresponding frequency domain (Onubogu, Pua and Faidz, 2021)

5.3 Summary

In this chapter, the behaviors observed during experimental and theoretical cavity loss modulations of the EDFLL and the EDFRL under several initial conditions have been presented. In summary, the results of the external cavity-loss modulation of the EDFRL revealed some significant observations (Onubogu, Pua, and Faidz, 2021):

- The dynamical behaviors of the EDFRL under external cavity loss modulation definitely confirm the occurrence of bifurcation.

- The sensitivity of the EDFRL under external cavity-loss modulation is indicated by the emergence of a resonance peak at the fundamental ω_r .
- During external cavity-loss modulation experiments of the EDFRL, when the MA is increased, the number of OB regions decreases as depicted in the bifurcation diagrams in Figures 5.2 (b), (c), and (d).
- During external cavity-loss modulation experiments of the EDFRL at MA ranging from 500 mV to 1000 mV, the bifurcation diagrams revealed the presence of two resonant peaks at the fundamental and first superharmonic resonance frequencies, indicating the system's dynamic nonlinear behavior.
- During variation of the MF in ascending and descending order, a general trend was noticed. For 500 mV and 900 mV MA, the peak amplitudes clearly get stronger around the fundamental ω_r and drop just after. The same trend was also seen around the 1st super-harmonic ω_r . Also, the output amplitude's intensity at the fundamental ω_r increases as seen in the bifurcation diagram in Figure 5.2 (b) and Figure 5.2 (c). But in Figure 5.2 (d), a decrease in the output amplitude is seen at the fundamental ω_r . This indicates that as the MA increases, the EDFRL's sensitivity to external cavity-loss modulation under MF variation with constant pump power rises until it reaches a maximum where sensitivity decreases at the fundamental ω_r .
- The EDFRL subjected to external cavity-loss modulation has a higher sensitivity to the acoustic wave emanating from the loudspeaker when the MA is greater than 200 mV but less than or equal to 1000 mV.

- It can be concluded that the dynamic response of the loss-modulated EDFRL can be modeled and predicted theoretically with an overall average accuracy of 91.07 % for the resonance frequency peaks (Table 5.4) and 95.96 % for the frequency after which saturation is observed (Table 5.5). Other authors such as Saucedo-Solorio, et al., (2003), Ghosh and Vijaya, (2014) and Kumar and Vijaya, (2015) have succeeded in producing theoretical results that described all the characteristics experimentally observed.

CHAPTER 6

CONCLUSION AND FUTURE WORK

6.1 Conclusion

An Erbium-doped fiber laser sensor has been designed and tested for its efficiency in pipeline leakage detection and location. The sensed environment is a ground-level water pipeline. Results obtained from the pipeline field test experiments showed that the EDFL sensor is capable of detecting leakage and the location of leakage with an overall calculated average accuracy of 90 %. This sensor has numerous advantages which include: simplicity, flexibility to bend to any shape, great sensitivity to external perturbations, acoustic wave detection capability with tunable sensitive frequency, applicability in harsh environments, low maintenance, high accuracy, cheap to manufacture, immunity to electromagnetic waves, etc. This is the first objective of this research. However, some instabilities were observed in the sensor as the signal from the Pico scope showed numerous peaks during sensing, especially for the sensor placed further away from the leak point. These numerous peaks can be confusing to the sensor reader. Therefore, to understand the reason behind the instabilities and the dynamic behavior of the EDFL sensor, it was necessary to carry out experimental and theoretical analysis to understand whether the bifurcation happening in the EDFL as experienced by other researchers (as discussed in the literature review) is the root cause of the instabilities.

Hence, the dynamics of the linear laser called the EDFLL and ring laser called the EDFRL under the pump and external cavity-loss modulations were investigated experimentally and theoretically. This is the second objective of this research. All experiments were carried out in the lab at UTAR, Sungai Long campus. For the numerical simulation to be carried out, an improved novel model that considers the EDFL's resonance frequency at a specific time was presented. This is the third objective of this research. The ω_r was considered because the EDFL is a resonator that is capable of having various ω_r values at various times. This was of great importance for the classification of the EDFL's sensitivity to acoustic waves. The improved novel model used for the numerical simulation was built from two rate equations of a class B laser for the laser power inside the cavity and the population inversion. Laser dynamic behaviors such as bifurcation including optical bi-stability (OB) regions and chaotic regions (occurring mostly at the ω_r) were identified in all results confirming the fact that this is probably the root cause of the unstable behavior of the EDFL sensor. From the experimental and theoretical pump and loss modulations of the EDFLL and the EDFRL, the following conclusions have been made:

- The response of the pump-modulated EDFLL can be predicted theoretically with an overall average accuracy of 91.09 % for the resonance frequency peaks (Table 4.2); 91.58 % for the frequency after which saturation is observed (Table 4.3) and 85.64 % for the width of the OB regions (Table 4.4).
- The response of the pump-modulated EDFRL can be predicted theoretically with an overall average accuracy of 86.60 % for the

resonance frequency peaks (Table 4.7) and 90.79 % for the frequency after which saturation is observed (Table 4.8).

- The response of the loss-modulated EDFLL can be predicted theoretically with an overall average accuracy of 91.04 % for the resonance frequency peaks (Table 5.2) and 91.70 % for the frequency after which saturation is observed (Table 5.3).
- The response of the loss-modulated EDFRL can be modeled and predicted theoretically with an overall average accuracy of 91.07 % for the resonance frequency peaks (Table 5.4) and 95.96 % for the frequency after which saturation is observed (Table 5.5).

The main significance of this research is that the modified theoretical model presented in Chapter 3 can be used to quickly predict the results of the sensor for further improvement in the future. The experimental and theoretical results indicated that the EDFLL and EDFRL can be utilized for sensing purposes in places having high background noise including water pipelines (either buried or on the surface). This is possible because of their high sensitivity even at low frequencies notwithstanding the noise. This is the main proposed application of this sensor. Nevertheless, the EDFL sensor can also be applied in underground oil and gas pipelines, but each will have unique features and sensor characterization is necessary to suit distinct purposes. Furthermore, the behavior of the EDFL portrayed its potential use in other engineering applications such as optical switches, bio-mimicking, and also as for multi-stable switching.

6.2 Recommendation for Future Works

For performance improvement, the EDFLL and EDFRL sensors should be used for real pipeline leakage detection in the field to further confirm their sensitivity in detecting leak points on the pipeline.

The experimental and theoretical analysis performed on the laser configurations aided in understanding the dynamic behavior of the EDFLL and the EDFRL. However, the new strange dynamic behavior identified from the theoretical results obtained when pump modulating the EDFRL from high frequency to low frequency under some initial conditions requires further studies to understand its cause and also the possible applications of this strange behavior.

Integration of the pump and external cavity-loss modulations on the EDFLL and the EDFRL is suggested to get better control of the bifurcations to further improve the sensor. It might also be useful to understand the behavior of the EDFRL under internal cavity-loss modulations based on its proposed application.

Lastly, it is suggested to apply the modified theoretical model in predicting the results of the sensor for further improvements.

REFERENCES

Afanador Delgado, S.M., Echenausía Monroy, J.L., Huerta Cuellar, G., García López, J.H. and Reátegui, R.J., 2022. Implementation of Logic Gates in an Erbium-Doped Fiber Laser (EDFL): Numerical and Experimental Analysis. *Photonics*, 9, pp.977.

Afanador Delgado, S.M., Echenausía Monroy, J.L., Huerta Cuellar, G., García López, J.H. and Reátegui, R.J., 2023. Numerical and Experimental Data of the Implementation of Logic Gates in an Erbium-Doped Fiber Laser (EDFL). *Data*, 8, pp.7.

Allwood, G., Hinckley, S. and Wild, G., 2012. Optical fiber sensors in physical intrusion detection systems: A review. *Journal of Latex Class Files*, [e-journal] 11(4), pp.1–13. DOI: 10.1109/JSEN.2016.2535465.

Arellano-Sotelo, H., Kir'yanov, A.V., Barmenkov, Y.O, and Aboites, V., 2011. The use of nonlinear dynamics of erbium-doped fiber laser at pump modulation for intra-cavity sensing. *Optics & Laser Technology*, 43(1), pp.132-137.

Bush, J., Davis, C.A., Davis, P.G., Cekorich, A. and McNair, F.P., 1999. *Buried fiber intrusion detection sensor with minimal false alarm rates*. In Proceedings of SPIE 3860 Photonics East, Fiber Optic Sensor Technology and Applications. Boston, Massachusetts, 9th December, pp.285–295.

Canavese, G. et al., 2015. A novel smart calliper foam pig for low-cost pipeline inspection- Part A: Design and laboratory characterization. *Journal of Petroleum Science and Engineering*, 127, p. 311-317.

Catalano, A., Bruno, F., Pisco, M., Cutolo, A., and Cusano A., 2014. *Intrusion detection system for the protection of railway assets by using fiber Bragg grating sensors: a case study*. In Proceedings 2014 IEEE Third Mediterranean

Photonics Conference. Trani, Italy, 7-9 May. DOI: 10.1109/MePhoCo.2014.6866483.

Crosby, M.G., 1937. Frequency modulation noise characteristics, in proceedings of the institute of radio engineers, [e-journal], 25 (4), pp. 472-514, DOI: 10.1109/JRPROC.1937.229050.

Digonnet, M.J.F., 2001. *Rare earth doped fiber lasers and amplifiers. Revised and expanded*. 2nd ed. Marcel Dekker, New York.

Doherty, C.M, Lindroos, M., Barton, D.P., 2003. *Structural health monitoring of aircraft using CVM*. In 4th Australian Pacific Vertiflite Conference on Helicopter Technology. Melbourne, Australia.

Esqueda De La Torre, J.O., García López, J.H., Jaimes-Reátegui, R., Pisarchik, A. and Huerta-cuellar, G., 2022. *Effects of Optical Laser Injection in Multistable Erbium Fiber Lasers. Chaos Theory and Applications, Dissemination and Research in the Study of Complex Systems and Their Applications* (EDIESCA 2022), pp.226-233. DOI: 10.51537/chaos.1197559

Feng, X., Tam, H.Y., Lu, C., Wai, P.K.A. and Guan, B., 2009. *Multiwavelength Erbium-Doped Fiber Laser Employing Cavity Loss Modulation*. In *IEEE Photonics Technology Letters*, 21(18), pp. 1314-1316.

Frings, J. and Walk, T., 2010. Pipeline leak detection using distributed fiber optic sensing. *3R international – Special-Edition*, 2, pp. 57- 61.

Fu, H., Chen, D. and Cai, Z., 2012. Fiber Sensor Systems Based on Fiber Laser and Microwave Photonic Technologies. *Sensors*, 12, pp.5395-5419.

Fu, Q., Wan, H. and Qiu, F., 2010. Pipeline Leak Detection based on Fiber Optic Early-Warning System. *Symposium on Security Detection and Information Processing, Procedia Engineering*, 7, pp. 88-93.

Galindez-Jamioy, C.A. and López-Higuera, J.M., 2012. Brillouin Distributed Fiber Sensors: An Overview and Applications. *J. Sens.*, 204121.

García-López, J.H., Jaimes-Reátegui, R., Afanador-Delgado, S.M., Sevilla-Escoboza, R., Huerta-Cuellar, G., Casillas-Rodríguez, F.J., López-Mancilla, D. and Pisarchik, A.N., 2014. *Optoelectronic flexible logic-gate using a chaotic erbium doped fiber laser, experimental results*. In: Latin America Optics and Photonics Conference. OSA Technical Digest (online) (Optical Society of America)

García-López, J.H., Jaimes-Reátegui, R., Afanador-Delgado, S.M., et al., 2018. *Experimental and Numerical Study of an Optoelectronics Flexible Logic Gate Using a Chaotic Doped Fiber Laser. Recent Development in Optoelectronic Devices*. InTech. DOI: 10.5772/intechopen.75466.

Ghosh, A. and Vijaya, R., 2014. Linear and non-linear resonance features of an erbium-doped fiber ring laser under cavity-loss modulation. *Pramana – Journal of Physics*, 83, pp.147-159.

Ghosh, A., Goswami, B.K and Vijaya, R., 2010. Nonlinear resonance phenomena of a doped fibre laser under cavity-loss modulation: Experimental demonstrations. *Pramana – Journal of Physics*, 75, pp.915-921.

Gorshkov, B.G. et al., 2022. Scientific Applications of Distributed Acoustic Sensing: State-of-the-Art Review and Perspective. *Sensors*, 22, 1033.

Graham, W. and Steven, H., 2010. *Optical Fibre Bragg Gratings for Acoustic Sensors*, Proceedings of 20th International Congress on Acoustics, ICA 2010, 23-27 August, Sydney, Australia.

Gursel, A.T., 2018. *Fiber Lasers and Their Medical Applications. Optical Amplifiers - A Few Different Dimensions*. InTech. DOI: 10.5772/intechopen.76610.

He, Z. and Liu, Q., 2021. Optical Fiber Distributed Acoustic Sensors: A Review. *J. Light. Technol.*, 39, pp.3671–3686.

Inaudi, D. and Glisic, B., 2010. Long-range pipeline monitoring by distributed fiber optic sensing. *Journal of Pressure Vessel Technology*, 13, pp.0117011-0117019.

Jaimés-Reategui, R., Afanador-Delgado, S.M., Sevilla-Escoboza, R., Huerta-Cuellar, G., Hugo, G-LJ., Lopez-Mancilla, D., Castañeda-Hernandez, C. and Pisarchik, A.N. 2014. Optoelectronic flexible logic gate based on a fiber laser. *The European Physical Journal Special Topics*, 223, pp.2837-2846.

Keren, S. and Horowitz, M., 2001. Interrogation of fiber gratings by use of low-coherence spectral interferometry of noiselike pulses. *Optics Letters*, 26, pp.328–330.

Kumagai, T., Sato, S. and Nakamura T., 2012. *Fiber-optic vibration sensor for physical security system*. In Proceedings of IEEE International Conference on Condition Monitoring and Diagnosis. Bali, Indonesia, 23 – 27 September, pp.1171–1174. DOI:10.1109/CMD.2012.6416369.

Kumar, G. and Vijaya, R., 2015a. Dynamical features of loss and pump modulation in an erbium-doped fiber ring laser. *Journal of Optics*, 17, 125402, pp.1-9.

Kumar, G. and Vijaya, R., 2015b. Dynamics of erbium-doped fiber ring laser under cavity loss modulation. *Physica D: Non-linear phenomena*. 304-305, pp.34-41.

Kumar, G. and Vijaya, R., 2017a. Dynamical bistability of a loss modulated erbium doped fiber ring laser. *Applied Physics B*, [e-journal], 123, 152. <https://doi.org/10.1007/s00340-017-6729-4>.

Kumar, G. and Vijaya, R., 2017b. Control of dynamics in a loss-modulated erbium-doped fiber ring laser. *Journal of the Optical Society of America B*, 34, pp.574-582.

- Kraus, M., Ahmed, M.A., Michalowski, A., Voss, A., Weber, R., and Graf, T., 2010. Microdrilling in steel using ultrashort pulsed laser beams with radial and azimuthal polarization. *Optics Express*, 18, pp.22305–22313.
- Ke, J., Yi, L., Xia, G. and Hu, W., 2018. Chaotic optical communications over 100-km fiber transmission at 30-Gb/s bit rate. *Optics Letters*, 43, pp.1323–1326.
- Lacot, E., Stoeckel, F. and Chenevier, M., 1994. Dynamics of an erbium doped fiber laser. *Physical Review A*, 49, pp.3997-4008.
- Li, J. and Zhang, M., 2022. Physics and applications of Raman distributed optical fiber sensing. *Light Sci Appl.*, **11**, pp.128.
- Liu, C., Li, Y., Yan, Y., Fu, J. and Zhang, Y., 2015. A new leak location method based on leakage acoustic waves for oil and gas pipelines. *Journal of Loss Prevention in the Process Industries*, [e-journal] 35, pp. 236-246. <https://doi.org/10.1016/j.jlp.2015.05.006>.
- Liu, T., Jiang, J., Wang, S. and Liu, K., 2022. *Optical Fiber Sensing Technologies: Principles, Techniques and Applications*. Wiley, Germany.
- Luca, P., Luca, S., Marco, S. and Andrea, G., 2022. Rayleigh-Based Distributed Optical Fiber Sensing. *Sensors*, [e-journal], 22(18), pp.6811 <https://doi.org/10.3390/s22186811>.
- Luo, L., Tee, T.J. and Chu, P.L., 1998. Bistability of erbium-doped fiber laser. *Optics Communications*, 146, pp.151-157.
- Luo, L.G. and Chu, P.L., 1998. Optical secure communications with chaotic erbium-doped fiber lasers, *Journal of the Optical Society of America B*, 15, pp.2524-2530.
- Mohanaprasad, K., Law, Z., Morris, A.G.E., Pua, C.H., 2020. Adaptive Independent Component Analysis–Based Cross-Correlation Techniques along

with Empirical Mode Decomposition for Water Pipeline Leakage Localization Utilizing Acousto-Optic Sensors, *Journal of Pipeline Systems Engineering and Practice*, 11(3): 04020027.

Morin, F., Druon, F., Hanna, M. and Georges, P., 2009. Microjoule femtosecond fiber laser at 1.6 μm for corneal surgery applications. *Optics Letters*, 34, pp.1991–1993.

Moura Jr, J.R.V. and Steffen Jr, V., 2005. *Damage detection techniques for aeronautic structures*. In: 23rd International Modal Analysis Conference (IMAC XXIII).

Onubogu, N.O. and Pua, C.H., 2022. *Dynamic behavior of a pump-modulated erbium-doped fiber linear laser with single fiber Bragg grating*. In A. Sivasubramanian, P.N. Shastry, P.C. Hong (Eds.), *Futuristic Communication and Network Technologies, Lecture Notes in Electrical Engineering*. Singapore: Springer. https://doi.org/10.1007/978-981-16-4625-6_28.

Onubogu, N.O., Pua, C.H., Lin, H.S. and Faidz, A-R., 2019. *Dynamics of a highly sensitive erbium-doped Fabry-Perot fiber (EDFBF) laser sensor under pump modulation*. In: 24th Microoptics Conference (MOC), Toyama, Japan, 17-20 November, pp. 262-263. doi: 10.23919/MOC46630.2019.8982878.

Onubogu, N.O., Pua, C.H. and Faidz, A-R., 2021. Dynamic features of a non-polarized Erbium-doped fiber ring laser subjected to external cavity-loss modulation. *Optik* 225, 165846, pp.1-8

Onubogu, N.O., Pua, C.H., Lin, H.S. and Faidz, A., 2020. The dynamic behavior of non-polarized erbium-doped fiber ring laser under experimental pump modulation. *Optik*, 207, 164442.

Onubogu, N.O., Pua, C.H., Faidz, A-R and Rose, W.C., 2022. Numerical analysis of the behavioral response of pump-modulated linear and ring erbium-doped fiber lasers, *Optik*, [e-journal] 266, 169519. <https://doi.org/10.1016/j.ijleo.2022.169519>.

- Paget, C., Atherton, K., and O'Brien, E., 2004. *Damage assessment in a full-scale aircraft wing by modified acoustic emission*. In 2nd European Workshop on SHM. Munich, Germany, 7-9 July 2004.
- Pendão, C. and Silva, I., 2022. Optical Fiber Sensors and Sensing Networks: Overview of the Main Principles and Applications. *Sensors*, 22(19), pp.7554.
- Philippov, V., Codemard, C., Jeong, Y., Alegria, C., Sahu, J.K., Nilsson, J. and Pearson, G.N., 2004. High-energy in-fiber pulse amplification for coherent lidar applications. *Optics Letters*, 29, pp.2590–2592.
- Ping, L., Nageswara, L., Mudabbir, B., Liu, B., Benjamin, T., Chorpeneing, Michael, P. B., and Paul, R.O., 2019. Distributed optical fiber sensing: Review and perspective. *Applied Physics Reviews* 6, 041302.
- Pisarchik, A.N. and Barmenkov, Y.O., 2005. Locking of self-oscillation frequency by pump modulation in an erbium-doped fiber laser. *Optics Communications*, [e-journal], 254, pp.128–137, <https://doi.org/10.1016/j.optcom.2005.05.028>.
- Pisarchik, A.N., Barmenkov, Y.O. and Kir'yanov, A.V., 2003. Experimental characterization of the bifurcation structure in an erbium-doped fiber laser with pump modulation. *IEEE Journal of Quantum Electronics*, 39 (12), pp.1567–1571.
- Pisarchik, A.N., Kir'yanov, A.V., Barmenkov, Y.O. and Jaimes-Reategui, J., 2005. Dynamics of an erbium-doped fiber laser with pump modulation: theory and experiment. *Journal of the Optical Society of America B*, 22(10) pp.2107–2114.
- Pua, C.H., Ahmand, H., Harun, S. and De La Rue, R., 2012a. Direct airborne acoustic wave modulation of Fabry–Perot fiber laser (FPFL) over 100 kHz of operating bandwidth. *Applied optics*, 51, (15) pp.2772-2777.
- Pua, C.H., Ahmand, H., Harun, S. and De La Rue, R., 2012b. Study of Dual-wavelength mode competition in an Erbium-doped fiber laser (EDFL)

produced by acoustic waves, *IEEE Journal of Quantum Electronics*, 48(12), pp. 1499-1504.

Pua, C.H., Chong, W.Y. and Ahmad, H., 2013. Instantaneous response of wide area intrusion sensor with long haul monitoring capability. *IEEE Photonics Technology Letters*, [e-journal] 25 (23), pp.2255-2258. DOI: 10.1109/LPT.2013.2284608.

Rao, Y.J., 1997. In-fibre Bragg grating sensor. *Meas. Sci. Technol.*, 8, pp.355–375.

Rajeev, P., Kodikara, J., Chiu, W.K. and Kuen, T., 2013. Distributed optical fiber sensors and their applications in pipeline monitoring. *Key Engineering Materials*, 558, pp. 424-434.

Reátegui, J., 2004. *Dynamic of complex system with parametric modulation: Duffing oscillators and a fiber laser*. Tesis de Doctorado en Ciencias (Óptica), Centro de Investigaciones en Óptica, A.C. León, Guanajuato. Available at: <https://cio.repositorioinstitucional.mx/jspui/bitstream/1002/796/1/10381.pdf> [Accessed 30th May, 2021].

Reategui, J., Kir'yanov, A.V., Pisarchik, A.N., Barmenkov, Y.O. and Il'ichev, N.N., 2004. Experimental study and modelling of coexisting attractors and bifurcations in an Erbium-doped fiber laser with diode-pump modulation. *Laser Physics*, 14(9), pp.1–5.

Roach, D., 2018. Use of Comparative Vacuum Monitoring Sensors for Automated, Wireless Health Monitoring of Bridges and Infrastructure. In: *Proceedings of the Ninth International Conference on Bridge Maintenance, Safety and Management (IABMAS 2018)*. Melbourne, Australia, 9-13 July 2018. London: CRC Press.

Ronghua, C., Hangtao, Z. and Liya, L., 2018. *A Novel Long Distance Fiber Bragg Grating Sensor System with Low Threshold Pump Power and High*

OSNR. International Symposium on Communication Engineering & Computer Science (CECS 2018), Advances in Computer Science Research, 86.

Saucedo-Solorio, J.M., Pisarchik, A.N., Kir'yanov, A.V. and Aboites, V., 2003. Generalized multistability in a fiber laser with modulated losses. *Journal of the Optical Society of America B*, 20, pp.490-496.

Selleri, S. and Poli, F., 2008. *Doped fiber lasers: From telecom to industrial applications*. 2008 10th Anniversary International Conference on Transparent Optical Networks, Athens, Greece, pp.206-209, doi: 10.1109/ICTON.2008.4598408.

Sharma, U., Kim, C.S. and Kang, J.U., 2004. Highly stable tunable dual-wavelength Q-switched fibre laser for DIAL applications. *IEEE Photonics Technology Letters*, 16, pp.1277–1279.

Sola, I.J., Martin, J.C. and Alvarez J.M., 2002. Nonlinear response of a unidirectional erbium-doped fiber ring laser to a sinusoidally modulated pump power. *Optics Communication*, 212(4-6), pp.359-369.

Subramaniam, T.K., 2015. Erbium Doped Fiber Lasers for Long Distance Communication Using Network of Fiber Optics. *American Journal of Optics and Photonics*. 3(3), pp.34-37.

Wooler, J. and Crickmore, R., 2005. *Fibre optic seismic intruder detection*. In Proceedings SPIE 5855, 17th International Conference on Optical Fiber Sensors. Bruges, Belgium, 23-27 May, pp.278–281. <https://doi.org/10.1117/12.624006>

Woon, S.L., Kwan, K., Chong, W., Lin, H. and Pua, C.H., 2017. Cascaded acoustic wave sensors based on Erbium-doped fiber laser dynamics for intrusion zone identification. *IEEE sensors*, 17(6), pp.1893-1898.

Woon S.L., Pua C.H., Lin H.S. and Rahman F.A., 2018. *Application of Erbium-Doped Fibre Laser Dynamics in Pipeline Leak Detection and*

Location Estimation, In proceedings: IEEE 7th International Conference on Photonics (ICP). Langkawi, Malaysia, pp.1-3. doi: 10.1109/ICP.2018.8533164.

Wu, D., Peng, B. and Xu, Q., 2010. *A building structure health Monitoring System based on the characteristic of TFBG*. In: The 9th International Conference on Optical Communications and Networks (ICOCN2010). Nanjing, China, 24-27 October.

Wu, Y., Bian, P., Jia, B., and Xiao Q., 2013. *A novel Sagnac fiber optic sensor employing time delay estimation for distributed detection and location*. In Proceedings SPIE 8896, Electro-Optical and Infrared Systems: Technology and Applications X. Dresden, Germany, 25th October. <https://doi.org/10.1117/12.2028311>.

Wu, Q., Okabe, Y. and Sun, J., 2014. Investigation of dynamic properties of erbium fiber laser for ultrasonic sensing. *Optics Express*, 22, pp.8405–8419.

Yan, S.Z. and Chyan, L.S., 2010. Performance enhancement of BOTDR fiber optic sensor for oil and gas pipeline monitoring. *Optical Fiber Technology*, 16, pp.100-109.

Yan, Z., Shi-jiu, J and Zhi-gang, Q., 2006. *Study on the distributed optical fiber sensing technology for pipeline leakage detection*. Advanced Laser Technology 2005. In Proceedings of SPIE 6344, The International Society for Optical Engineering. pp.634465-1 – 634465-6. DOI: 10.1117/12.694438.

Yue, L., Xue, F., Wei, Z. and Xiao-Ming, L., 2009. An experiment of dynamical behaviors in an erbium-doped fiber-ring laser with loss modulation. *Chinese Physics B*, 18, pp.3318-3324.

Zhihui, F., Dingzhong, Y., Wen, Y., Jian, K. and Yonghang, S., 2009. Widely tunable compact erbium-doped fiber ring laser for fiber-optic sensing applications. *Optics and Laser Technology*, 41(4), pp.392.

APPENDIX A

DATASHEET FOR ERBIUM DOPED-FIBER ISOgain



VERSION: NEWPORT 16/3
RELEASE DATE: 8 NOVEMBER 2013

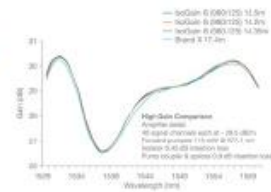
Erbium Doped Fiber IsoGain™

Fibercore's IsoGain™ range of Erbium Doped Fibers (EDFs) offer a wide selection of absorption and cut-off wavelengths to allow the best choice of fiber for each type of Erbium Doped Fiber Amplifier (EDFA) design.

Fibercore's low absorption fibers offer best-in-class efficiency for C-band amplifiers whilst higher absorption fibers are optimized for L-band EDFAs.

High cut-off wavelength (HC) fibers have larger core diameters, reducing non-linear effects and increasing efficiency at higher pump powers.

The core composition of Fibercore's IsoGain™ has been engineered to generate a substantially flattened wavelength response that closely matches that of other leading fiber types.



Supported by Fibercore's GainMaster™ simulation software

Advantages:

- High efficiency core composition
- 'HC' variants optimized for high pump power EDFAs
- High absorption fibers for L-band amplifiers and mini/micro C-band EDFAs
- Wide range of absorption values for EDFA design optimization

Typical applications:

- EDFAs / Telecoms
- ASE Light Sources
 - Gyros
 - Current Sensors
 - Distributed Sensor Systems
- Fiber Lasers
- Biomedical Illumination
- Optical Coherence Tomography (OCT)

Related Products:

- Erbium Doped Fiber MetroGain™
- Dual-Clad Erbium/Ytterbium Doped Fiber (CP1500Y)
- GainMaster™ Simulation Tool

Product Variants:

- I-4 (980/125) For high efficiency C-band EDFAs
- I-4 (980/125)HC For high efficiency, high power C-band EDFAs
- I-6 (980/125) Increased absorption for high efficiency C-band EDFAs
- I-12(980/125) Mid level absorption fiber for short length C-band and L-band EDFAs
- I-12(980/125)HC High cut off wavelength, mid level absorption fiber for higher power short length C-band and L-band EDFAs
- I-15(980/125)HC High cut off wavelength, mid/high level absorption fiber for higher power short length C-band and L-band EDFAs
- I-25 (980/125) Very high absorption fiber for short length L-band EDFAs
- I-25H(1480/80) 80µm cladding diameter, high cut off wavelength, high absorption fiber for small coil diameter mini and micro EDFAs

T: +1 (949) 863 3144
E: sales@newport.com
www.newport.com



Specifications

High Efficiency C-Band Erbium Doped Fibers

	I-4(B80/125)	I-4(B80/125)HC	I-6 (B80/125)
Cut-Off Wavelength (nm)	870 – 970	1000 – 1320	870 – 970
Numerical Aperture	0.22 – 0.24		
Mode Field Diameter (µm)	5.4 – 6.6 @1550nm	5.2 – 5.8 @1550nm	5.5 – 6.3 @1550nm
Absorption (dB/m)	5.0 – 6.7 @1531nm	7.7 – 9.4 @1531nm	7.2 – 8.4 @1531nm
Proof Test (%)	1 (100 kpsl)		
Attenuation (dB/km)	≤10 @1200nm		
Polarization Mode Dispersion (ps/m)	≤0.005		
Cladding Diameter (µm)	125 ± 1		
Core Concentricity (µm)	≤0.3		
Coating Diameter (µm)	245 ± 15		
Coating Type	Dual Acrylate		

L-Band and C-Band Erbium Doped Fibers

	I-12(B80/125)	I-12(B80/125)HC	I-15(B80/125)HC	I-25(B80/125)
Cut-Off Wavelength (nm)	900 – 970	1200 – 1320	1200 – 1320	900 – 970
Numerical Aperture	0.21 – 0.23	0.23 – 0.26		
Mode Field Diameter (µm)	5.7 – 6.6 @1550nm	5.0 – 5.5 @1550nm	4.8 – 5.4 @1550nm	5.2 – 6.3 @1550nm
Absorption (dB/m)	14 – 21 @1531nm	17 – 21 @1531nm	27 – 33 @1531nm	35 – 45 @1531nm
Proof Test (%)	1 (100kpsl)			
Attenuation (dB/km)	≤10 @1200nm			
Polarization Mode Dispersion (ps/m)	≤0.005			
Cladding Diameter (µm)	125 ± 1			
Core Concentricity (µm)	≤0.3			
Coating Diameter (µm)	245 ± 15			
Coating Type	Dual Acrylate			

Reduced Cladding Erbium Doped Fiber For Mini and Micro EDFAs

	I-25H(1480/80)
Cut-Off Wavelength (nm)	900 – 1025
Numerical Aperture	≥0.30
Mode Field Diameter (µm)	3.8 – 4.7 @1550nm
Absorption (dB/m)	23 – 27 @1531nm
Proof Test (%)	1 (100kpsl)
Attenuation (dB/km)	≤30 @1200nm
Polarization Mode Dispersion (ps/m)	≤0.005
Cladding Diameter (µm)	80 ± 1
Core Concentricity (µm)	≤0.5
Coating Diameter (µm)	160 ± 10
Coating Type	Dual Acrylate

Visit fibercore.com/fiberpedia for our encyclopedia of industry terms/knowledge base.

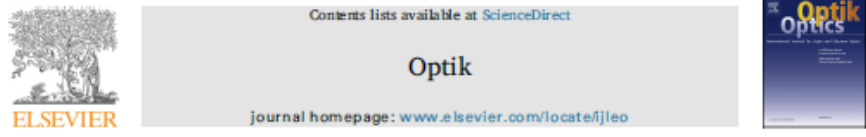
T: +1 (949) 853 3144
E: sales@newport.com
www.newport.com



APPENDIX B

PUBLICATION 1

Optik - International Journal for Light and Electron Optics 207 (2020) 164442



Original research article

The dynamic behavior of non-polarized erbium-doped fiber ring laser under experimental pump modulation



Nneka Obianuju Onubogu, Chang Hong Pua*, Homg Sheng Lin, Abd-Rahman Faizd

Lee Kong Chian Faculty of Engineering and Science, Universiti Tunku Abdul Rahman, Jalan Sungai Long, Bandar Sungai Long, 43000, Kajang, Selangor, Malaysia

ARTICLE INFO

Keywords:
Erbium-doped fiber ring laser
EDFRL
Pump modulation
Bifurcation
Optical bi-stability
Chaos

ABSTRACT

An Erbium-doped fiber ring laser subjected to sinusoidal pump modulation has been studied experimentally and its bifurcation diagram analyzed. Data from oscilloscope is used to analyze the interesting spectral features observed via the time domain response and frequency domain response which shows the different dynamical regimes occurring when the modulation frequency and amplitude are being varied respectively. Linear and non-linear (chaos) dynamical behaviors are observed, as well as optical bi-stability. The dynamical response of an Erbium-doped fiber ring laser can easily be studied through pump modulation.

1. Introduction

Erbium is the most common choice for constructing a fiber laser due to its validated capability to support the generation and amplification of short optical pulses in the spectral region of 1550 nm. Hence it is very useful for optical communication applications, sensing, medicine, etc. Erbium-doped fiber laser is a class B laser as its polarization can be eradicated without heat transfer and its dynamics can be ruled by the two-rate equations for field and population inversion [1]. Erbium-doped fiber laser is very sensitive when subjected to external perturbations which may disturb its normal operation and generate a non-linear response. Therefore, it is of valuable importance to study and observe its dynamic behavior under pump modulation as it has a vast range of applications [2–8]. Many studies on experimental and theoretical pump modulated Erbium doped fiber laser have been carried out by several authors [1,2,9–17], having various ring laser cavity configurations. The present work differs from them in that the ring laser set-up is different as it does not include a polarizer. These authors have also studied the non-linear dynamic behavior and chaos of fiber laser subjected to pump modulation and have obtained similar results. Pump modulated fiber lasers need large modulations in order to display its non-linear dynamics unlike in loss modulated fibers [18]; however, from an experimental point of view, it is much easier to achieve compared to cavity loss modulation [1] and the former is not always the case.

In this research work, the linear and nonlinear dynamical behaviors of the single-mode Erbium-doped Fiber Ring Laser (EDFRL) is demonstrated experimentally under pump modulation of the frequency (kHz) of the laser pump power. Bifurcation diagrams presented in this paper illustrate the dynamical changes occurring at different frequencies as the control parameters are altered and shows behaviors such as bifurcation, optical bi-stability, chaotic routes to chaos and chaos at different modulation frequencies while keeping the input amplitude constant. To understand the dynamical regimes of the EDFRL, time and frequency domains are presented. The waveforms obtained throughout the experiment as seen in the time domain diagrams is different from what has been

* Corresponding author.

E-mail addresses: nneka.onubogu@utar.my (N.O. Onubogu), punch@utar.edu.my (C.H. Pua), linhs@utar.edu.my (H.S. Lin), faizdar@utar.edu.my (A.-R. Faizd).

<https://doi.org/10.1016/j.ijleo.2020.164442>

Received 10 January 2020; Accepted 16 February 2020
0030-4026/ © 2020 Elsevier GmbH. All rights reserved.

APPENDIX C

PUBLICATION 2

Optik - International Journal for Light and Electron Optics 225 (2021) 165846



ELSEVIER

Contents lists available at ScienceDirect

Optik

journal homepage: www.elsevier.com/locate/ijleo



Original research article

Dynamic features of a non-polarized Erbium-doped fiber ring laser subjected to external cavity-loss modulation



Nneka Obianuju Onubogu, Chang Hong Pua^{*}, Abd-Rahman Faizd

Lee Kong Chian Faculty of Engineering and Science, Universiti Tunku Abdul Rahman, Jalan Sungai Long, Bandar Sungai Long, 43000, Kajang, Selangor, Malaysia

ARTICLE INFO

Keywords
Cavity-loss modulation
Erbium-doped fiber ring laser
EDFRL
Bifurcation
Chaos
Optical bi-stability

ABSTRACT

An experimental study of an Erbium-doped fiber ring laser subjected to external cavity-loss modulation using a loudspeaker as the modulator has been carried out and analyzed via modulation of the driving amplitude and frequency in the range of 1–20 kHz. The linear and non-linear (chaotic) dynamical behaviors have been observed from the bifurcation, time domain and frequency domain diagrams presented. The bifurcation diagram showed that the loss modulated laser is more sensitive to the acoustic wave generated from the loudspeaker when the driving amplitude is < 200 mV and < 1000 mV (< 16.5 mW and < 82.5 mW optical power). At driving amplitudes of 500 mV – 1000 mV (41.25 mW – 82.5 mW optical power), the ring laser system behaves like a damped non-linear oscillator. Optical bi-stability was also observed in the bifurcation diagrams near or exactly at the fundamental resonance frequency and first super harmonic resonance frequency. The availability of different control parameters during external cavity-loss modulation in an Erbium doped fiber laser makes the study of its non-linear response features easy in a very precise way. The control parameters considered in this paper are the driving amplitude and the modulation frequency.

1. Introduction

Erbium doped fiber lasers (EDFL) have gained increased attention due to its many advantages and vast applications which include secure optical communications, LIDAR technology, sensing purposes (chemical sensing, water flow sensing, acoustics sensing, etc.) and a range of other applications [1–12]. EDFL are characterized by slow relaxation times and are highly sensitive to external disturbances that in most cases interrupt their usual operation causing a range of dynamic behaviors. These dynamic behaviors can be attained via three popular methods: pump modulation [13–20], loss modulation [21–27] and controlled feedback methods [28]. Pump modulation is very common and there are so many existing studies on pump modulated EDFLs [13–20] and fewer on loss modulated EDFLs [21–27], because it is believed from the experimental point of view that pump modulation is easier to achieve compared to loss modulation [13]. However, the features displayed by the Erbium-doped fiber ring laser (EDFRL) from the two types of modulation are almost the same.

The focus of this paper is on loss modulation. Loss modulation is of great importance as chaotic (non-linear) features can be easily generated at low modulation amplitudes [29] compared to pump modulation where large modulations are needed to display chaotic features. This is the main drive for studying loss modulation. For this reason, loss modulated EDFLs can be used as model systems in

^{*} Corresponding author.

E-mail addresses: nneka.onubogu@utar.my (N.O. Onubogu), puach@utar.edu.my (C.H. Pua), faizdar@utar.edu.my (A.-R. Faizd).

<https://doi.org/10.1016/j.ijleo.2020.165846>

Received 19 August 2020; Received in revised form 9 October 2020; Accepted 20 October 2020

Available online 25 October 2020

0030-4026/© 2020 Elsevier GmbH. All rights reserved.

APPENDIX D

PUBLICATION 3

Optik - International Journal for Light and Electron Optics 266 (2022) 169519



Numerical analysis of the behavioral response of pump-modulated linear and ring erbium-doped fiber lasers

Nneka Obianuju Onubogu ^a, Chang Hong Pua ^{a,*}, Abd-Rahman Faizd ^a, William C. Rose ^b

^a Lee Kong Chian Faculty of Engineering and Science, Universiti Tunku Abdul Rahman, Jalan Sungai Long, Bandar Sungai Long, 43000 Kajang, Selangor, Malaysia

^b Department of Kinesiology and Applied Physiology, University of Delaware, Newark, DE 19716, USA

ARTICLE INFO

Keywords:
Erbium-doped fiber laser
Rate equations
Pump modulation
Bifurcation
Chaos

ABSTRACT

Objective: The behavioral response of an erbium-doped fiber laser having two different configurations (linear cavity and ring cavity) and subjected to pump modulation is analyzed numerically. These same laser configurations with the same initial conditions have previously been studied experimentally.

Methodology: For the numerical analysis, a modified laser model based on the rate equations of a three-level class B laser which is quite similar to that of a non-linear oscillator is presented.

Results: The numerical model generates all the linear and non-linear spectral features observed during the experimental analysis. The experimental and numerical bifurcation, time domain and frequency domain diagrams match reasonably well. The dynamic behavior of the EDFRL is numerically analyzed at low modulation frequencies (below 7 kHz) when the resonance frequency ranges from 2 kHz to 10 kHz. The results for the descending chirp of the EDRPL under certain pump modulation conditions showed a new strange dynamic behavior requiring further studies.

Significance: The EDFRL can be used for sensing purposes in locations with high background noise as it is sensitive even at low frequencies irrespective of the noise. Numerical analysis is a fast and reliable way to obtain remarkable information on the spectral behavior of the EDFL.

1. Introduction

The merits of erbium-doped fiber lasers (EDFLs) have made them popular for so many years and counting in the areas of secure optical communication, medicine, sensing, LIDAR technology, etc. [1–10]. These merits include their immunity to electro-magnetic interference, narrow line-width, one-mode operation, slow relaxation times, long interaction length of the laser pumped light with the active erbium ions, high amplification or gain, low noise, great sensitivity to external perturbations leading to a series of dynamic behaviors, etc., [7]. More so, EDFLs are very compact in size and affordable which makes them applicable in hand-held detectors [11]. Hence, it is of great interest to many researchers to study the dynamic features of the EDFL especially under modulation owing to its many developing prospective applications.

* Corresponding author.

E-mail addresses: nneka.onubogu@utar.my (N.O. Onubogu), puaoh@utar.edu.my (C.H. Pua), faidzar@utar.edu.my (A.-R. Faizd), rosewc@udel.edu (W.C. Rose).

<https://doi.org/10.1016/j.ijleo.2022.169519>

Received 19 April 2022; Received in revised form 1 June 2022; Accepted 16 June 2022

Available online 20 June 2022

0030-4026/© 2022 Elsevier GmbH. All rights reserved.

APPENDIX E

PUBLICATION 4

Dynamics of a highly sensitive Erbium-doped Fabry-Perot Fiber (EDFBF) Laser Sensor under pump modulation

Publisher: **IEEE**

[Cite This](#)

[PDF](#)

Nneka Obianuju Onubogu ; Chang Hong Pua ; Horng Sheng Lin ; Abd-Rahman Faidz [All Authors](#)

33

Full

Text Views



Abstract

Document
Sections

1. Introduction
2. Configuration and

Abstract:

This study experimentally investigates changes occurring in a highly sensitive Erbium-doped Fabry-Perot fiber (EDFPF) laser sensor under pump modulation by varying the modulation frequency from 1 kHz to 60 kHz. The dynamic behaviour of the EDFBF laser sensor and the laser spectrum of the routes to chaos are presented graphically.

Dynamics of a highly sensitive Erbium-doped Fabry-Perot Fiber (EDFBF) Laser Sensor under pump modulation

Nneka Obianuju Onubogu⁽¹⁾, Chang Hong Pua^{(1)*}, Horng Sheng Lim⁽¹⁾, and Abd-Rahman Faizd⁽¹⁾

⁽¹⁾ Lee Kong Chian Faculty of Engineering and Science, Universiti Tunku Abdul Rahman

^{(1)*} Bandar Sungai Long, Jalan Sungai Long, 43000, Kajang, Malaysia, nneka.onubogu@utar.my, pua.ch@utar.edu.my

Abstract: This study experimentally investigates changes occurring in a highly sensitive Erbium-doped Fabry-Perot fiber (EDFBF) laser sensor under pump modulation by varying the modulation frequency from 1 kHz to 60 kHz. The dynamic behaviour of the EDFBF laser sensor and the laser spectrum of the routes to chaos are presented graphically.

1. Introduction

Acousto-optic sensing has been made possible over the years with the use of optical fiber-based methods such as Raman Scattering, Rayleigh scattering, Fiber Bragg Grating (FBG), and Brillouin scattering. However, these methods entail monitoring of wavelength scattering which involves costly instruments as the set-up is complicated with slow response time. For this reason, Erbium-doped fiber lasers were introduced and are now gaining popularity due to their numerous merits such as low cost, flexibility, extreme resistance to heavy environments, simplicity, low maintenance costs, high sensitivity, wide tunable wavelength, etc. [1]. Research has previously been carried out on the application of the Erbium doped fiber laser (EDFL) for intrusion zone identification [2], pipeline leakage sensing and location estimation [3]. In another research by Pua et al, EDFL has been proven to be a highly sensitive sensor with sensitivity of about -60 dBA when the resonant frequency is varied from 5 kHz to 85 kHz [4]. The highly sensitive Erbium-doped Fabry-Perot fiber (EDFPF) laser sensor in this paper is similar to the sensors in [2-4], and is proposed mainly for pipeline leakage monitoring.

To study the dynamics of the EDFPF, pump modulation is performed in order to trigger the non-linear behavior of the laser. A few researchers have performed pump modulation on EDFL [5-8]. Pump modulated EDFL has drawn lots of attention because it exhibits chaotic features at high frequencies which has unique applications [9]. Also, the modulation process via semi-conductor lasers is quite easy.

2. Configuration and working principle of the EDFPF laser sensor

The configuration of the EDFBF laser sensor under pump modulation is shown in Fig. 1. It consists of the Erbium doped fiber (EDF) of 10 m length which is the active medium of the laser; a 980 nm pump laser diode having a single wavelength 980/1550 nm; wavelength division multiplexing (WDM) coupler; single mode fiber (SMF), 1550 nm single side Fiber Bragg grating (FBG), and a high-speed photodetector to change the optical output to electrical output.



Fig. 1. Schematic diagram of the EDFBF laser sensor

The working principle of the EDFBF laser sensor is very simple. Laser is propelled by the laser pump into the WDM coupler which couples the 980 nm and 1550 nm wavelengths. The lasing light then moves to the EDF and to the sensing arm. Erbium ions absorb 980 nm of photons and freely releases photons at 1520-1560 nm but the FBG reflects only 1550 nm photons. The Erbium ions are then stimulated by the reflected 1550 nm photons to release photons at 1550 nm. The FBG and the other end of the fiber with flat cleave forming the laser cavity needed in the setup with reflectivity of 0.98 and 0.04, respectively. The output power of the laser is observed using photodetector and oscilloscope. To activate the laser dynamics of the EDFBF laser sensor, low feedback is used to create an unstable lasing condition.

3. Experiments and results

For the pump modulation experiment, the resonance frequency of the EDFPF laser and its amplitude were set at 7 kHz and 0.2 V_{pp} respectively. The laser was pumped at 95 mW power from the laser pump to the EDF. Direct modulation was carried out by varying the modulation frequency from 1 to 60 kHz using a manual function generator with a sinusoidal signal. During pump modulation from low to high frequency and vice versa, the peak to peak amplitude of the optical output were measured for every frequency change and presented graphically in Fig. 2. Fig. 3 shows the behavior of the

APPENDIX F

PUBLICATION 5

Dynamic Behavior of a Pump-Modulated Erbium-Doped Fiber Linear Laser with Single Fiber Bragg Grating



Nneka Obianuju Onubogu and Chang Hong Pua

Abstract An experimental analysis of the dynamical behavior of a pump-modulated Erbium-doped fiber laser (EDFL) with single fiber Bragg grating has been carried out and reported in this paper. The linear laser cavity here resembles a Fabry Perot interferometer. While varying the modulation frequency with a consistent signal amplitude and pump power, a wide range of features were observed which include: bifurcation, regions of optical bi-stability, period doubling, intermittently chaotic paths to chaos and chaos. Based on the region of chaos observed around the resonant frequency, the propensity of the laser to be used as a sensor to detect acoustic waves is briefly discussed, as the EDFL displayed tunable sensitive frequency capability.

Keywords EDFL · Pump modulation · Bifurcation

1 Introduction

Erbium-doped fiber lasers (EDFL) are known to have very outstanding features such as single-mode operation, high amplification, self-pulsations, high sensitivity to external disturbances, etc. These characteristics have made them a good laser source for many applications including optical communication, medicine, science and technology, reflectometry, pipeline sensing, intrusion zone identification, airborne acoustic sensing, etc. [1–6]. The characteristic of “high sensitivity to external disturbances” has gained more focus over the years as it leads to nonlinear dynamics during pump or loss modulation [7], which has an immense range of applications. Experimental pump modulation has been carried out on fiber lasers doped with Erbium by various authors [8–20]; however, our configuration is different from theirs and is quite simple and affordable. More so, it is customizable as other optical devices or

N. O. Onubogu · C. H. Pua (✉)
Lee Kong Chian Faculty of Engineering and Science, Universiti Tunku Abdul Rahman, Bandar Sungai Long, Jalan Sungai Long, 43000 Kajang, Malaysia
e-mail: puach@utar.edu.my

N. O. Onubogu
e-mail: nneka.onubogu@utar.my

© The Author(s), under exclusive license to Springer Nature Singapore Pte Ltd. 2022 281
A. Sivasubramanian et al. (eds.), *Futuristic Communication and Network Technologies*,
Lecture Notes in Electrical Engineering 792,
https://doi.org/10.1007/978-981-16-4625-6_28

